Laser Processing, Thermomechanical Processing, and Thermomechanical Fatigue of NiTi Shape Memory Alloys

by

Boyd Panton

A thesis
presented to the University of Waterloo
in fulfilment of the
thesis requirement for the degree of
Doctor of Philosophy
in
Mechanical Engineering

Waterloo, Ontario, Canada, 2016

Author's Declaration

I hereby declare that I am the sole author of this thesis. This is a true copy of the thesis, including any required final revisions, as accepted by my examiners.

I understand that my thesis may be made electronically available to the public.

Boyd Panton

Abstract

NiTi shape memory alloys (SMAs) have revolutionized engineering design across all industries, with major contributions in the medical, aerospace, and automotive industries. These fascinating materials possess the shape memory effect, pseudoelastic effect and biocompatibility, which make them so highly desired. Since their discovery mid-way through the 20th century a large research effort has been underway to gain fundamental understanding of the mechanisms responsible for their properties. The material properties depend on a large number of variables including the microstructure, the texture, the stress/strain state, and the temperature. An understanding of the interdependence of these variables is still being developed, with particular focus on their evolution when either multi-axial loading, or fatigue cycling are applied to the material. Furthermore, the advanced manufacturing techniques required to properly process NiTi have only recently become a reality, with further advancements being developed to continue pushing the limits of these materials. One limitation of NiTi is that standard manufactured products have only one transformation temperature. A number of techniques have been developed in an attempt to address this limitation and increase the functionality of SMAs. A highly accurate and repeatable technique was recently developed that uses a high energy density process (e.g. laser) to alter the composition of NiTi in localized regions. Laser processing enables the tailoring of different regions of a single piece of NiTi to have different transformation properties. However, there have been no in-depth studies of the evolution of the properties of these laser processed materials over multiple mechanical or thermal cycles. This lack of fundamental knowledge significantly limits both the understanding and possibilities for the application of laser processed NiTi. In addition to this limitation, the most widely used form of NiTi SMA is wires, but the major studies on laser processing have focused on sheets. Investigation of the evolution of laser processed NiTi wires over multiple mechanical or thermal cycles would not only benefit laser processing technologies, but it would also improve the general understanding of SMAs, with benefits to other areas including other local processing techniques, welding and joining, mechanical and thermomechanical fatigue. The current study investigated the evolution of the properties of laser processed NiTi when the materials were subjected to thermal cycling, mechanical cycling, and fatigue cycling. The knowledge gained

was used to identify limitations in the current technology, and develop thermomechanical treatments to address these limitations.

The first part of the investigation focused on a wire that had a single laser processed spot (i.e. a laser weld). Few investigations have been attempted to characterize the mechanical fatigue properties of NiTi joints, and to the author's knowledge there have been no previous investigations on the thermomechanical fatigue properties of these joints. The current work investigated the thermomechanical fatigue properties of Nd:YAG pulsed laser welded, and post-weld heat treated NiTi wires. The welded wires maintained over 86 % of the base metal ultimate tensile strength; however, they had reduced actuation stability and stroke, and had significantly reduced cycle life. Use of a post-weld heat treatment successfully increased both the actuation stability and the cycle life by an order of magnitude compared to the welded wires.

The second part of the investigation focused on the development and characterization of laser processing techniques for NiTi wires. The process altered the composition of the NiTi wire with a reduction of 0.23 at.% Ni for each laser pulse after the first pulse. The first laser pulse removed 0.40 at.% Ni, which was a larger amount than the following pulses, because the wire drawn surface finish was less reflective than the laser processed surface. The coarse grained laser processed NiTi had 71 % of the base metal ultimate tensile strength, 40 % of the base metal ductility, significant reduction in the stability of the shape memory properties, and an almost complete loss of the fatigue life of the base metal. Using the fundamental knowledge gained from this investigation a thermomechanical treatment was developed to improve the properties of the laser processed NiTi. The treated laser processed NiTi had an ultimate tensile strength matching the base metal and a ductility 70 % greater than the laser processed NiTi. Significant improvement to the shape memory properties were achieved, with a return of pseudoelasticity, and an 80% greater shape memory recovery than the untreated laser processed NiTi. Furthermore the low strain (i.e. 2%) thermomechanical fatigue lives of the treated laser processed NiTi were equal to the base metal. Finally, actuators were developed with two distinct memories, with the treated actuator having 33 % lower plastic strain, and 42 % greater shape memory recovery than the untreated actuator.

This technology was exploited to develop a self-biasing actuator. A shape memory alloy (SMA) actuator that is biased internally (i.e. self-biasing) would not need an external bias to achieve multiple actuation cycles. This would reduce cost, complexity and weight compared to standard one-way SMAs. The self-biasing actuators that have been developed to date have a lack of geometric and actuation stability. The current study developed a self-biasing NiTi actuator using a laser based vaporization process to alter the bulk composition of a NiTi wire. The martensitic laser processed NiTi region was the actuator, and un-processed austenitic base metal region was the internal bias. It was discovered that the laser processed region of the self-biasing actuator was unstable during high stress thermomechanical cycling due to the coarse grained microstructure. Cold-working of the half martensitic and half austenitic component resulted in similar deformation characteristics to single phase NiTi, which enabled the formation of a uniform nanocrystalline microstructure in both regions. When thermomechanically cycled 6000 times under stresses ranging from 180 to 400 MPa, it was discovered that this treated self-biasing actuator exhibited the stabilization behaviour of traditional one-way actuators. This behaviour was due to the uniform nanocrystalline microstructure, which impeded dislocation activity and ensured minimal plastic deformation.

Acknowledgements

I would like to acknowledge the contributions of many people who have helped me throughout my degree. I want to thank my family and friends for all of their love and support throughout my time at the University of Waterloo. I would like to thank my supervisor Prof. Y. Norman Zhou for his guidance and all of the opportunities that he has provided me. I want to thank Dr. M. Ibraheem Khan and all of the members of Smarter Alloys for their training, assistance, and the opportunities that they have provided. I want to thank Dr. Andrew Pequegnat for his supervision, mentorship, help and partnership in research. I want to thank Mr. Siu Kei Tang for his partnership during the initial development of the laser processing and wire drawing processes.

I want to thank all of my research collaborators in no specific order; Joao Oliveira, Prof. Zhi Zeng, Dr. Adelina Han, Dr. Michael Kuntz, Greg Seviora, Matt Daly, Prof. Corneliu Craciunescu, Andrew Michael, Tirdad Niknejad, and Jeff Wang. I would like to thank all students that I have worked with; Suleman Azam, Mark Liang, Tim Thompson, Yeshwanth Kesavan, Raymond Kuo, Anthony Zhou, Daniel Zhou, and Hung Yang.

I want to thank all of my colleagues in the Centre for Advanced Materials Joining (CAMJ) from whom I have learned priceless knowledge and lessons. I would like to thank all of the technicians at the University. Without their help I would not have been able to design and manufacture my experimental apparatuses. I would like to thank the researchers at the Canadian Centre for Electron Microscopy (CCEM) all of their support with transmission electron microscopy. I would like to thank the researchers at the University of Toronto.

I would like to thank the Natural Sciences and Engineering Research Council of Canada (NSERC), which supported this works.

Lastly I want to thank all of those that I have forgotten to add to this list.

Dedication

To my beautiful, loving fiancée Cyrille Viola,

& my father, my mother, and my brother

Contents

List of Figures

List of Tables

List of Equations

1 Introduction

1.1 Background

The shape memory effect was first observed in the early 20th century in the Au-Cd and In-Th systems [1, 2]. These systems had negligible change in shape, making the shape memory effect only of academic interest until the discovery of NiTi in the mid-20th century [3]. NiTi has a significant shape memory effect of up to 10 % recovery [4], but needed decades of research to develop both the fundamental knowledge for application and the proper manufacturing techniques before NiTi was first implemented in industry in the latter half of the 20th century [5, 6]. In the modern day shape memory alloys (SMAs) have become widely used in the medical industry and have enabled revolutions in design throughout the engineering world [5, 7-11]. In many of these designs, traditional motors and actuators are being replaced with NiTi SMAs, and this replacement is forecasted to significantly increase over the next decade [5]. SMAs are of particular interest in actuation applications due to their high stress, high actuation strain, and high energy density. Further improvement to their actuation frequency and the number of transformation properties per NiTi component is desired to increase the range of applications for these materials [12].

SMA components with a gradient of properties or regions of different properties would enable greater functionality for countless applications including medical tools and implants [13], multiple position actuators [14], self-biasing actuators [15], or SMAs with complex responses that are activated at distinct temperature ranges [16]. Previous methods explored to make multi-functional SMAs include antagonistically positioning SMAs, local heat treatment techniques, the two-way shape memory effect, and local alteration of SMA properties [17-19]. Local property modification is the most flexible method which and can be used in a wide scale and range of applications [13, 14, 16, 20, 21]. A highly versatile method of tailoring local properties using high energy density sources (e.g. laser) was recently developed at the University of Waterloo [16]. This process has been proven to create multiple transformation temperatures and pseudoelastic plateaus in a single NiTi component [13]. Application of this technology is currently limited by a lack of fundamental knowledge of the evolution of the properties of the

laser processed NiTi over multiple thermal or mechanical cycles. The current study investigated the thermal, mechanical and thermomechanical cycling of laser processed NiTi. The objective of this study was to gain a fundamental understanding of the process-structure-properties relationship of these materials, which would increase the depth of knowledge of SMAs, and expand the potential beneficial use of laser processed or other multi-functional SMAs throughout industry.

1.2 Objectives

The motivation for this work was to gain a fundamental understanding of the process-structure-properties relationship of laser processed NiTi when it was cycled thermally and mechanically. This knowledge was used to design thermomechanical treatments to improve the properties of the laser processed NiTi. This knowledge provides a deeper understanding of NiTi SMAs, and enable the wider use of laser processed SMAs to benefit society. SMAs have already enabled a revolution in engineering designs, and SMAs with multiple properties across a single component can enable a second revolution, which can benefit humanity immensely. This study involved:

1. Investigation of the effect of welding (i.e. single laser processing spot) of NiTi SMAs on the thermomechanical fatigue properties. There have been no previously published investigations in this area. Part of this investigation was to determine if any post-weld processes could be implemented to improve the material properties.
2. Characterization of the laser processing of NiTi wires. Investigation of the structure-properties relationship of the laser processed wires with focus on multiple thermal and mechanical cycles. Identification of the underlying mechanisms behind any limitations in the properties (e.g. stability, fatigue life) of these materials and development of thermomechanical treatments to improve the properties.
3. Development of a self-biasing (i.e. moves on heating and cooling) actuator using the laser processing technology. This would further increase the functionality and potential applications of SMAs. The adoption of a self-biasing actuator by industry would require it to achieve tens of thousands of cycles while maintaining geometric and actuation stability. This has not yet been achieved by other self-biasing methods.

1.3 Thesis Organization

The thesis is divided into 8 chapters.

Chapter 1 is an introduction, the objectives and the motivation behind this work.

Chapter 2 is a literature review of NiTi SMAs, including their physical metallurgy, manufacturing, and physical, transformation and fatigue characteristics. The limitations of current laser processing technologies are identified and the motivations for the current work are expanded.

Chapter 3 describes the experimental methods used for this study.

Chapter 4 investigates the effect of laser welding on the thermomechanical fatigue of NiTi SMA wires. There was a significant reduction in the fatigue life and stability of actuation after laser welding, which was partially recovered by the application of a post-weld heat treatment.

Chapter 5 investigates the laser processing of NiTi SMA wires. The laser processed wires had significant reduction in physical, transformation and fatigue properties compared to the base metal. The thermomechanical treatment applied to the wires recovered a large portion of the properties, with full recovery of the ultimate tensile strength, improvements to the pseudoelastic and shape memory properties and low strain fatigue values in the same order of magnitude as the commercially available actuator wire.

Chapter 6 discusses the development of a self-biasing actuator developed using the processes from Chapter 5. The treated self-biasing actuator had a stabilized actuation, with low plastic strain build-up after thousands of cycles.

Chapter 7 details the main conclusions of the study and recommendations for future work.

Chapter 8 lists the author's contributions to research.

2 Literature Review

The study of the thermomechanical fatigue of laser processed shape memory alloys requires a fundamental understanding of the crystallography, microstructure, phase transformation kinetics, material processing and manufacturing methods, and the mechanism of fatigue unique to SMAs. The following literature review examined this vast field of knowledge, and was used to build key relations essential to the success of the project as outlined in the results chapters.

2.1 NiTi Physical Metallurgy

The NiTi SMA is a near equiatomic (i.e. ~Ni 50.0 at. % Ti) Ni and Ti intermetallic compound, which is in between the Ti_2Ni and Ni_3Ti intermetallics in the Ni-Ti binary phase diagram shown in Figure 2.1. As indicated in the phase diagram the undesirable brittle Ti_2Ni phase forms during solidification of a Ti-rich NiTi. It can also form in Ni-rich NiTi when the environment contains any amount of oxygen, due the higher solubility of oxygen in Ti_2Ni [22]. Forming this compound can lead to solidification cracking during rapid solidification processes such as welding [16, 23]. Other detrimental phases can form during ingot casting including TiC carbides, which form due to a eutectic reaction with the graphite crucibles used in vacuum induction melting (VIM). The high reactivity of NiTi requires inert or vacuum atmospheres to impede reactions with the atmospheric contaminants but even these methods are incapable of completely stopping the peritectic reaction that forms $Ni_2Ti_4O_X$ and TiO oxides [22, 24]. During the casting process a greater amount of carbides form than oxides in part due to the faster kinetics of eutectic reactions compared to peritectic reactions [25-27]. Methods of coating the crucible have been developed to limit the formation of these detrimental carbides [28]. After casting, during the forming processes these inclusions can fracture and form particle void assemblies (PVA) that serve as crack initiation points for failure [26, 27, 29-31]. The oxides are generally larger than carbides and fracture more readily to form the PVAs [31].

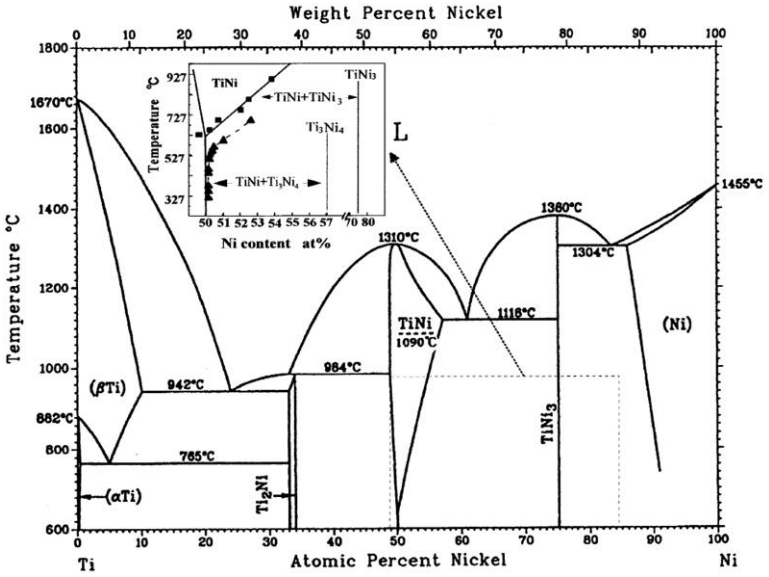

Figure 2.1: The Ni-Ti Phase diagram [6, 32]

NiTi is a stoichiometric intermetallic at room temperature, but the diffusion of Ni and Ti greatly increases above 923 K (650 °C) [6]. Solutionizing above this temperature followed by quenching will form a supersaturated solid solution, which can then be aged to form beneficial precipitates [6]. These metastable phases are indicated by the insert in Figure 2.1. Their form is dependent on ageing time and temperature with longer times and higher temperatures resulting in the phase being absorbed by the matrix (i.e. $Ni_4Ti_3 \rightarrow Ni_3Ti_2 \rightarrow Ni_3Ti$) [33]. The metastable Ni_4Ti_3 is the preferred phase used for strengthening the microstructure, forming coherent lenticular precipitates in the matrix [34, 35]. Fine, homogenous distribution of this beneficial phase requires Ni supersaturation, and the homogeneous distribution of grain boundaries, dislocations and other high energy areas that act as preferential nucleation sites [6, 36].

NiTi has a phase change that occurs near room temperature, from the parent B2 austenite phase to the product B19’ martensite phase as illustrated by Figure 2.2. The B2 phase is a cubic CsCl type structure with lattice parameter 0.3015nm, and the B19’ martensite phase is a monoclinic structure with lattice parameters a =0.2889, b = 0.4210, c = 0.4622 and $\beta = 96.8°$ [37, 38]. Heavy cold work, the presence of precipitates, or nanocrystalline grains can restrict the maximum strain that can be accommodated by the structure without plastic deformation [36, 39]. This restriction

of strain results in an intermediate small strain transformation to a rhombohedral (R-phase) structure that enables the transformation between the B2 and B19' phases (Figure 2.3).

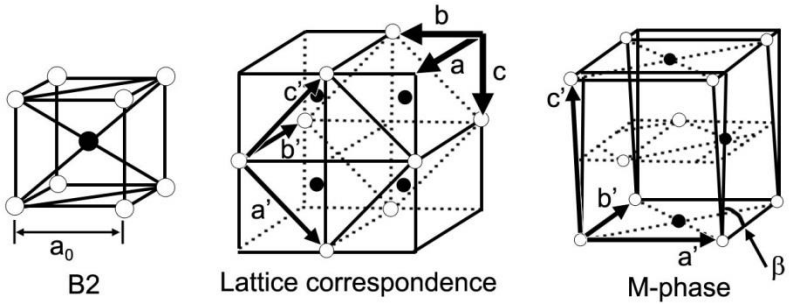

Figure 2.2: Crystal structure of the parent austenit (B2) and product martensite (B19') phases and the lattice correspondence between the two phases [40]

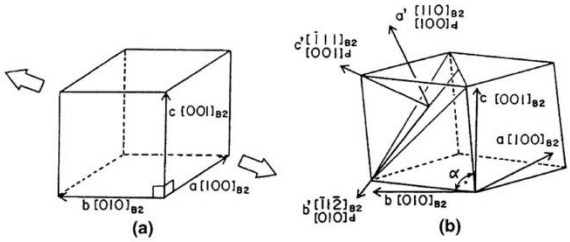

Figure 2.3: Lattice change from B2 to R-phase. The axes a', b' and c' represent the principal axes in that lattice deformation [41]

2.2 The Reversible Martensite Transformation in Shape Memory Alloys

The word 'martensite' was first used to describe quench hardened steel microstructures, but is now used to describe a wide breadth of materials that have a variety of crystallographies, properties and growth kinetics [42]. The martensitic transformation is a diffusionless phase transformation from a parent phase to a coherent product phase of the same composition that occurs via the homogeneous shear of the crystal lattice that propagates through the material as a wave [42]. The transformation occurs between the martensite start (M_s) and finish (M_f) temperatures, with the reverse martensite to austenite transformation occurring between the austenite start (A_s) and finish (A_f) temperatures [43]. Martensite formation in carbon steels is not reversible in part due to the large volume change between the phases (Table 2.1), which results in large plastic strains [40]. The introduction of large amounts of plastic strain in martensitic steels results in a transformation hysteresis of hundreds of degrees Kelvin, with A_s being in a

temperature range (i.e. 1003 K (730 °C)) where carbon diffuses rapidly. This results in the supersaturated body-centred tetragonal martensite decomposing into carbides and body centred cubic ferrite before reforming austenite [40].

Table 2.1: Percent volume change between austenite and martensite in NiTi (SMA), CuAlNi (SMA) and an Iron-Nickel-Carbon alloy [44]

NiTi	CuAlNi	Iron-Nickel-Carbon Alloy
0.023 %	0.297 %	-2.586 %

The combination of the nearly constant volume (Table 2.1) and high elastic limit in NiTi enables the elastic accommodation of martensite in the austenite matrix with minimal plastic deformation [44]. This lack of plastic deformation maintains coherency between the phases and enables them to grow or shrink depending on the thermodynamics of the system [42, 44]. The limited deformation causes the hysteresis to be on the order of tens of degrees and not in the range where significant diffusion could impede the reverse transformation [40]. In addition to these critical properties a number of other criteria are required to achieve the unique reversible martensite transformation possessed by SMAs:

- A parent phase with a single low energy state
    - B2 austenite in NiTi
- Multiple low energy product phases (If only 1 variant exists, significant slip will occur)
    - 24 variants can form in B19' [45]
- The ability of the material to form and change microstructures freely
    - i.e. self-accommodation of martensite variants reorientation of these variants, and their relation to the recoverable strain of the shape memory effect [44, 46]

2.3 Ductility of the NiTi Intermetallic Compound

Intermetallics generally possess limited plasticity; however, the NiTi intermetallic can be cold worked up to 60 % [6, 47]. The exact reasons for the ductility of this material are still under investigation [48, 49]. The near stoichiometric NiTi intermetallic exists over a range of compositions meaning it can accommodate local chemical inhomogeneity resultant from 'like' atoms being in contact [50, 51]. Compared to a stoichiometric intermetallic, this makes NiTi less

resistant to diffusion driven phenomena including grain growth, recrystallization, recovery, grain boundary sliding and dislocation climb [52]. Furthermore, the bonds in intermetallics are a mixture of metallic, covalent and ionic bonds [51]. The added constraints of these directional bonds relate to the brittle nature of intermetallics, which increases with a decrease in unit cell symmetry, and with an increase in atoms per unit cell [51]. The B2 strukturbericht CsCl-type cubic crystal structure of the NiTi system (Figure 2.2) has high symmetry and only 1.5 atoms per unit cell. Comparatively, the brittle non-stoichiometric Ti_2Ni unit cell has low symmetry and 96 atoms [53].

Several other important factors contribute to the unusually high ductility of the NiTi intermetallic. The critical stress for dislocation motion of solution treated NiTi is as low as 150 MPa [54]. This low stress is believed to be a result of the low elastic constants c' and c_{44}, with the c_{44} being between 1/3 and ½ that of standard intermetallics [6, 54]. Additionally the elastic anisotropy of the material is as low as 2, where intermetallics can be as high as 10 [55-57]. This low elastic anisotropy ensures that in boundary fracture does not occur, increasing ductility. Finally the martensite phase has 24 variants, numerous twinning and slip modes (Table 2.2), which serve to further increase the ductility of the material. The ductility of the stabilised austenite phase is less than the martensite phase because it has fewer slip and twin modes for deformation .

Table 2.2: Twinning modes of B19' martensite [6]

Twinning Mode	K_1	H_1	K_2	η_2	s (shear)
$\{\bar{1}\bar{1}1\}$ Type I[1]	$(\bar{1}\bar{1}1)$	$[0.54043\ 0.45957\ 1]$	$(0.24695\ 0.50611\ 1)$	$[\bar{2}\bar{1}1]$	0.30961
	$(\bar{1}11)$	$[0.54043\ \overline{0.45957}\ 1]$	$(0.24695\ \overline{0.50611}\ 1)$	$[\bar{2}11]$	0.30961
{111} Type I	(111)	$[\overline{1.51172}\ 0.51172\ 1]$	$(\overline{0.66875}\ 0.33750\ 1)$	[211]	0.14222
	$(1\bar{1}1)$	$[\overline{1.51172}\ \overline{0.51172}\ 1]$	$(\overline{0.66875}\ \overline{0.33750}\ 1)$	$[2\bar{1}1]$	0.14222
{011} Type I[1]	(011)	$[1.57271\ 1\bar{1}]$	$(0.72053\ 1\ \bar{1})$	[011]	0.28040
	$(01\bar{1})$	$[\overline{1.57271}\ 11]$	$(\overline{0.72053}\ 1\ 1)$	$[01\bar{1}]$	0.28040
{011} Type II[1,2]	$(0.72053\ 1\bar{1})$	[011]	(011)	$[1.57271\ 1\bar{1}]$	0.28040
	$(\overline{0.72053}\ 11)$	$[01\bar{1}]$	$(01\bar{1})$	$[\overline{1.57271}\ 11]$	0.28040
Compound	(001)	[100]	(100)	[001]	0.23848
	(100)	[001]	(001)	[100]	0.23848
$\{20\bar{1}\}$[3]	$(20\bar{1})$	$[\bar{1}0\bar{2}]$	$(00\bar{1})$	[100]	0.4250

(1) Lattice invariant strain
(2) Dominant twinning mode
(3) $\{20\bar{1}\}$ deformation twinning mode, which appears under heavy deformation

2.4 Deformation of NiTi

The deformation characteristics of NiTi depend on the phase in which and the temperature at which testing is performed (Figure 2.4) [58]. The modulus, detwinning stress, and transformation stress are all change significantly with temperature. The material can also exist in a mixed phase state between transformation temperatures (i.e. $M_s>T>M_f$, $A_f>T>A_s$), making properties like the elastic modulus a composite of multiple phases [48].

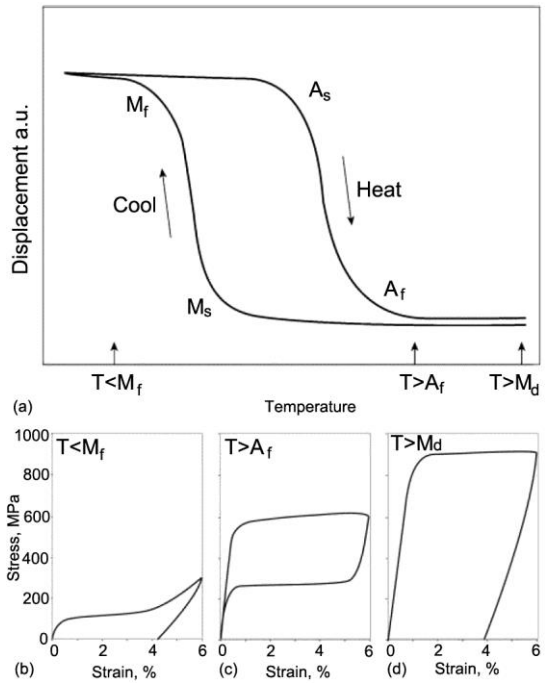

Figure 2.4: a) Displacement-Temperature schematic indicating NiTi transformation temperatures, and monotonic stress strain curves b) below M_f (100 % martensite), c) above A_f (100 % Pseudoelastic Austenite) and d) above M_d (stabilized austenite) the temperature where the stress for slip is below that for stress induced martensite [59]

2.4.1 The Shape Memory Effect

The lattice invariant strain in NiTi martensite is recoverable because it is predominantly accommodated by twinning, and not dislocation motion or stacking faults [60, 61]. This twinning mechanism minimizes lattice strain, dislocation activity and change in system energy during deformation. The twins organize by 'self-accommodation' meaning the twinning across the microstructure occurs in a pattern that minimizes the total increase in energy of the system,

which enables the transformation to be reversible [44]. When a single crystal of NiTi is stressed, the variants that form in the centre of the crystal minimize the energy by accommodating the maximum strain with minimal dislocation activity, while the variants at the crystal boundaries serve to satisfy boundary conditions (i.e. conform to the existing geometry). The two competing requirements results in fine zig-zag deformation patterns [46, 62]. If no load is applied and the transformation is cycled thermally then the self-accommodation of the martensite will cause no macroscopic shape change [44]. The only visible sign that a phase transformation has taken place is the occurrence of surface relief from the deformation of the lattice [63]. The repetitive formation of this surface relief can hasten fatigue crack nucleation [64].

Thermal martensite variants all have the same energy state [44]. When a load is applied the variants rearrange as shown in Figure 2.5 B→C [11]. There is no driving force to return the variants to their original orientation during unloading, so only the elastic strain is recovered as shown in Figure 2.5 C→D [11]. The remaining deformation is recovered upon heating to the single variant austenite phase as shown in Figure 2.5 D→E→F→A→B. This recovery requires rearrangement of the atom to the original configuration [44]. The maximum recoverable strains are limited by texture and loading orientation as discussed in the following sections. Loading to above the maximum strain causes permanent plastic deformation and reduces the possible recoverable strains [44].

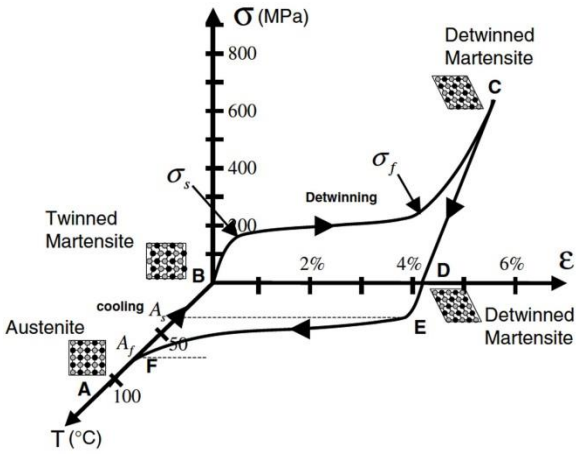

Figure 2.5: Stress-strain-temperature data illustrating the shape memory effect for a typical NiTi SMA [12]

2.4.1.1 Transformation Temperatures

The transformation temperatures are measured either by changes in the electrical resistance (Figure 2.6) or differential scanning calorimetry (DSC) (Figure 2.7) [40, 65]. The transformation temperatures are related to the Helmholtz free energy of the system, with the austenite phase minimizing this energy at high temperatures, and the martensite minimizing it at low temperatures [44]. The equilibrium between the austenite and martensite phases and the resultant transformation temperatures can be altered if either the chemical or elastic strain is changed.

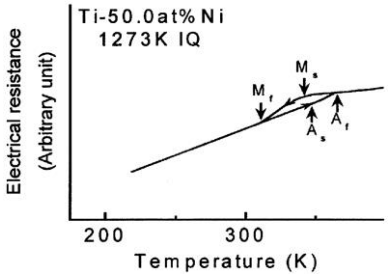

Figure 2.6: Electrical resistance vs temperature curve showing the transformation temperatures of the Ti-50.0at %Ni alloy [65]

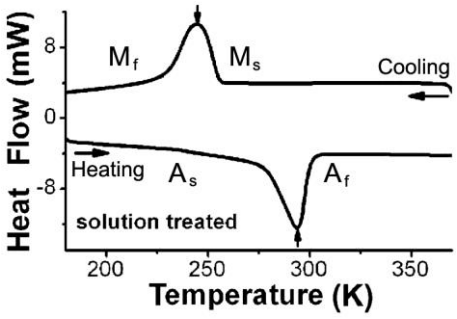

Figure 2.7: DSC curves showing the transformation temperatures of the Ti-50.6at.% Ni alloy [66]

Altering the composition can be done through bulk alloying, or by forming of secondary phases. Work by Tang et al. [67, 68] which was later confirmed and refined by Frenzel et al. [22] (Figure 2.8), compared previously reported M_s temperatures to alloy compositions, showing that a change of 0.1 at.% Ni can result in a 10 K change in the transformation temperature of the material [69]. This variation is much smaller than the compositional tolerances for most engineering materials, meaning NiTi production requires much tighter tolerances resulting in higher costs. Below 49.7 at.% Ni the Ti_2Ni phase forms and consumes the excess Ti in the system, thereby maintaining the composition of the matrix, and ensuring a constant temperature as the Ni content is further decreased [67]. During casting of the alloy undesired additions to the composition such as oxygen or carbon can enter the melt and deplete the system of Ti, thus reducing the transformation temperatures [22, 24]. The transformation temperatures are also affected by the elastic stress, the orientation of the stress, the texture of the material, the thermomechanical treatment history, and thermal or strain cycling [70].

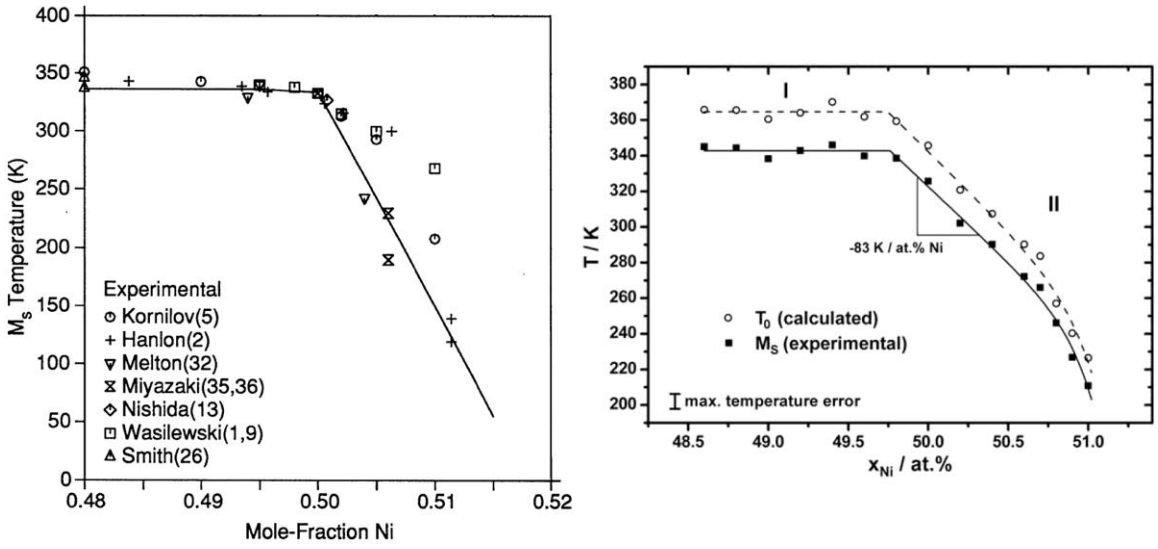

Figure 2.8: Dependence of M_s Temperature on Ni composition of NiTi, left) Tang et al. [67], right) Frenzel et al. [22]

2.4.1.2 Transformation Induced Plasticity

The hysteresis observed between the peaks in Figure 2.7 is a result of the resistance of the microstructure to the motion of the martensitic interface (i.e. internal friction). This internal friction occurs due to the alteration of local stress fields by the presence of secondary phases, and defects in the crystal lattice [71, 72]. This change in the local stress field influences the preferential martensite variants that form in these regions and increases the stress required to reorient these variants to accommodate the passage of the martensitic interface [73].

The complete reversible accommodation of the transformation in these localised regions is not always possible, leading to plastic deformation via dislocation creation and motion in the <100>{011} slip system followed by entanglement with sessile dislocations [72, 74, 75]. This deformation mechanism is called transformation induced plasticity. Transformation induced plasticity can increase dislocation density by two orders of magnitude after only 100 cycles [72, 75]. The resultant microstructure after thermal cycling is banded austenite and retained martensite. The increase in dislocation density in thermally cycled SMAs increases the driving force necessary for phase transformation (i.e. lowers transformation temperatures), may lead to R-phase forming, increases internal friction (i.e. higher critical stress to reorient martensite), and increases the stored elastic energy (i.e. alters the elastic modulus) [76]. When an SMA is

thermomechanically cycled this microscopic build-up of plastic deformation results in a macroscopic plastic strain and decrease in actuation strain as shown in Figure 2.9.

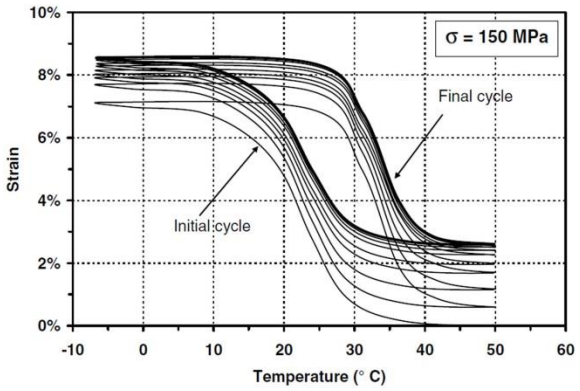

Figure 2.9: Thermal cyclic loading (50 cycles) of a NiTi shape memory alloy wire under constant load of 150 MPa [12]

2.4.2 Stress Induced Martensite and Pseudoelasticity

Elastically straining NiTi adds energy to the system and decreases the driving force required for the martensite transformation (i.e. increases the M_s temperature) [77]. If pseudoelastic austenite exists at the test temperature (i.e. $A_f < T < M_d$) and a sufficient stress is applied then the M_s will increase to the point where the pseudoelastic austenite shears into stress induced martensite (Figure 2.10 B→C). The stress induced martensite transformation propagates in an isostress state (i.e. pseudoelastic) that may have a serrated profile due to the Lüders-like propagation of strain bands across the specimen [78, 79]. Upon removal of the stress, the transformation temperatures will decrease and the stress induced martensite will transform back into pseudoelastic austenite (Figure 2.10 D→A). The critical stress for slip of the material must be above the critical stress for stress induced martensite (i.e. Figure 2.11 A); otherwise the material would plastically deform before stress induced martensite formed (i.e. Figure 2.11 B) [80]. As discussed previously, the temperature at which the stress for slip is less than the stress for stress induced martensite is called the M_d temperature and is indicated in Figure 2.11. Above M_d (Figure 2.11) the austenite is mechanically stable and behaves like a standard elasto-plastic material as was observed in Figure 2.4 [80]. Solutionized NiTi generally displays little to no PE properties and

requires strengthening via cold work, grain refinement, and precipitate formation to exhibit these properties [6].

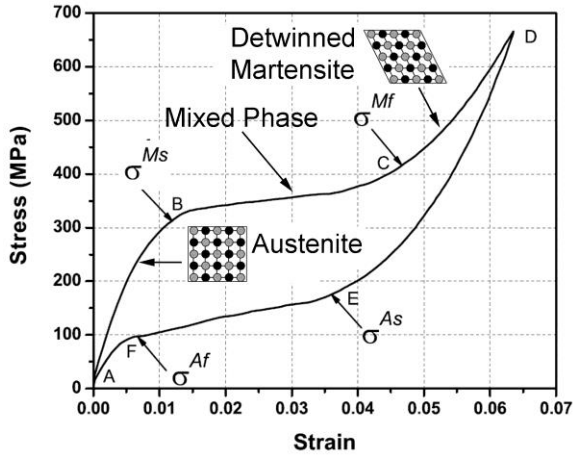

Figure 2.10: Standard tensile stress-strain curve of PE austenite [12]

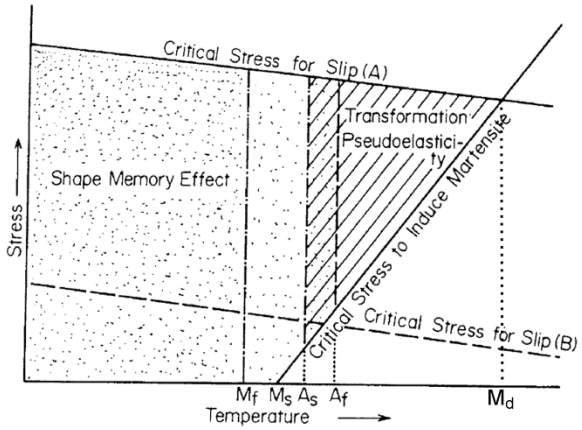

Figure 2.11: Schematic diagram representing region of shape memory effect and transformation pseudoelasticity in temperature-stress coordinates; (A) represents critical stress for slip for case of high critical stress and (B) represents critical stress for slip for [80]

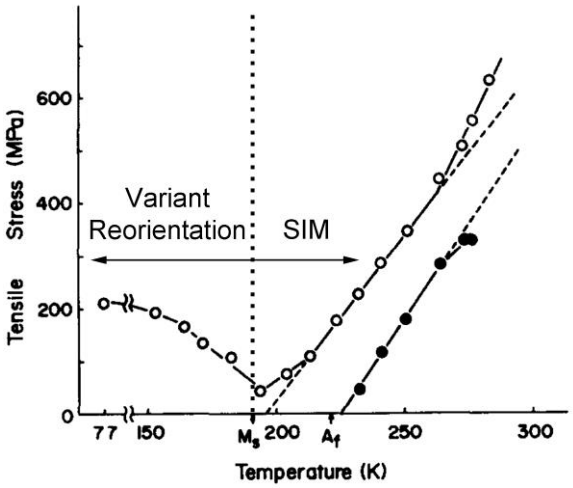

Figure 2.12: Critical stresses as a function of temperature for: open circles) inducing stress-induced martensite (SIM) ($T>M_s$) and for detwinning thermal martensite ($T<M_s$), closed circles) Reverse SIM transformation [81]

The stress at which pseudoelastic austenite forms stress-induced martensite increases as the test temperature is increased above the M_s because a greater elastic energy is required to overcome the increasing temperature differential. The increase in stress has a linear relation with temperature (Figure 2.12) for which the most useful model is the Clausius-Clapeyron relation shown in Equation 2.1 [82]. Where $d\sigma$ is the change in the stress required for stress-induced martensite, dT is the change in test temperature, σ is the uniaxial applied stress, ΔH^* the enthalpy of transformation per unit volume, ε the transformation strain, and T is the temperature. In this equation the transformation from parent to product phase is negative. The left side of the equation is the rate of change of stress with respect to the temperature which changes with material processing method and is generally between 3 and 20 MPa $°C^{-1}$ [58].

$$\frac{d\sigma}{dT} = -\frac{\Delta H^*}{\varepsilon T} \tag{2.1}$$

During the forward and reverse stress-induced martensite transformations the material releases and absorbs heat respectively due to the exothermic and endothermic nature of the transformations [83]. This effect can change the material temperature in turn changing the stress-

induced martensite plateau stress [83]. The detwinning stress of thermal martensite is a thermally activated process, so the stress for detwinning increases with decreasing temperature as shown in Figure 2.12 [6]. The presence of the R-phase results in additional intermediary detwinning of stress-induced martensite features in the stress-strain curves as shown in Figure 2.13.

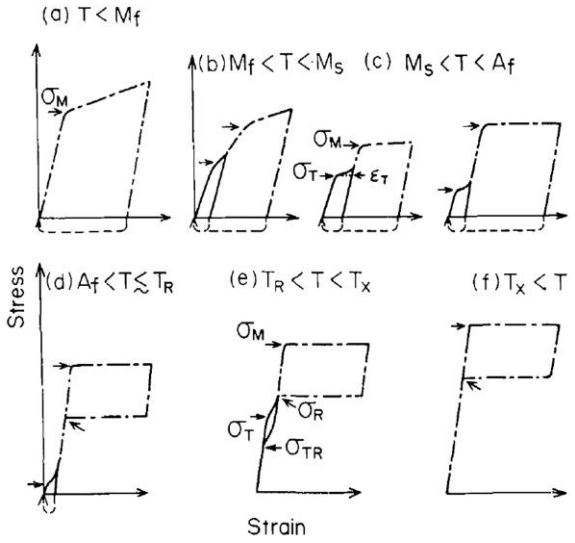

Figure 2.13: Classification of stress-strain curves according to test temperatures for Ti-Ni alloys. a) B19' shape memory effect (SME), b) B19' and R-phase SME, c) R-phase SME and non-recovered stress induced martensite (SIM), d) Recovered SIM and R-phase SME, e) SIM and R-phase SIM, f) SIM [84]

The hysteresis observed between the forward and reverse stress-induced martensite plateaus is related to the same internal friction effects encountered in thermally cycled SMAs as discussed in the previous section. However, in the case of successive tensile cycling the critical stress for stress-induced martensite is reduced as shown in Figure 2.14. As was the case with thermal cycling the forward stress-induced martensite transformation ($M_s \rightarrow M_f$) experience a greater reduction that the reverse ($A_s \rightarrow A_f$), resulting in a reduction in the hysteresis after cycling. It is hypothesized that this reduction in stress and hysteresis occurs because dislocation networks created by prior deformation and the stored elastic strain enable easier transformation of preferred variants during successive cycles [85, 86]. This effect may be the cause of a particularly interesting aspect of the pseudoelastic the material; its ability to 'remember' the deformation history [48]. If a torsional load is first applied, and then a uniaxial tensile load

applied, upon removal of the loads the material will first recover the tensile strain and second the torsional strain as shown in Figure 2.15 [87]. The reasons for this effect are hypothesized to be related to the reorganization of the dislocation networks; however this remains to be proven [87]. Recent investigations have proposed that the dislocation networks that evolve in the microstructure alter the transformation from a wave propagating across the material, to a uniform transformation occurring throughout the material [88].

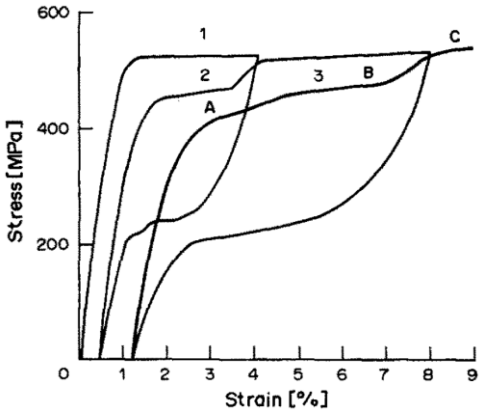

Figure 2.14: The underaged NiTi wire is prestrained twice: curve 1 shows the first prestraining to 4 % and curve 2 shows the second postponing to 8 %. A deformation (heavy line) then exhibits two yield drops (A and B) before the original flow stress is achieved (C) [85]

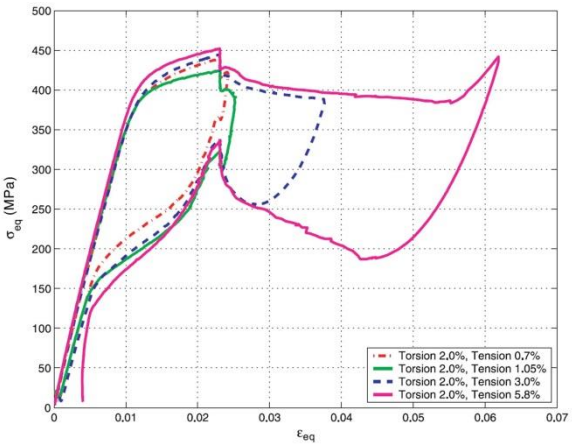

Figure 2.15: Equivalent stress–strain plots in torsion (2 %), followed by tension (0 %, 0.7 %, 1.05 %, 3 %, 5.8 %) and reverse unloading (Type II) [87]

2.4.3 The Two-Way Shape Memory Effect

The two-way shape memory effect achieves a change in shape during both the heating and cooling cycles. There are a number of methods used to train an SMA to exhibit the two way shape memory effect, including the introduction of dislocations, formation of preferentially oriented precipitates, thermal cycling, and constrained aging [6, 19]. The first method uses the dislocations formed during severe plastic deformation of the martensitic phase to inhibit full shape recovery during transformation to the austenitic state [19]. The presence of these dislocations during the reverse transformation leads to preferential formation of certain martensite variants which results in the material possessing a two-way shape memory effect [19]. The other methods of achieving the two-way shape memory effect alter the microstructure to

achieve the same effect. The two-way shape memory effect can achieve approximately 2 % recoverable strain, however the actuation strain degrades and the plastic strain can substantially increase as cycling progresses and the microstructure evolves [6, 89]. This degradation can be greater than 5 % plastic strain under stresses as small as 100 MPa; furthermore, significant degradation in the actuation occurs under stress-free thermal cycles, which limits the applicability of the two-way shape memory effect for high precision devices [89]. The methods used to cause the two-way shape memory effect are also used to 'train' actuators so that they are stable for the load and strain of a specific application as will be discussed in Section 2.5.2.

2.4.4 Texture Dependence of Deformation

Single crystals of NiTi have anisotropic properties with different moduli of elasticity, strain reversibility, slopes and hysteresis of stress-induced martensite when loaded in different crystallographic directions [90]. The recoverable tensile strain can vary from 3 % in the <100> direction to 10.5 % in the <111> direction (Figure 2.16) [4]. The unidirectional nature of shear strain on the habit planes contributes to this anisotropic, asymmetric deformation [91]. In addition, the orientation of the crystal with respect to the load affects twinning, which influences the anisotropy of stress-induced martensite [92].

In a polycrystalline material the grains are joined at the grain boundaries and need to move together while maintaining a continuous displacement across the grain boundaries [44]. When the boundary is parallel to a tensile load it is similar to a single crystal deformation; however, when it is perpendicular to a tensile load it exhibits a complex deformation that is brittle [93, 94]. Triple junctions are more complicated; requiring the formation of complex twin microstructures to accommodate strain, thus restricting the deformation in these regions [44]. The restrictions imposed by the grain boundaries and multiple grain junctions can lead to localized plasticity even at macroscopically low stresses [44, 46].

When polycrystalline NiTi is loaded grain boundary variants maintain the strain between grains, while variants in the grain interiors arrange to enable the greatest overall strain of the material, with neighbouring grains competing for preferential deformation [44]. The anisotropic properties of a single NiTi crystal make the deformation characteristics of a polycrystalline material highly

dependent on the texture. The material properties, including the elastic modulus, the yield stress, ductility, work hardening, the transformation stresses and hysteresis, transformation strains and recoverable strains can all change depending on the texture and the orientation of the load with the texture [95-98]. An example of this anisotropy is the difference of martensite deformation in tension and compression shown in Figure 2.17. The grains in this example were oriented such that they provided more recoverable modes of deformation in tension than in compression. The tensile specimens had pseudoelastic recovery but the compressive specimens did not; only the elastic stain was recovered [99-101].

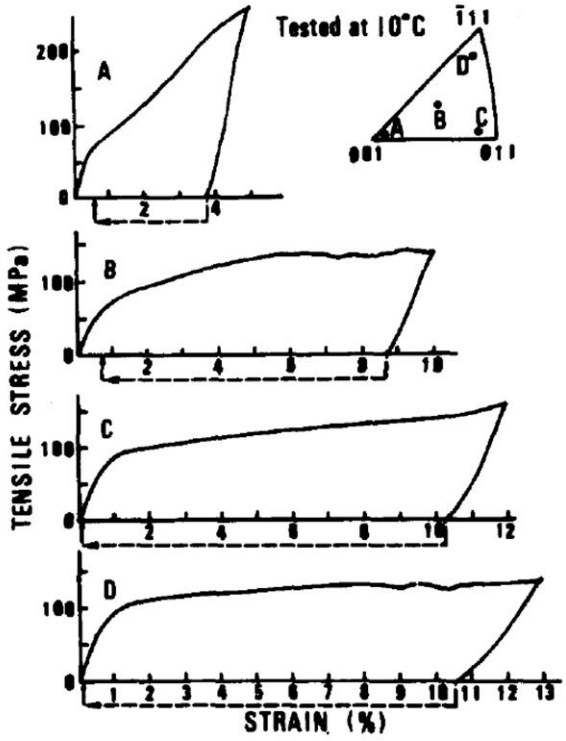

Figure 2.16: Orientation dependence of the recoverable strain of a single crystal in A) the <001> direction, B) a mixed texture, C) the <011> direction, D) the <111> direction. Deformed below A_s and then heated above A_f [4]

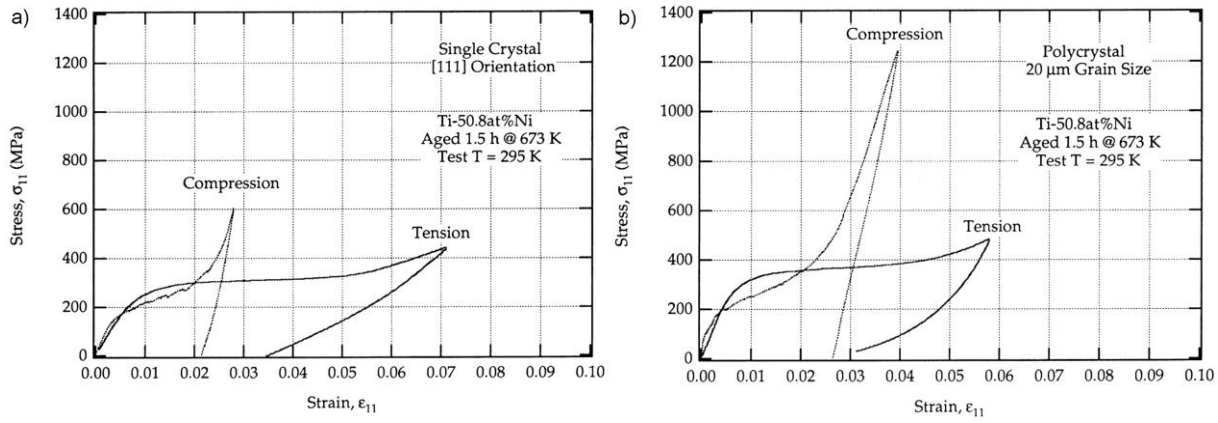

Figure 2.17: Tensile and compressive stress-strain curves for peak-aged NiTi (1.5h at 673 K): a) [111] orientation, b) polycrystal (with <111> texture) [100]

Material texture depends on the processing route with tubes, sheets, rods, and different sizes of these forms all having unique textures which are not significantly altered by heat treatments [102]. Uneven distribution of stress throughout the textured microstructure can lead to unpredicted localisation of strain, and in turn unexpected fatigue failure [103]. This dependence on texture can lead to significant issues when cutting a component out of a textured material, for example when a stent is laser cut from NiTi tubing [103]. Luckily the texture of drawn NiTi wires is in the <111> direction which is the direction that has the largest recoverable strains [104]. This enables polycrystalline NiTi wires to have between 5.5 % [105] and 8 % recoverable strain, depending on the processing route [81].

2.5 Fatigue of Shape Memory Alloys

Thermal and mechanical fatigue testing of NiTi material has been conducted for more than 40 years but has not resulted in a universally applicable constitutive model [59]. Initial testing in the 1960s-1980s was done with substandard material purity and processing methods (i.e. grain size ~100μm) so the conclusions of these investigations are not applicable to modern day manufactured materials (i.e. grain size <1μm) [59, 86, 106]. To make matters worse, much of the current research is proprietary and unpublished [59]. The published results of thermal or mechanical cycling of SMAs are often contradictory, and more emphasis is required to relate the

microstructural and bulk mechanical properties to develop adequate quasi-static models and evolving material fatigue models [107].

Classical fatigue models assume a stable microstructure throughout the life of the material [108]. This assumption does not hold with SMAs, which have significant variation in microstructure and thus bulk properties -primarily the reorientation of thermal martensite and the formation of stress-induced martensite - that change as fundamental variables of fatigue testing (i.e. stress, strain, and temperature) are changed [108]. The fatigue behaviour differs substantially depending on what phase is stable; thermal martensite, pseudoelastic austenite, a mixed phase (i.e. between M_s and M_f or A_s and A_f) or stable austenite [108]. The presence of precipitates, inclusions, other defects and their effect on the evolution of transformations further complicates the modelling of the material behaviour [6]. The dependence of the material behaviour on the crystallographic texture and the loading path make simple tension-compression cycling difficult to model, with multi-axial loading being poorly understood, and modelled with minimal success [87]. Recently synchrotron micro-X-ray diffraction has been used to separate elastic and transformation strain during cycling, which can be used to develop a fundamental understanding of the evolution of the NiTi microstructure during mechanical and thermal fatigue cycling [103, 109]. This is required for the modelling of NiTi with traditional FEA stress computations, and describing the evolution of the material [109]. The combination of these noted issues results in the fatigue behaviour of a specific material and testing parameters being applicable only to this specific case [59]. This means that no generic S-N or ε-N curves can be produced for NiTi, only application specific curves [110]. This results in the costly requirement of fatigue testing each application [111-114]. This is an acceptable increase in cost with pseudoelastic applications that can be cycled at relatively high frequencies (e.g. 50 Hz) [115]. Shape memory effect cycle frequencies are usually in the sub-Hz range, which can lead to testing time of over one year and be an impediment for any companies interested in entering the market with an SMA actuating device [59].

Further impeding the studies of these materials is the lack of standards describing how fatigue testing for either pseudoelastic or shape memory effect materials should be performed and analysed [116]. This has resulted in every lab developing their own testing and using various

analysis methods, making comparison between results difficult. If standards were developed they could help accurately compare the fatigue lives of materials offered by different manufacturers, a number of whom make substantial claims (e.g. 4 % actuation strain for 100,000 cycles) and until recently offered little evidence to back up their claims [117-119].

2.5.1 Mechanical Fatigue of Shape Memory Alloys

The majority of work in fatigue of SMAs has been focused on pseudoelastic alloys because of their much earlier adoption into industry than their shape memory effect counterparts [59]. The focus of this thesis is thermomechanical fatigue, but due to the lack of literature in this area, a thorough review of mechanically induced fatigue of NiTi is useful. Pseudoelastic materials are tested in a similar manner to other materials: by mechanically straining with methods such as rotation-bending fatigue, bending fatigue or hydraulically actuated tension/compression fatigue [59]. Tension-tension testing of NiTi is known to have the lowest life compared to bending or rotation-bending fatigue, because the continual crack growth, and a maximum volume of cross section is subjected to maximum strains, as opposed to the partial tension and compression of the other methods [59, 120].

2.5.1.1 Stress Life

The stress in NiTi is only related to the strain while in the limited elastic strain regions. In the plateau regions the strain increases while the stress remains constant. This makes the S-N analysis of total fatigue life less meaningful than the ε-N analysis. Use of the S-N method has erroneously found the fatigue life of pseudoelastic austenite greater than thermal martensite at 400 MPa, not because of the superiority of the material but because the strain in the austenite was only 2 % while that of the martensite was 9 % [121]. Similar conclusions were made when increasing the test temperature, which saw an increase in fatigue life, but this was resultant from the increase in modulus and critical stress for stress-induced martensite which reduced the strain amplitude of the test [58, 122]. There has been no study relating S-N and ε-N effects with significant conclusions. Only one study has ever related the three major failure analysis methods (i.e. S-N, ε-N, and damage tolerant approaches), and this was performed by the pioneering investigators Melton and Mercier [121, 123]. They used substandard material and did not compare microstructural effects; which can be significant considering that after only 10 cycles

retained martensite has been observed due to permanent deformation in the microstructure [86, 106, 124, 125].

2.5.1.2 Strain Life

The majority of pseudoelastic NiTi fatigue studies are conducted with the strain-life method, which allows control of the ratio of martensite and austenite [59]. When testing at zero-mean stress, thermal martensite had the highest fatigue life of all the microstructures (i.e. martensite, pseudoelastic austenite, mixed phase, stable austenite) for equivalent strain values because the stress for detwinning martensite is much lower than that needed to from stress-induced martensite [126, 127]. Pseudoelastic austenite fatigue lives were longer when the test temperature was closer to A_f because the stress for stress-induced martensite was lower [128]. Long fatigue lives (e.g. 10^6) required cycling only in the elastic region with a constant phase fraction, in which case typical fatigue damage accumulation occurred [113, 129]. Dislocation free transformation between austenite and martensite is required for a high cycle fatigue life, but the high shear strain typical of the transformations leads to dislocation creation even under zero-load conditions, making high fatigue life of pseudoelastic phase transformations impossible [108]. Cycling between martensite variants, or between austenite and martensite led to shorter fatigue lives because of the increase in plastic deformation. Strains typical of low fatigue life pseudoelastic austenite are significantly higher than standard materials measuring 10 % at 1000 cycles compared to 1 % or less of standard materials [121]. The stable austenite phase had the lowest fatigue life because a limited number deformation routes are available to accommodate the strain. When cycling between the linear elastic region into the stress-induced martensite plateau the deformation is related to the Coffin-Manson region [130, 131]. The formation of stress-induced martensite and not plastic deformation results in the inability to directly compare this material using this method.

Many applications experience non-zero mean strain, such as cardiovascular or gastrointestinal stents, which use interference fits with the surrounding biology that leads to strain in the pseudoelastic plateau [111, 132, 133]. When cycling with non-zero mean stress it was found that increasing the mean strain did not always lead to a reduction in the fatigue life; leading to the conclusion that the Goodman and Soderberg constructions [134, 135] are not valid for NiTi [113,

129]. Increasing mean strains in pseudoelastic austenite into the middle of the stress-induced martensite plateau saw an increase in the strain amplitude that reached 10^6 cycles [75, 112, 114]. When in the stress-induced martensite plateau the strain amplitude is the major contributor to fatigue life of pseudoelastic austenite and not the mean strain. Multi-axial deformation of NiTi is poorly understood and there is very limited work on multi-axial fatigue [136].

2.5.1.3 Damage Accumulation, Crack Growth and Fracture

There are few studies that use damage tolerance analysis, mainly because of the dimensionally small sizes (e.g. 0.2mm stent strut) of medical industry devices [133]. Crack initiation in these small components can be difficult to measure, and failure could occur in only hours or days after nucleation [137]. Therefore, emphasis has been placed on control of crack nucleation instead of crack growth. Small cracks are theorized to have much lower crack initiation and propagation resistances, but there is no reported data on small crack measurement [138]. This makes it impossible to currently use the damage tolerant method for product life prediction. Total life analysis is deemed acceptable in components that have critical crack lengths below 15-50 μm, above which parts are rejected [138]. New applications in areas including aerospace and orthopaedics have large cross sections in which cracks may have stable growth before failure; in which case damage tolerance analysis may be beneficial.

Fatigue crack growth in NiTi is dependent on the phase. The high ductility of thermal martensite resulted in the stress intensities (i.e. ΔK_{th} from the Paris law) required for crack initiation being the highest compared with the other microstructures, and it having the best growth resistance [139, 140]. The stress intensity and growth resistance decreased as the temperature increased through the pseudoelastic austenite phase with the lowest values being for stabilized austenite due to its limited deformation mechanisms [139, 141]. Normalizing the stress intensity factors with the modulus enables evaluation of the strain intensity range revealing that the materials have similar crack growth rates to other biomedical materials like titanium or stainless steel [142]. The stable crack growth rate exponent m = 2.5 was shown to be independent of the specimen thickness, geometry, the loading (R) ratio and the phase of the material [121, 139, 141-143]. Increasing R (i.e. tension-tension testing) led to lower fatigue thresholds. Testing specific product forms is required to evaluate crystallographic texture issues, which affect the fracture

initiation point and direction [115]. The crystallographic texture, component geometry and loading direction affect the direction of crack growth and the deformation around the crack tip [144]. Synchrotron X-ray diffraction has revealed that the traditional peanut plasticity zone found in linear-elastic fracture mechanics models is not found in NiTi; rather, the texture of the surrounding grains determined suppression of or transformation of the surrounding grains [144]. Most important to note is that the build-up of plastic deformation is a necessity to resist crack growth in NiTi [143]. A fully cold worked material needs to be annealed or the residual stress will lower the stress intensity and cracks will initiate earlier [143].

There are only six studies in fracture toughness, and of these only one had a specimen thickness significantly larger than the plastic zone [115, 140, 145-148]. The results are potentially erroneous; however a few conclusions can be made from the work. Steady state fracture toughness can vary across product forms and microstructures; however, the fracture toughness for both martensite and pseudoelastic austenite were measured to be approximately 30 MPA $m^{1/2}$ [115, 140, 145-148]. This is due to the formation of stress-induced martensite at the crack tip in pseudoelastic austenite, meaning the crack is growing through the same microstructure (i.e. martensite) in both cases. The adiabatic heating observed during these transformation, was found to have little effect on the crack growth kinetics [115, 149-151]. Above M_d in the stabilized austenite phase, where the crack propagates through austenite the fracture toughness increased to 53 MPa $m^{1/2}$ related to the increase in yield strength [148].

Fractography of NiTi fatigue specimens is very similar to standard metals [115]. Martensite and pseudoelastic austenite fracture surfaces are similar because failure occurred through the martensite as mentioned above. The crack propagation is texture dependent and branches in a tortuous path dictated by the microstructure [115]. Cracks formed preferentially at near surface inclusions or other stress risers such as precipitates, oxide or carbides and wire drawing striations [145]. If these inclusions were below the critical flaw size (i.e.15-50um) they were proven to not affect the fatigue life of the material [126, 138]. The fracture surface of low and high fatigue specimens are very similar, with a small crack propagation region and large ductile overload failure region [127]. This signifies that the majority of fatigue cycles are in crack initiation and

not propagation [127]. In high cycle fatigue specimens the fatigue striations are worn, absent or require high magnification to view.

2.5.2 Thermomechanical Fatigue of Shape Memory Alloys

Thermomechanical fatigue testing is generally performed by applying a constant or linearly varying (e.g. weight or spring) stress or strain to a material and thermally cycling between martensite and austenite until failure. Fatigue failure of SMAs can be by fracture, but failure can also include the change in physical and SMA properties that may lead to the component no longer performing as required (i.e. reduction in actuation strain) [107].

There is limited published work in the thermomechanical fatigue of SMAs and there is no comprehensive review of this field. Most investigations reported as 'fatigue' only observe a few cycles (e.g. 10-1000), partly due to the testing frequencies of 0.05 Hz and below, because of limitations of heat transfer upon cooling [152-155]. Actuation frequency has recently been increased by decreasing the diameter of the wire, but these innovations require a higher grade material for acceptable fatigue lives [119]. The first investigations of thermomechanical fatigue were performed on coiled springs, which had significant strain (i.e. 3 %) for very high cycle lives (i.e. 10^8 cycles); however the difference in geometry makes comparison to linear wire actuators difficult [106, 156]. Most thermal fatigue investigations focus on the stability and plastic build-up in the two-way shape memory effect, but these were generally done with little to no load applied [89, 157]. In the limited thermomechanical fatigue investigations of loaded thermal cycled failure of SMAs, a large number investigated ternary or off-chemistry NiTi alloys (e.g. NiTiCu or $Ni_{60}Ti_{40}$), which are incorporated into the following review [153, 154, 158].

Transformation induced plasticity is limited in thermomechanically cycled NiTi by microstructures that have a nanocrystalline microstructure and strengthening Ni_4Ti_3 precipitates [159-163]. Higher annealing temperatures result in larger grained microstructures that are less resistant to dislocation motion. These microstructures can have longer lives as shown in Figure 2.18, because a greater number of cycles are required for dislocations to pile up and cause cracking [143, 153]. The higher dislocation activity reduces transformation strain and increases

plastic strain compared to smaller grain microstructures (i.e. lower heat treatment temperatures) as shown in Figure 2.19 [163].

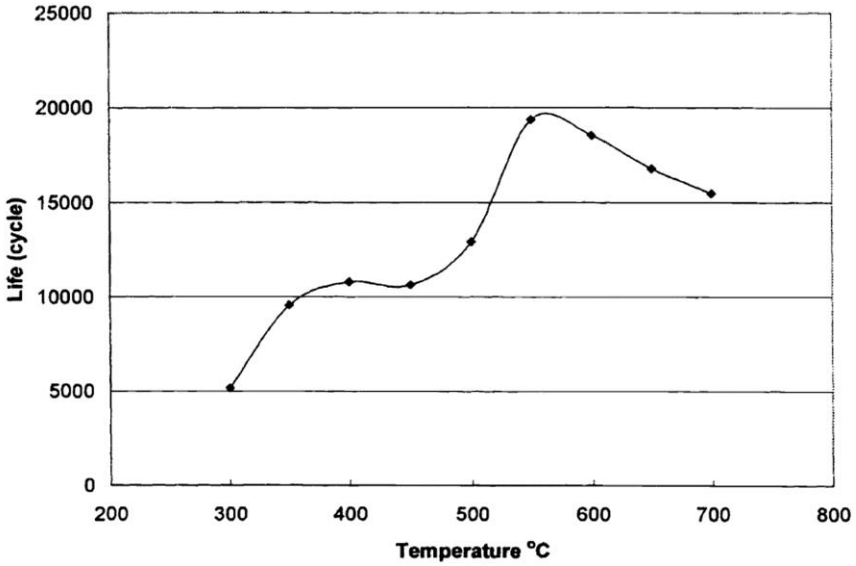

Figure 2.18: Fatigue life of TiNiCu alloy annealed at various temperatures for 15min [153]

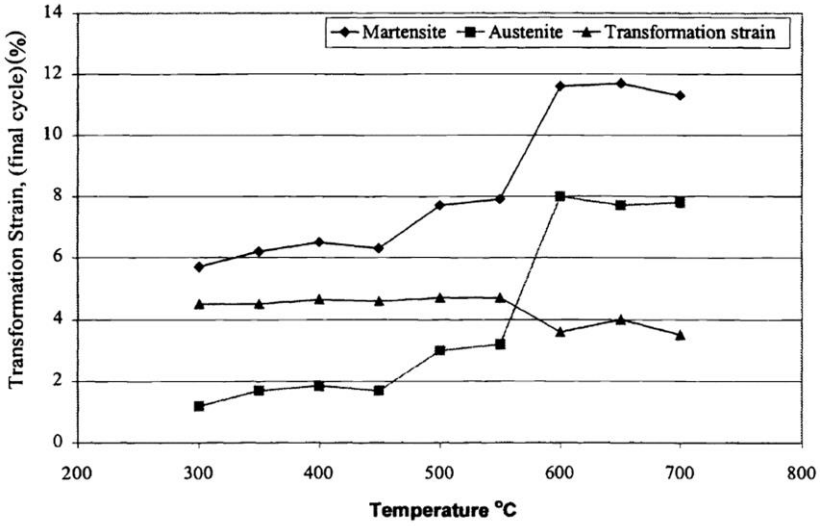

Figure 2.19: Influence of annealing temperature on transformation and plastic strain development [153]

Even with the optimized microstructure, accumulation of plastic strain is significant in the initial thermomechanical cycles, so the properties must be stabilized (i.e. trained) before use in an actuation system [152, 164, 165]. As the initial plastic strain is increased, it becomes more

difficult to cause further plastic deformation and the material will stabilize with a lower rate of increase in plastic strain [72, 74, 125]. The 'training' of an SMA involves artificially inducing plastic buildup before putting the SMA into service, which is usually done by cycling an actuator for a number of cycles at higher stresses than the application [166, 167]. The training increases the fraction of martensite variants preferentially oriented in the trained direction, with dislocation structures formed to maintain the stability of these variants [168, 169]. Other methods of training include thermal cycling slightly above the martensite yield stress, or applying a load and constraining motion while thermally cycling [108, 157, 161]. The improvement in stability after training can be shown in Figure 2.20, where RS is the recovery strain and RD is the remnant deformation. This training was initially investigated for creating the two-way shape memory effect [170, 171]. Similar to the 'training' the use of intermittent overload cycles can improve the fatigue life of an actuator because of beneficial plastic hardening [172].

Functional and fatigue properties of SMAs are highly linked to the stress-strain-temperature relationship of a specific application [108, 152, 158, 166, 173]. Practical actuation applications are limited to 200-300 MPa and 2-4 % strain due to fatigue life issues. Plastic deformation is higher at higher stresses, but within the mentioned range there is little effect on the fatigue life (Figure 2.21).

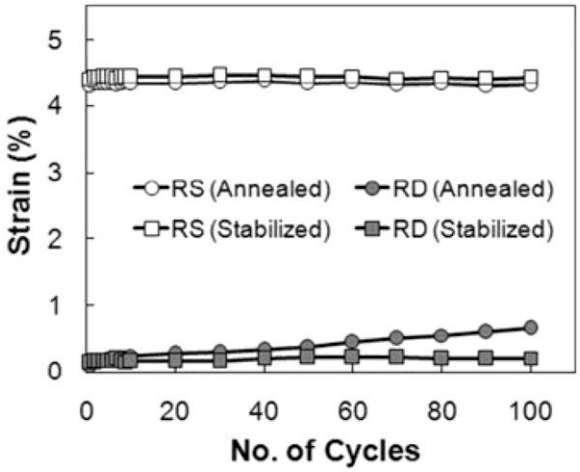

Figure 2.20: Strain versus number of cycles plot upon of NiTi SMA wires under a stress of 200 MPa before and after stabilization treatment [159]

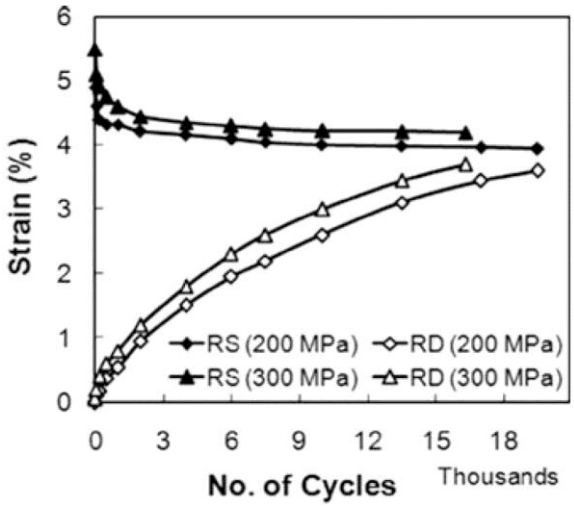

Figure 2.21: Strain versus number of cycles plot of NiTi SMA wire at 200 and 300 MPa [159]

Fatigue life reduces with increasing strain; doubling actuation strain reduced fatigue life by more than half as shown in Figure 2.22. SMA fatigue life is also very sensitive to overheating. Increasing the maximum test temperature by only 10 K can reduce the fatigue life by over 50 %, and increasing from 10 K over A_f to 40 K over A_f decreased fatigue life by almost 75 % (Figure 2.23). Partially transforming (mixed phase) results in a much higher fatigue life than fully transforming [158, 161, 173]. With partial transformation there is very little plastic buildup because the martensite transformation is for the most part accommodated elastically, as opposed to full transformation which will have a comparably large amount of plastic deformation resultant from the transformation of poorly aligned variants [157, 174]. Of the three control parameters (i.e. stress, strain, temperature) the fatigue life has the highest sensitivity to overheating, so actuator heating must be controlled precisely.

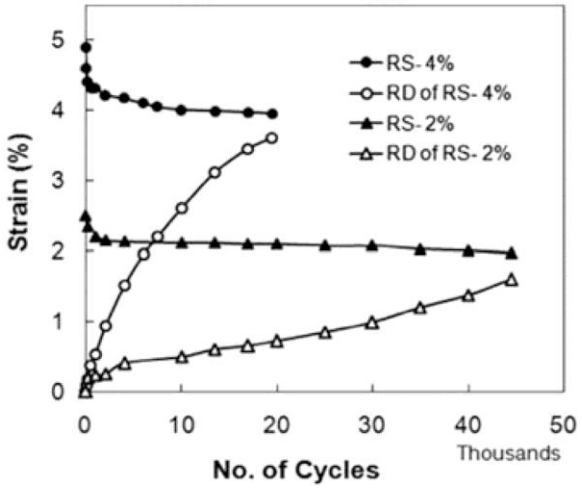

Figure 2.22: Strain versus number of cycles plot of NiTi SMA wire at 200 MPa with actuation strain (RS) at 2 and 4 %. RD is residual strain [159]

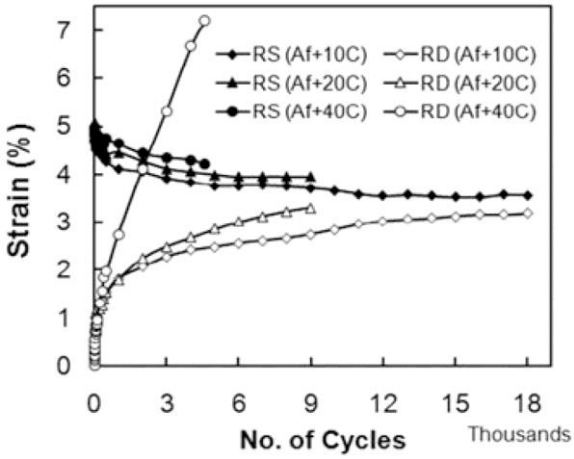

Figure 2.23: Strain versus number of cycles plot showing fatigue life as a function of Tmax in the wire; conducted at a stress of 200 MPa [159]

When thermally cycling via joule heating a resistance feedback loop can be used to detect the transformation temperature of the material [175]. Stopping heating after the transformation is detected can lead to an order of magnitude increase in the fatigue life [176]. This feedback loop can also be used to control the amount of transformation (actuation). Current pulsing with a ramp up and down instead of a square wave has been shown to increase the stability of an actuator [177]. Heat input can be further reduced by the use of electrically conductive coatings [178].

The heating of NiTi wires by current leads to interlinked cracks forming in the core of the wire (Figure 2.24), which affects the fatigue life of the wire [179]. These cracks form as a result of strain inhomogeneity due to temperature inhomogeneity across wire cross section. The formation of these cracks increases the temperature inhomogeneity (i.e. increased local resistance) and accelerates the damage. During cycling, the brittle oxide layer on the outer diameter of the wire cracks in many places [154]. These and other defects serve as crack initiation points, with final fracture being similar to what is observed in mechanical fatigue of NiTi, but the surface cracks and internal cracks may merge and reduce the life of the part [108, 158].

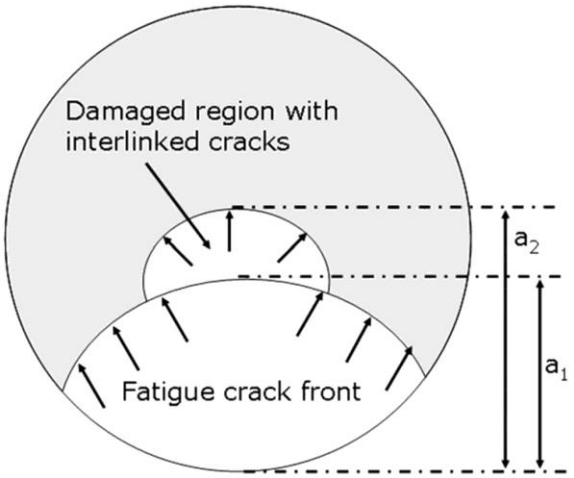

Figure 2.24: Schematic representation of a propagating fatigue crack interaction with the damaged core region; a1: fatigue crack depth, and a2: effective crack depth after interaction with the damaged zone. [179]

The thermomechanical fatigue of NiTi is a function of the stress, strain, material processing, and percent transformation. The maximum fatigue lives reported in academic literature range from under 1.5 % actuation strain at 80 MPa stress for 100,000 cycles, to 4 % actuation strain at 109 MPa for 500,000 cycles [173, 180]. The stresses for the corresponding actuations of the above studies are significantly lower than what is reported by industry which one manufacturer achieving 3.5 % actuation for 120,000 cycles at 200 MPa with only 0.3 % plastic deformation and another achieving an astounding 10^6 cycles with 1% actuation at 350 MPa and less than 0.2 % plastic deformation [118, 119]. The results from the latter report are summarized in Figure 2.25. It is important to note that these results are under ideal actuation conditions; which likely will not be present in application, or may require a complex control system.

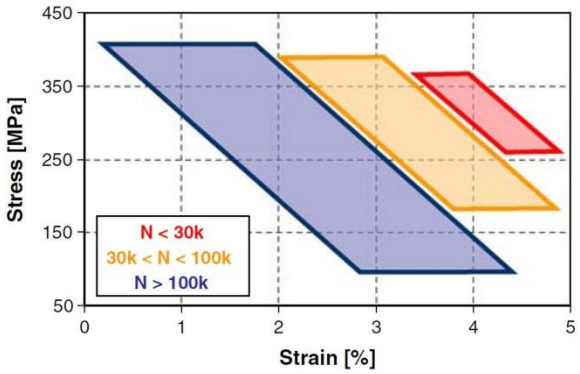

Figure 2.25: Fatigue lifetime for Smartflex 76 under different stress-strain conditions [119]

2.6 Manufacturing of Shape Memory Alloys

The manufacturing of NiTi SMAs is not a trivial task [181]. With the modern day technology in use it is still common to receive material with widely different transformation properties from what was specified, or even within a single component (e.g. a pseudoelastic sheet containing pseudoelastic and shape memory effect properties). Inability to provide custom defect-free components is also an issue in this field. A review of the manufacturing processes is useful to design both laser processing, and post-laser processing thermomechanical treatments for optimal material performance.

2.6.1 Refining and Casting NiTi

The extreme sensitivity of NiTi to the chemical composition makes contamination a potential cause of loss of production [181]. Raw materials and alloying methods must be chosen to minimize impurities. Ni and Ti are not found in nature in their metallic form, and the ores require costly refining processes (e.g. the Van Arkel de Boer, and Kroll-reduced processes) in order to produce the 99.99 % pure titanium sponge, and 99.94 % electrolytic nickel used to make NiTi [69, 182]. VIM and vacuum arc re-melting (VAR) are of similar cost and both suitable to produce ingots with the inclusion size and density lower than the ASTM F2063 standard. These are the two main furnace melting processes used to make NiTi ingots, providing a transformation temperature control of ±5 °C [69, 126, 182]. The induction coil heated graphite crucible of the VIM process contaminates the melt with C (i.e. 300-700ppm C), but the ingots have excellent homogeneity due to mixing by eddy currents [181]. The contamination can be minimized by

coating the graphite crucible with the Ti bars/disk to create a TiC diffusion barrier, reducing the time the ingot is molten, and running consecutive ingots [28, 183]. The VAR process uses DC current to melt a compacted Ni and Ti electrode into a water-cooled copper crucible and results in much less contamination because the melted region is not in contact with the crucible [69]. This lack of complete melting causes inhomogeneity in the ingot that is rectified by flipping over the ingot, or even cutting it up and re-melting it several times, but this adds cost and risk of atmospheric contamination [181]. The combination of the two processes in the VIM/VAR process is used to get a higher purity VAR ingot in the initial melt and the homogeneity of the VIM process after the second melt [181]. After casting the ingots are commonly solutionized to ensure homogeneity [184].

There is a push by industry for smaller cross section components and very fine wires, for medical applications and fast actuation [185, 186]. In these small components the ASTM F2063 standards for inclusion size are no longer acceptable because the defects consume a much larger area of the cross section. Greater purity ingots are needed for these next generation NiTi components [185, 186]. High purity VIM and VAR methods have been developed to serve this need [31]. E-beam vacuum melting has also been used to prepare high purity NiTi alloys (i.e. 0.007 %-0.016 % C for E-beam, vs 0.04 % to 0.06 % C for VIM), and there is an effort to scale up the current production size which is currently limited to 2kg [187-189]. Obstacles in the use of this technique include the difficulty in controlling the composition due to Ni evaporation during E-beam melting.

2.6.2 Bulk Material Deformation

As-cast NiTi has poor ductility, limited SMA properties and poor fracture resistance properties [69, 181, 190, 191]. Further processing is required for acceptable stability, and fatigue. Post-casting processing includes hot working, cold working, heat treatments, joining, machining, and surface treatments. The most common final products are plates, sheets, tubes, ribbons and wires. The most prevalent form of NiTi is wires, which are cold drawn. This review will focus on the manufacturing requirements for wires. The following sections will detail the requirements.

2.6.2.1 Hot Work

Hot working NiTi brings the material closer to the final product form and changes the microstructure [181]. Hot working of NiTi is done in the range of 300-900 °C, with significant softening occurring near 400 °C and 100 % elongation possible at 900 °C due to the reduction in critical flow stress with increase in temperature [192-194]. Degradation of material due to oxidation can occur at the higher temperatures (900-1000 °C), with cracks forming at the edges because of embrittlement by oxides [195]. The temperature of 800 °C provides good workability without the massive oxidation of the higher temperature range [195]. Significant oxidation can still occur at these temperatures so methods have been developed to minimize oxidation, which include canning with Cu or mild steel sleeves, or extrusion [118, 196, 197]. Dynamic recrystallization and precipitation formation begins between 400-600 °C; however, long range recrystallization does not occur and the microstructure is typically elongated grains [198, 199]. Swaging is most often used as the initial high deformation process for forming bars for wire drawing. Swaging can produce high reduction with low energy, is more dimensionally precise than forging, yields 4-6 pieces per minute, and has higher surface quality and mechanical properties, but it does have issues related to stress distribution over the component surface and the resultant metal flow [200].

2.6.2.2 Cold Work

Hot working is generally followed by cold working steps, to provide final product shape, finish, fine microstructure and mechanical properties [181]. Cold forming leads to much greater retained martensite and amorphization than hot forming [201]. Marforming (i.e. $T < M_f$) makes finer subgrains than ausforming (i.e. $T > M_d$) because dislocation annihilation and dynamic recrystallization do not occur at the lower temperature [196]. Ausformed parts are less sensitive to heat treatment because they are more thermally stable [196]. The finer microstructure of marforming results in a higher strength, stability and fatigue life than ausforming [162]. Ausforming at lower temperatures avoids these recrystallization issues but does not have as fine a grain structure as marforming due to the limited available deformation mechanisms [196, 198]. NiTi work-hardens quickly so is limited to between 30 and 40 % cold work, after which a full

anneal of 600-800 °C is required [181]. Initial cold work of bars is done first by swaging, then by rolling and finally by wire drawing.

2.6.2.3 Wire Drawing

Many different forms of wires can be drawn. This review will focus on the drawing of wire with a circular cross section. The process of wire drawing usually limits the maximum reductions per pass to between 30 and 35 %, and much lower amounts are normal as in the case of many non-ferrous materials [202]. The deformation involved in wire drawing is not as simple as an idealised one dimensional tensile deformation, or even a multi-axial deformation of rolled sheets. The circumferential reduction of the wire as it passes through the die is the result of a complex interaction between the wire and the walls of the die. Assuming uniform flow through the die, the true strain of wire reduction is found in 2.2, the strain rate in 2.3, and the wire reduction in cross sectional area in Equation 2.4 [202]. In Equation 2.2 ε_t is the wire drawing true strain, and d_0, d_1 are the original and final diameter respectively. In equation 2.3 V_{DRAW} is the drawing speed. In equation 2.4, r is the wire drawing reduction, and A_0 and A1 are the initial and final area. Non-uniform strain occurring at the die entrance and exit can lead to redundant strain that can be incorporated into these equations with a correction factor.

$$\varepsilon_T = ln\left[\left(\frac{d_0}{d_1}\right)^2\right] \quad [202] \tag{2.2}$$

$$strain\ rate = \varepsilon_T V_{Draw} \quad [202] \tag{2.3}$$

$$r = 1 - \left(\frac{A_1}{A_0}\right) \quad [202] \tag{2.4}$$

The die angle α is the angle between die wall and the wire centreline (Figure 2.27). This angle and the reduction are used to calculate the area of the idealised deformation zone; the trapezoid shown in Figure 2.27, which is characterized by the variable Δ. The effect of Δ on the deformation zone can be shown in Figure 2.28. The value of Δ greatly affects the wire drawing deformation, and the optimization of this value as close to 1 as possible leads to optimal wire drawing conditions [202]. Certain engineering constraints such as the requirement to keep the drawing stress at less than 0.6 of the existing wire's yield stress lead to the optimal values of Δ

often being between 2-3. The drawing stress (D) is the sum of the uniform work (W_U), redundant work (W_R) and the frictional work ($W_{Friction}$) as shown in Equation 2.5.

$$D = W_U + W_R + W_{Friction} \quad [202] \tag{2.5}$$

The uniform work is work required to thin and stretch the wire. Both the redundant and frictional work reduces the total possible reduction in wire diameter [202]. The redundant work is related to the change in direction of material flow at the die entrance and exit that have no effect on wire geometry but require energy. The redundant work increases substantially as Δ increases because of non-uniformity in strain across the cross-section (Figure 2.28) [203]. This non-uniformity leads to uneven hardness across the wire cross section which can require more inter-anneal steps than a more uniform strain. This effect can be used beneficially to harden the surface with a very light pass, causing a residual compressive stress that can increase wire fatigue life resistance [204].

The frictional work is resultant from the interaction between the die surface and the wire. The wire temperature can increase due to the work and friction in the die region and must be cooled to avoid localized recrystallization, lubricant deterioration, die-sticking or transformation from the preferable marforming to the undesirable ausforming of NiTi [205]. With adequate lubrication, lower values of Δ are preferred for reducing friction. High Δ can lead to high wear on the wire causing local fracture in the form of 'fines' flaking off. These fines clog the lubricant and die, leading to poor quality material or breakage [206].

With adequate lubrication, a low Δ (i.e. low approach angles / larger reductions) reduces die wear [207], frequency of intermediate annealing (hardening of surface because redundant work), risk of breakage (compressive not tensile stresses in core) [208], improves ductility and minimizes bulging at the entrance and thinning after exiting from the die (i.e. drawing stress higher than wire flow stress) [209]. Throughout the wire drawing stages the Δ should be kept constant (i.e. same die angle and percent reduction) to ensure consistent drawing mechanics. Maintaining equivalent draw stress to flow stress ratios also ensures consistency [202]. It is also

important to align the die concentric with the wire so that the forces are distributed evenly across the die cone and deformation occurs evenly.

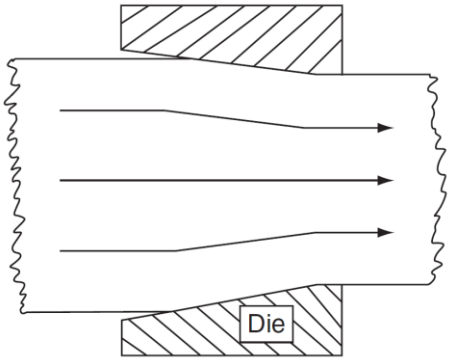

Figure 2.26: Flow of the wire through the drawing die. Note the deflections upon entering and exiting the deformation zone [202]

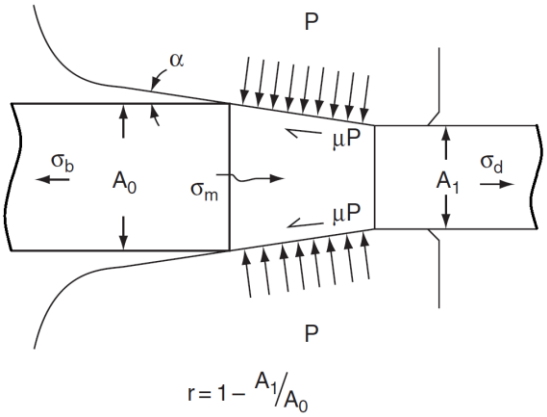

Figure 2.27: An analytical schematic illustration of a wire drawing pass [202]

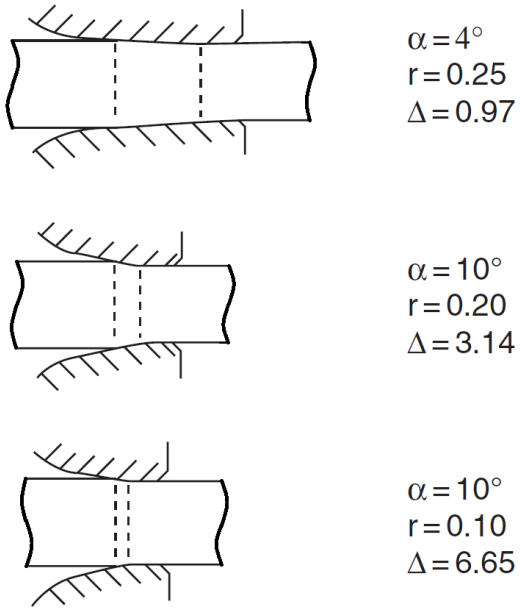

Figure 2.28: Illustrations of three different deformation zones as wire being drawn through the die, and associated values of Δ, die semi-angle, and reduction [202]

The effectiveness of the lubricant directly impacts the surface quality of the drawn wire and thus the fatigue properties of the wire. When no lube is used the surface has heavy striations and string bonds form between the wire and die, which results in a fracture surface and metal stuck in the die [210]. With non-continuous lubricant local effects termed ‘crows feet’ form due to sticking/shear fracture. The formation of these chevrons have a large number of drawbacks, including entrapping debris and lubricant, reducing lubricant efficacy leading to die wear, reduction in physical and fatigue properties and the potential for breaking the wire, which can

jeopardize the net positive income of a drawing process [210]. The ideal bright drawing is possible if a thin continuous film of lubricant is achieved, but attempting to achieve this condition can result in the non-continuous lubrication issues mentioned above [210]. If the lubricant layer is too thick it provides excellent lubrication, but a poor wire finish. This is due to a shear stress developing between the die and the wire, which causes a shear band to form with grain to grain variation in strain leading to a poor surface devoid of surface ironing and covered in asperities [211]. If the lubricant is a medium amount then there will be a mixture of regions, with bright anneal properties and deep gouges typical of thick lubricants [210].

2.6.2.4 Wire Drawing Shape Memory Alloys

NiTi is more difficult to wire draw than stainless steel, copper or other engineering materials, but with proper lubrication and die design industry can draw wires as small as 17um with an acceptable time and cost [181]. Thin oxide films can be used as lubricant, but thick oxide films have cracks and spalling which impeding wire drawing, in which case MoS_2 is advised to be used [212]. Few published works on wire drawing NiTi exist, with the majority of work being proprietary to industry and kept secret. None of the publications detail the final steps of cold work by wire drawing; rather they may specify the total percent cold work. Final cold work percentages between 20-50 % have been identified as being suitable for good physical properties, transformation stability and fatigue life [58, 69, 213-215]. The most complete work on wire manufacturing is by Grossman et al., but even this publication leaves the last cold work steps unmentioned [184].

The number of passes between equivalent reductions can affect the uniformity of hardness across the cross section (Figure 2.29) [212]. The use of multiple passes reduced the drawing stress and chance of breaking. Multiple passes around the M_s result in the lowest critical stress for deformation (Figure 2.12), reducing the drawing stress (Figure 2.30) and maximizing the number of passes possible between inter-annealing. Drawing in R-phase results in an even lower stress because it has the lowest critical stress for deformation [216].

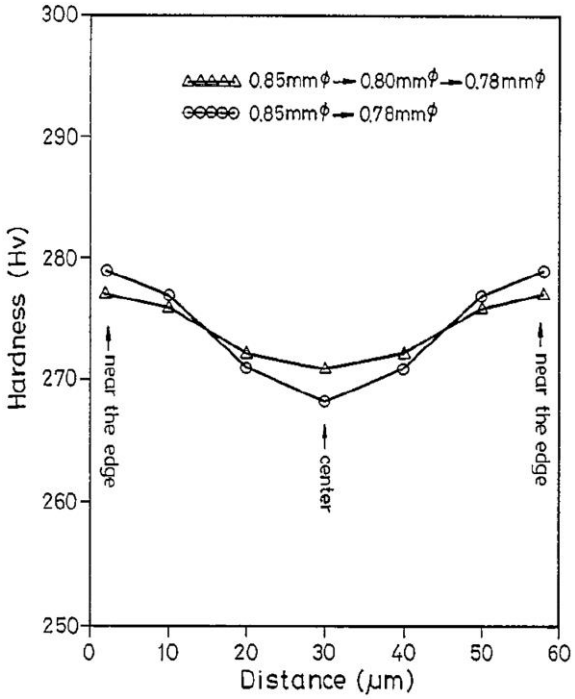

Figure 2.29: The hardness curves across the wire section for $Ti_{50}Ni_{50}$ wires drawn from 0.85mm dia to 0.78mm dia [184]

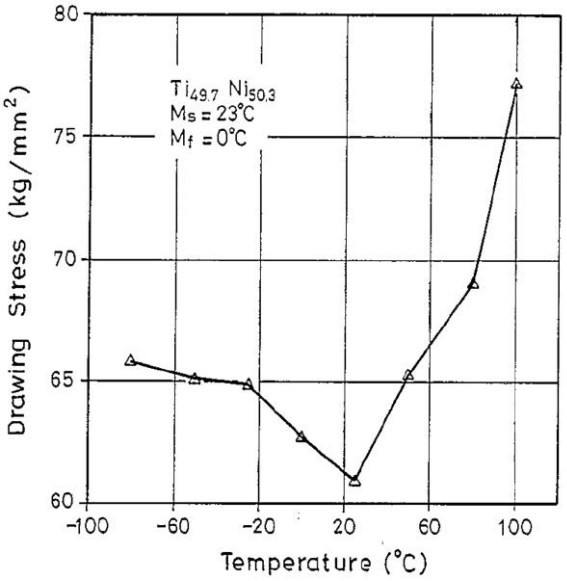

Figure 2.30: The drawing stress vs. drawing temperature for the as-annnealed $Ti_{49.7}Ni_{50.3}$ wire [184]. See Figure 2.12 for relation to NiTi deformation.

2.6.3 Heat Treatment

Final heat treatment is required after cold work to bring back SMA properties, provide strengthening by precipitates in Ni-rich NiTi and increase resistance to fatigue crack nucleation [143]. The combination of percent cold work, heating temperature and time dictate the final microstructure [58, 181]. At intermediate temperatures (350-475 °C) the nucleation and diffusion processes are optimized for maximum, coherent fine precipitate formation [58, 217]. A heat treatment temperature of around 400 °C for about 1 hour has been identified as providing the most stable properties for both Ni-rich and Ti-rich NiTi [6, 69, 218, 219]. Quenching after heat treatment is required to avoid the formation of Ni_3Ti [220].

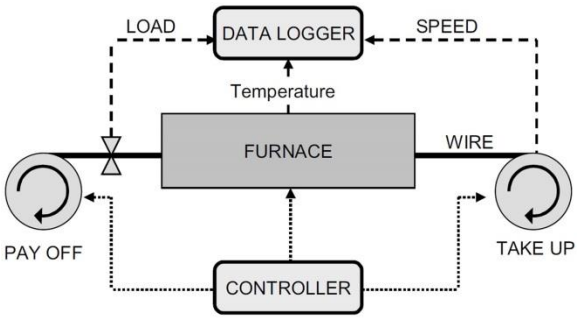

Figure 2.31: Functional diagram of annealing [118]

The morphology, nucleation and growth of the Ni_4Ti_3 precipitates, and the NiTi matrix can be affected by small changes in superimposed external stresses [73, 221, 222]. Large production facilities use continuous production strand heat treatment (Figure 2.31), and need to monitor and control the tensile loading which are reported to be between 35-300 MPa with temperatures of 350-600 °C [58, 118]. The tensile load, annealing temperature and time are crucial for stabilization and functional properties. The initial stages of heating lead to spring back due to any remnant shape memory effect. The applied strain will straighten the wire and potentially reduce the wire diameter.

Heat treating wires by electropulse has shown promise, producing similar microstructures and properties to conventional heat treatment methods [223]. This method may be a suitable replacement of continuous strand annealing for specific applications, where the wire can be heat treated in-situ in the application [224, 225].

Shape setting heat treatments are used to set the wire's 'memory' to specific shapes. These treatments are generally performed between 325-525 °C for 5-30min, followed by a water quench [69].The desired form is ensured by constraining the NiTi with a stainless steel fixture, at high temperatures the austenite grains are stress relieved and will return to this new form after deformation and shape memory effect activation.

2.6.4 Surface Properties

High cycle fatigue lives of electropolished NiTi were slightly longer than black oxide surfaces; however, low cycle fatigue was unaffected [126]. The effects of poor oxide surfaces and the

hardening of the surface region are magnified when the size of component is reduced and total area of oxide to total cross sectional area ratio is increased, where it can have significant effect on low cycle fatigue [158]. Striations created by the wire drawing process must be removed by electropolishing or chemical etching or fatigue cracks will nucleate from these areas [226, 227]. Hydrogen embrittlement can occur during manufacturing processes including the mentioned chemical etching and can reduce fatigue life of NiTi by a small amount [228]. If there are no surface defects, then failure initiates at the previously mentioned PVAs (Section 2.1.1) [227]. Crack initiation was observed at these points even in high purity materials, with higher oxygen content leading to lower fatigue lives in both the low cycle fatigue and high cycle fatigue regions [227].

2.7 Laser Processing - Welding of Shape Memory Alloys

2.7.1 Laser Welding of Shape Memory Alloys

Despite the importance of welding and joining in manufacturing there is a relatively small amount of literature detailing the welding and joining of SMAs. Mechanical joining techniques are generally used to integrate NiTi SMAs into systems, but these techniques have limitations in joint geometry and maximum load. These limitations can be overcome with metallurgical bonding, which has a number of advantages that include high strength connections to control systems [229], and reduction of cost by joining NiTi with less expensive materials [230-232]. The counterpoint to these advantages are the difficulties that can be encountered during joining of NiTi, which include solidification cracking, formation of brittle intermetallics and oxides, and degradation of the material properties [16, 23].

Nd:YAG laser welding was chosen for the current study because it is a superior method for joining SMAs, achieving NiTi joint efficiencies of 80 % with minimal heat input [233]. The low heat input limits the deterioration of the strain of actuation, strength and ductility [234, 235], while preserving the functional properties (i.e. the shape memory effect and pseudoelasticity) of NiTi [236]. Characterization of the joint properties to date has focused on quasi-static tests, but integration of SMAs into actuator applications requires characterization of fatigue properties.

As was discussed in previous sections, the texture of NiTi is important for the maximum achievable recoverable strain. The texture along the axis of wires is in the preferred <111> direction which provides the maximum possible strain of all crystal directions [104]. During the solidification of laser welded spots in the wire the texture becomes the <100> direction [23]. This is the preferred growth direction of cubic metals. This change in texture directly affects the SMA properties, with a lower overall achievable strain in the FZ compared to the BM [23].

2.7.2 Fatigue of Welded Shape Memory Alloys

There have been a few investigations on the effect of welding on the mechanical fatigue of pseudoelastic NiTi [237-239]; but to date there have been no investigations on the thermomechanical fatigue of welded SMAs. The sole investigation on a small number of thermal cycles of a welded SMA involved a two-way shape memory effect actuator, which concluded that the effect on the actuator performance was minimal [240]. The same cannot be concluded for the cycle life, which has been shown to be greatly affected by coarse grained microstructures like those in the heat affected and fusion zones of the welded wires [59, 163, 237, 238, 241]. Furthermore, mechanical fatigue investigations of welded NiTi reported a reduction in the mechanical cycles to failures compared to the base material as a result of the alteration of the microstructure [242]. A post-weld heat treatment strengthened the microstructure and improved the cycle life of the weld [237, 241]. It is hypothesized that a similar result would occur for thermomechanical fatigue of welded NiTi; however, one must carefully chose the post-weld heat treatment as it can promote phase transformations that inhibit either the shape memory or pseudoelastic effects at a given operating temperature of operation.

2.7.3 Laser Processing of NiTi Shape Memory Alloys

The limitation of having one transformation property for a NiTi component has resulted in the development of numerous methods to increase the number of transformations possible. Previous methods explored to achieve multiple properties in a single component include antagonistically positioning SMAs, local heat treatment techniques, the two-way shape memory effect, welding, and local alteration of SMA properties [17-19, 243]. Of these methods the local property modification methods are the most flexible and can be used in a wide scale and range of applications [16, 19].

Local annealing techniques have been used to make SMA component with both the pseudoelastic and shape memory effects [18, 244-246]. Unfortunately these techniques are limited by a number of factors including the composition permitting pseudoelastic and shape memory effect to both exist at operating temperatures, geometries that accommodate local heating, lack of control over the transformation temperatures, and issues associated with the heat affected regions [18, 244-246].

Local-chemistry modification has been shown to be a more effective and flexible method of controlling local SMA properties [16, 247]. Powder metallurgy was used to make a proof of concept muti-phase actuator; however, this method is limited by carbon contamination, porosity, micro-chemical inhomogeneity and undesirable intermetallic formation [247, 248]. In comparison, laser processing can accurately modify local bulk composition and microstructure, while avoiding the aforementioned issues [16]. Proof of concept laser processed devices include; a multi-position micro-gripper, a two-memory linear actuator, multiple pseudoelastic components and a hybrid pseudoelastic-shape memory component [13, 14, 20, 249].

The laser processing technology uses the vaporization of liquid metal that occurs during laser welding to locally alter chemistry [16, 250]. This effect was initially studied in the laser welding of stainless steels, where the loss of chromium negatively impacts the corrosion properties of the weld [250-254]. The difference in vapour pressures of the alloying elements (shown in Figure 2.32), results in a difference in vaporization rates, and thus a change in composition of the solidified fusion zone as shown in Figure 2.33 [255].

In the NiTi system, Ni has a higher vaporization rate than Ti during laser welding [13, 16]. This difference in vaporization rates results in the solidified fusion zone having a Ni-lean composition compared to the base metal. A small change of 0.1 at.% Ni can result in a 10 K change in the M_s transformation temperature. The laser processing technology has been designed to provide precise control over these small changes in chemistry to enable a high resolution of control of the transformation temperatures [13].

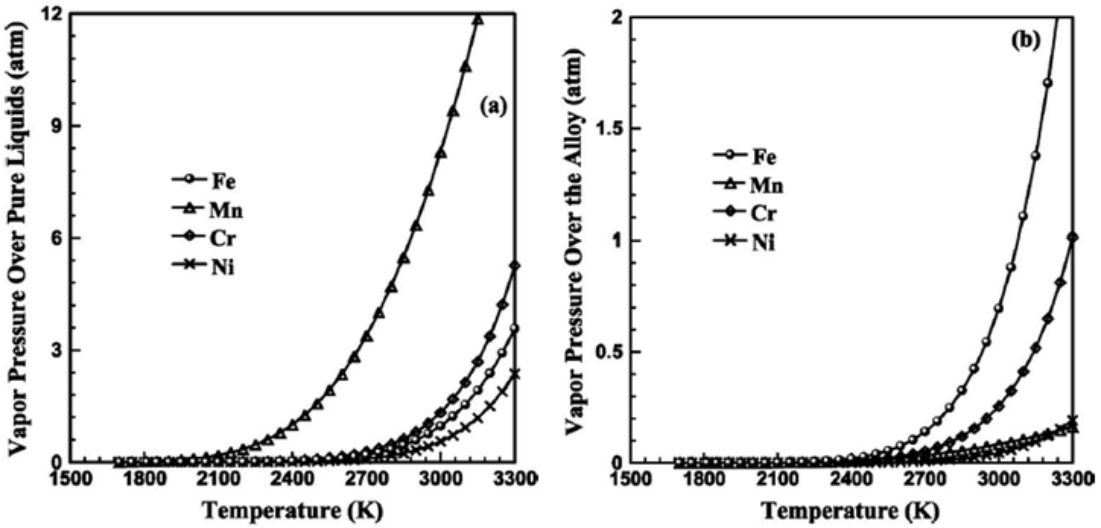

Figure 2.32: Equilibrium vapor pressures of the various alloying elements (a) over respective pure liquid and (b) over 304 stainles steel as a function of temperature [255]

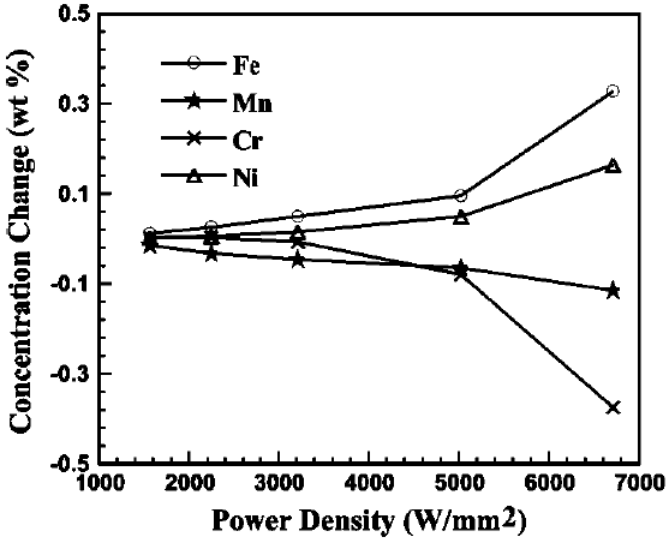

Figure 2.33: Concentration change of the various alloying elements as a function of power density. Laser power: 1067 W and pulse duration: 3ms. [255]

Laser processing of NiTi SMAs has a number of limitations that can be addressed through the development of a more fundamental understanding of the process-structure-properties relationship. Pequegnat et al. [13] identified that the yield stress of laser processed NiTi sheets was not sufficient to accommodate stress-induced martensite. A post-laser processing

thermomechanical treatment was applied to the sheets which consisted of a cold-work reduction and a heat treatment designed to strengthen the microstructure. This study was limited to single thermal and tensile cycles; the evolution of the material over multiple cycles was not investigated. The only investigation of multiple thermomechanical cycles of laser processed NiTi used a low stress, and only 200 cycles [20]. Characterization of these materials over thousands of cycles is required to gain a fundamental understanding of their evolution, so that they can be successfully manufactured for use by industry. The following areas have been identified to be addressed in the current study:

1. There is no literature on thermomechanical fatigue of laser welded NiTi (i.e. single laser spot processing). Chapter 4 presents the first study on the thermomechanical fatigue of lase welded NiTi, and investigated if a post-weld heat treatment could improve the properties of the material. This knowledge was used for the work presented in Chapter 5.
2. There is no in-depth study on the manufacturing or the thermomechanical cycling of laser processed NiTi wires. Chapter 5 of this study detailed an in-depth study on the manufacturing of laser processed NiTi wire, and fully investigate the process-structure-properties relationship of these materials as they were thermally, mechanically and thermomechanically cycled.
3. The above knowledge was used to design a thermomechanical treatment that improved the properties of the laser processed NiTi wires as they were cycled thermally, mechanically and thermomechanically.
4. The knowledge gained from the previous sections was used to design and manufacture a laser processed NiTi wire actuator that had a new type of two-way shape memory effect, which is detailed in Chapter 6. An actuator that could move on both heating and cooling, without an external load (i.e. self-biasing) is desired by industry, because the use of an external bias adds complexity, weight and space. This is of specific importance in micro-actuation devices where the assembly processes account for 80 % of the production cost [256]. These added costs have led to ongoing efforts by researchers to eliminate the dependence of cyclically actuating SMAs on an external bias; with the goal of creating a self-biasing actuator. Adoption of these self-biasing actuators by industry would require

them to achieve tens of thousands of cycles while maintaining geometric and actuation stability. This benchmark has thus far not been met. It is proposed that a stable multiple memory laser processed NiTi actuator could meet this requirement.

3 Experimental Setup

The experimental setup was separated to reflect the different results chapters. Section 3.1 refers to Chapter 4, section 3.2 refers to Chapter 5, and section 3.3 refers to Chapter 6. There is overlap between the experimental setup in Chapters 4-6. To limit repeating information only differences in testing methods were highlighted in the different sections.

3.1 Thermomechanical Fatigue of Laser Welded NiTi

3.1.1 Materials, Welding and Heat Treatment

The NiTi wire used in this investigation was purchased from Dynalloy Inc., is called flexinol, and measured 381 μm in diameter. These wires were of a proprietary composition, with Dynalloy Inc. publishing an austenite finish temperature of 90 °C. An oxide was present on the wire due to a final heat treatment by the manufacturer. This oxide was removed prior to welding with an etchant of 7 vol. % HF, 20 vol. % HNO_3, bal H_2O, to ensure quality joints [257]. This process reduced the average diameter of the wire to 370 μm.

Nd:YAG laser welding was chosen for the current study because it is a superior method for joining SMAs, achieving NiTi joint efficiencies of 80 % with minimal heat input [233]. The low heat input limits the deterioration of the strain of actuation, strength and ductility [234, 235], while preserving the functional properties (i.e. the shape memory effect and pseudoelasticity) of NiTi [236]. Laser welding was performed using a Miyachi Unitek LW50A pulsed Nd:YAG laser, which had a wavelength of 1.064 μm, a spot size of 600 μm and a top-hat energy distribution. The effect of joint fit-up was not the focus of this investigation. To remove this effect, bead-on-plate welds were made with single wires. The pulse profile had a peak power of 1kW and a width of 7ms including an up and down slope of 2 ms each. The downslope was used to minimize solidification cracking that can occur in Ti-rich NiTi [258, 259]. The pulse was designed to form a full penetration joint with the minimal energy required, to preserve the physical properties of the base metal.

A custom fixture (Figure 3.1) was designed to clamp the wire securely in place and shield it with an argon flow rate of 0.56 m^3h^{-1}. The wires were martensitic at room temperature, so the shape memory effect could be activated by the thermal cycle of the weld which caused the wire to

move during welding and distort the weld as shown in Figure 3.2 A and B. The ideal weld approximated the shape of the original wire. A weld with minimal distortion and no necking is shown in Figure 3.2C; this was the standard set for quality control, any irregularities in shape greater than this were deemed unacceptable and were discarded. This standard of quality was repeatedly achieved when a protocol of thermal cycling the wire prior to welding was initiated, so that no detwinned martensite remained to be recovered during the weld thermal cycle.

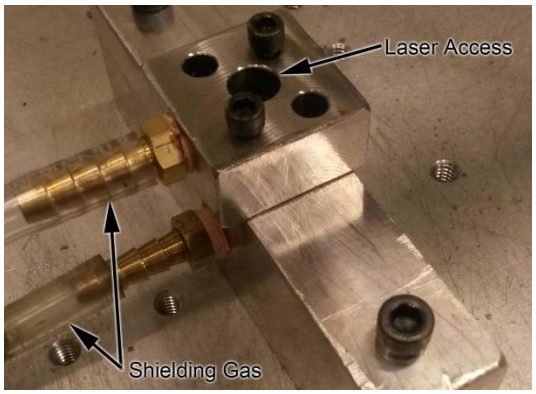

Figure 3.1: Image of the welding fixture. A base and a cap clamped together to secure the wire, with shielding gas from the top and bottom to ensure limited oxygen pickup by the weld

The welded wires were separated into two groups for comparison. The first group was the as-welded wires, and the second group was further processed with a post-weld heat treatment. The heat treatment consisted of a 3600 s heating cycle at 400 °C in an air furnace followed by a water quench. This protocol was used previously by Yan et al. [237] and Chan et al. [241] during their investigation of the effect of post weld heat treatments on the mechanical cycling fatigue of pseudoelastic NiTi wires. It was posited that this well-known heat treatment which benefits the shape memory properties, and shape memory fatigue would also improve the thermomechanical fatigue life of the welded wires. A separate batch of base metal was solutionized at 1000 °C for 3600 s and water quenched. This material was used as a reference for the transformation properties of the heat affected zone.

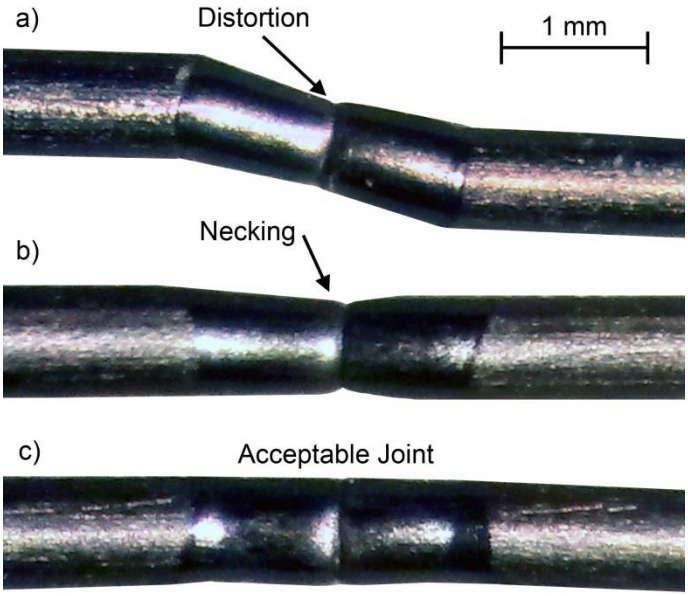

Figure 3.2: Weld joint quality control diagram a) fail due to distortion, b) fail due to necking, c) pass due to minimal irregularities.

3.1.2 Phase Analysis

A Thermal Analysis Q2000 system equipped with a refrigerated cooling system was used for differential scanning calorimetry (DSC). The ASTM F2004-05 standard was used, with modification of the standard including a test rate of 5 °C min^{-1} and a temperature range of -75 °C to 120 °C. The Thermal Analysis Universal 2000 software was used to locate the A_s, A_f, M_s, M_f, R-phase start and finish (R_s, R_f) temperatures. The software calculated the temperatures as the intersection of the tangent of the maximum slope of the reaction peak and base line. The DSC samples for the welds were cut out of the wire to only contain the fusion and heat affected zones, in order to compare these regions with the original base material.

3.1.3 Tensile and Thermomechanical Fatigue Testing

An Instron 5548 micro-tensile tester with an environmental chamber was used for tensile testing. A standard ASTM F216-07 testing protocol was used with a strain rate of 0.04 mm $mm^{-1}min^{-1}$. The tensile specimens had a gauge length of 20 mm, which was composed of a weld, a heat affected zone and the base metal as shown in Figure 3.3. The tester was used for tensile failure loads and characterization of single actuation cycles. At least three samples were tested per

parameter, and the tests were performed at room temperature (22 °C) and 10 °C above the A_f (i.e. 77 °C) of the base material. Pneumatic grips flat faces were used to clamp the wires. The wire lengths extended out of the backside of these grips, and there was no observed change in the length of the wires out of the back of the grips, which indicating minimal slippage of the wires occurred. A mechanical extensometer was attached to the wires, but resulted in significant deformation before testing, so it was not used. It was decided that strain would be measured using the cross head motion. The gauge length for this method was smaller than that recommended by the ASTM standard, but was chosen due to constraints of the environmental testing chamber. The region of the material around the grips can be affected by the pressure from the grips [260]. A series of tests was performed on different gauge lengths to determine the minimum gauge length required for accurate data (i.e. the gauge length from which increasing the gauge length no longer affected the elastic moduli or detwinning plateaus). The gauge length used in the current study was set above this minimum length to avoid significant effects from the grips. Comparison of the different specimens was performed with the knowledge that their data would all potentially have artefacts related to the above discussed testing methods.

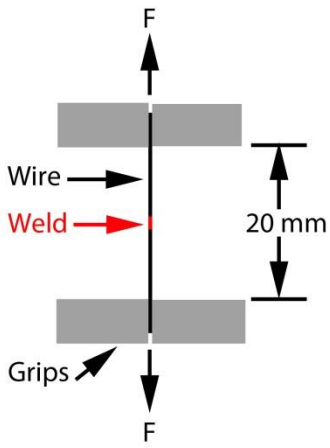

Figure 3.3: Schematic of welded tensile and fatigue specimens

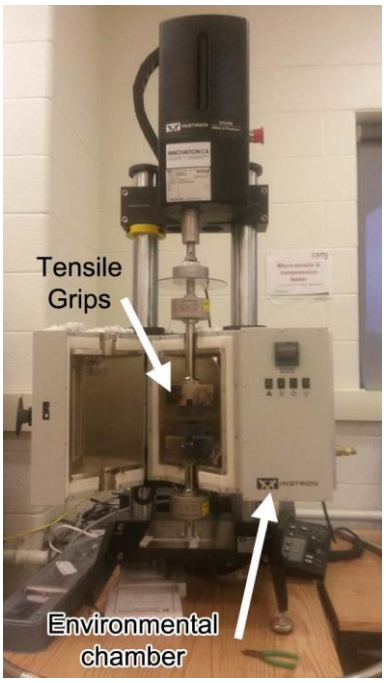

Figure 3.4: Tensile tester used for characterization of stress-strain response and zero load recovery of shape memory properties

Thermomechanical fatigue testing was conducted using a custom designed setup shown in Figure 3.5. The testing of NiTi can lead to erroneous results if testing equipment is not designed or used properly, therefore a comprehensive review of literature, ASTM standards for tensile and fatigue testing and available works including those by Shaw et al. [260-266] were reviewed for the manufacturing and design of the testing equipment. The test specimens had a gauge length of 20 mm and were held in the system as per the schematic of Figure 3.3. Serrated quench hardened steel, that was tightened by screws was used for the grips. This provided excellent gripping with no slippage, but had a heat sink effect on the wire. An Omega LCMFD 500N load sensor and a MT 2571 Heidenhain displacement sensor with ±0.2 µm sensitivity were used for characterization of the actuation properties. A NI PXI-1031 DAQ from National Instruments was used to monitor the sensors and control the Sorensen XG 33-25 power supply which supplied a current of 4 A, with a varying potential near 2 V to heat the wire for actuation for a period of 5 s, followed by a cooling of 8 s for each thermomechanical cycle. At least three samples were tested per load, with the load being set at the beginning of the test using a biasing spring.

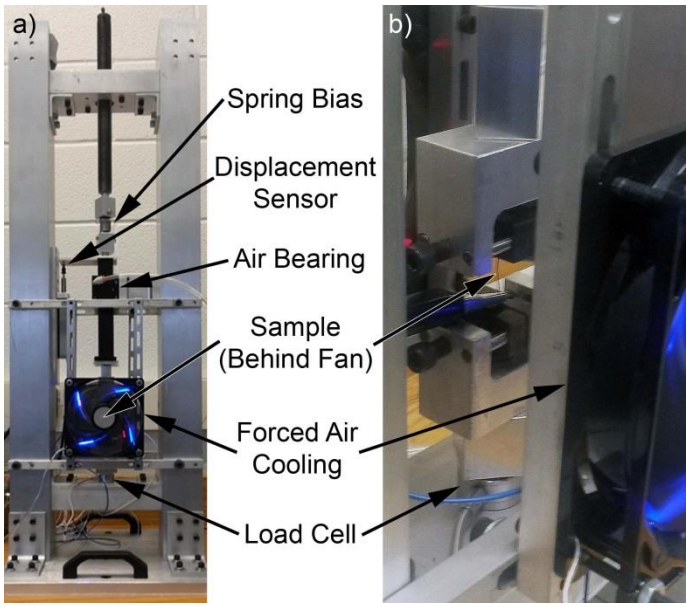

Figure 3.5: Thermomechanical fatigue tester in spring-biased configuration a) front view, b) side view with specimen in grips

3.2 Laser Processing and Thermomechanical Treatment of NiTi Wires

3.2.1 Materials and Laser Processing

A 700 μm diameter Ni-rich NiTi wire (NT-E9) manufactured by the Furukawa Electric Co. LTD., was used in this investigation. This wire was thermomechanically processed by the manufacturer to exhibit pseudoelastic behavior at room temperature. Prior to laser processing the wire was cleaned to remove any contaminants. No acid etching was required as the oxide layer was previously removed by the supplier and the remaining oxide was very thin [233].

Laser processing was performed using a Miyachi Unitek LW50A pulsed Nd:YAG laser with a wavelength of 1.064 μm. A laser spot size of 600 μm and energy of 16 J per laser pulse was used. An example of the laser processed NiTi wire is shown in Figure 3.6. The wire was fed through a custom fixture and shielded with Ar gas at a flow rate of 0.71 $m^3\ h^{-1}$ to prevent atmospheric contamination of the processed region. The design of the pulse was done to minimize expulsion and solidification cracking [259, 267]. A cylindrical cross section of the process region was designed to facilitate overlapping of the spots. The centreline of the laser

processed fusion zone was the weak point where failure occurred during initial wire drawing attempts. The centrelines were removed by overlapping the 1200 μm laser processed spots by 60 % in order to enable wire drawing. Overlapping the sports increased the removal of Ni per length of wire. This limited the current process to having one memory above room temperature after wire drawing. Using the base metal as the first memory, and the laser processed NiTi as the second memory, two memory actuators were manufactured by laser processing one half of a wire (i.e. Ti-rich, or high temperature) and leaving the remaining portion of the wire as base metal (i.e. Ni-rich, or low temperature). Additional single and two memory specimens were processed and subjected to a series of thermomechanical treatments defined in Section 3.2.2 which were designed to improve the properties of the material.

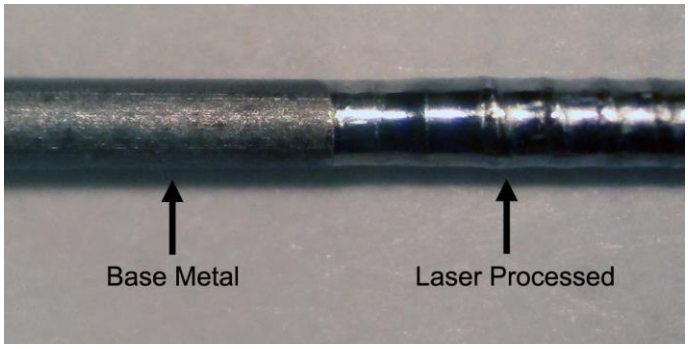

Figure 3.6: Laser processed NiTi wire

3.2.1.1 Laser Characterization

Repeatability of the laser process was important to ensure consistency over the length of the study, and for the knowledge transfer to future students and industry partners. The laser power was measured to ensure consistency before each use. The average power measured over the period of six months of use for the 16 J laser pulse (i.e. 16 J reported by the laser controller) was 11.21 J ± 0.05 J. If the average power measured from 10 consecutive pulses varied more than 2.5 % from the average of the measured powers then the system was diagnosed. During this time period the optics did not require re-alignment; the only requirement was cleaning of the protective glass on the collimator to return the laser to its original condition. If the laser was opened for maintenance or alteration then the optics were realigned and the system recalibrated to return to the optimal beam profile and power.

A 400 μm step index (SI) fibre was attached to the Nd:YAG laser. This fibre carried the beam to a collimator with a lens of 150/100 aspect ratio. This optics package would produce an ideal spot size of 600 μm. A Spiricon BeamGage was used to characterize the beam profile. The spot size measured was 649 μm, with an ellipticity of 0.996, flatness of 0.917, and an edge steepness of 0.956, indicating that the spot was circular and had a uniform energy across the spot.

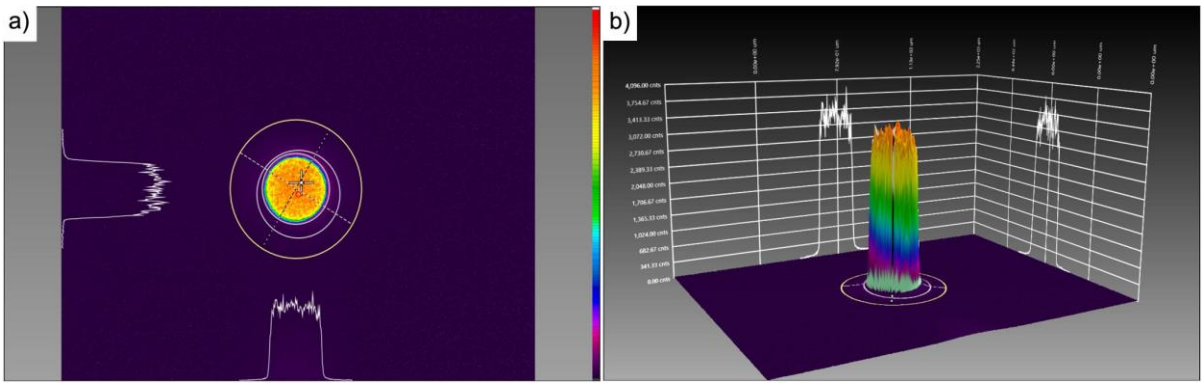

Figure 3.7: a) 2D-beam profile, b) 3D-beam profile

3.2.2 Post-Laser Processing Thermomechanical Treatment

The post-laser processing thermomechanical treatments are outlined in Table 3.1. The treatment was designed to homogenize the microstructure, and to reduce the grain size thus minimizing dislocation activity for improved cyclic actuation properties [59, 75]. The treatments began with a solutionization treatment at 1000 °C in an argon atmosphere for 3600 s followed by a water quench. A number of wire drawing steps and inter annealing stages were performed as per Table 3.1 to a final diameter of 460 μm. The true strain (ε_t) was calculated as shown in Equation 2.2. This final diameter had the equivalent of a total final area reduction of 45 % which is near the limit of the range identified for superior physical, stability and fatigue properties [58, 69, 213-215]. At this final diameter a final heat treatment of 400 °C in air for 3600 s and a water quench were applied.

There are a limited number of publications on the wire drawing of NiTi, which were used to aid in the design of the thermomechanical treatment [58, 69, 181, 184, 212-216]. The limits of the maximum potential reductions were investigated, along with the required total reduction for

stable shape memory properties. Commercial wire drawing rarely involves single stage reductions above 30-35 %, and many materials have much lower maximum reductions [202]. Larger reductions near the maximums possible for a material are desired for a number of reasons including higher UTS, less potential defects, less redundant work during the drawing process, and less die wear [202]. The total reduction possible with NiTi is much lower than other standard wire drawn engineering materials; NiTi is severely hardened when CW exceeds 30 % and becomes difficult to work further [215]. To ensure consistent drawing mechanics and thus consistent microstructure evolution through each die, the reductions were designed to be consistent. The reductions were kept in the between $\varphi = 0.1\text{-}0.15$ range, after the work by Grossman et al. [184]. The current investigation found that higher amounts of reduction per die resulted intermittent breaking of the wire. Reductions to $\varphi = 0.597$ (i.e. 45 % reduction) was achieved in this work, with this large total reduction being used to refine the grains to be nanocrystalline for superior fatigue performance [163]. The wire drawing parameters were designed to avoid the issues that can occur during wire drawing including surface defects, internal defects, and deformation issues at the die [202, 208]. The drawing speed of 0.5 mm s^{-1} was used for all wire reductions, which combined with the consistent reduction strain ensured a consistent strain rate through all dies according to Equation 2.3.

Table 3.1: Thermomechanical treatment schedule

Die Diameter (um)	ε_t Per Die	Total ε_t	Total Area Reduction (%)
	Laser Processing		
	Solutionization 1000 °C, 3600s		
660	0.118	0.118	
620	0.125	0.243	22.6
	Inter Anneal 600 °C, 600s		
580	*0.133*	0.133	12.5
540	0.143	0.276	24.1
500	0.154	0.430	35.0
460	0.167	0.597	45.0
	Final Heat Treatment 400 °C, 3600s		

The dies used in this study were purchased from Advanced Wire Die Ltd. The dies were tungsten carbide with a cobalt matrix, which has very good wear resistance [268]. Tool steel dies deform

relatively quickly, so were avoided in order to keep the die drawing properties consistent throughout the study [268]. A custom fixture was designed to hold the die and wire, while the tensile tester drew the wire as shown in Figure 3.8. The Instron model 4465 tensile tester was used to control the drawing speed and measure the drawing stress.

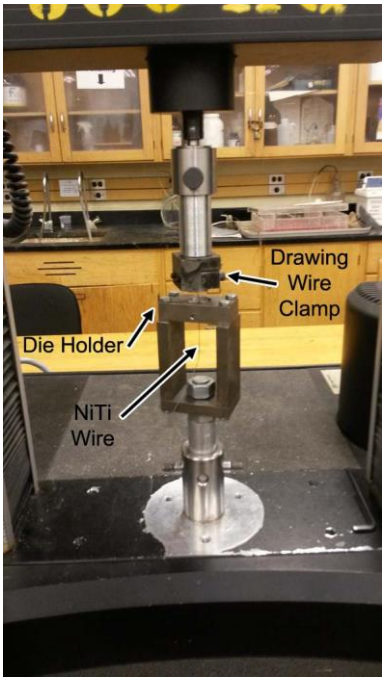

Figure 3.8: Wire drawing setup installed in tensile testing machine. Tensile tester used to monitor drawing force and control drawing speed

The wires were lubricated with a MoS_2 lube from McLube, McGee Industries Inc.. The MoS_2 was applied as a liquid, but required to dry before wire drawing. The MoS_2 was chosen as the lubricant for this study because it has a lower drawing stress than soap, which is commonly used for lubrication in wire drawing [210, 212].

The furnace temperatures were measured using a K-type thermocouple from Omega, in addition to their internal thermocouple readings. The Carbolite tube furnace used for solutionization had a set temperature of 1000 °C, which was measured by the thermocouple to be 969.6 °C ± 2.9 °C, across a hot zone measuring 203 mm. The Thermo Electron Corporation Lindberg/Blue M furnace used for the inter-anneal and final heat treatment was set to 400 °C and 600 °C, which was measured by the thermocouple to be 391 °C ± 2 °C, and 594 °C ± 2 °C respectively.

The thermomechanically treated laser processed wire is referred to as the treated laser processed NiTi. The two-memory actuators are referred to as the laser processed actuator, and the treated laser processed actuator.

3.2.2.1 Wire Quality Evaluation – Drawing Force, Surface Properties, Cross Section

It is recommended to keep drawing stresses below 0.6 of the wire ultimate tensile strength (UTS) of the wire to avoid any wire drawing related defects [202]. The drawing stresses of the initial laser processed NiTi were above this limit due to the uneven surface of the wire, and microstructural properties including texture. After the first inter-anneal the drawing stress reduced below the recommended limit. The wires were analysed to determine if any defects occurred due to these initial high drawing stresses. The key points of this analysis are presented below.

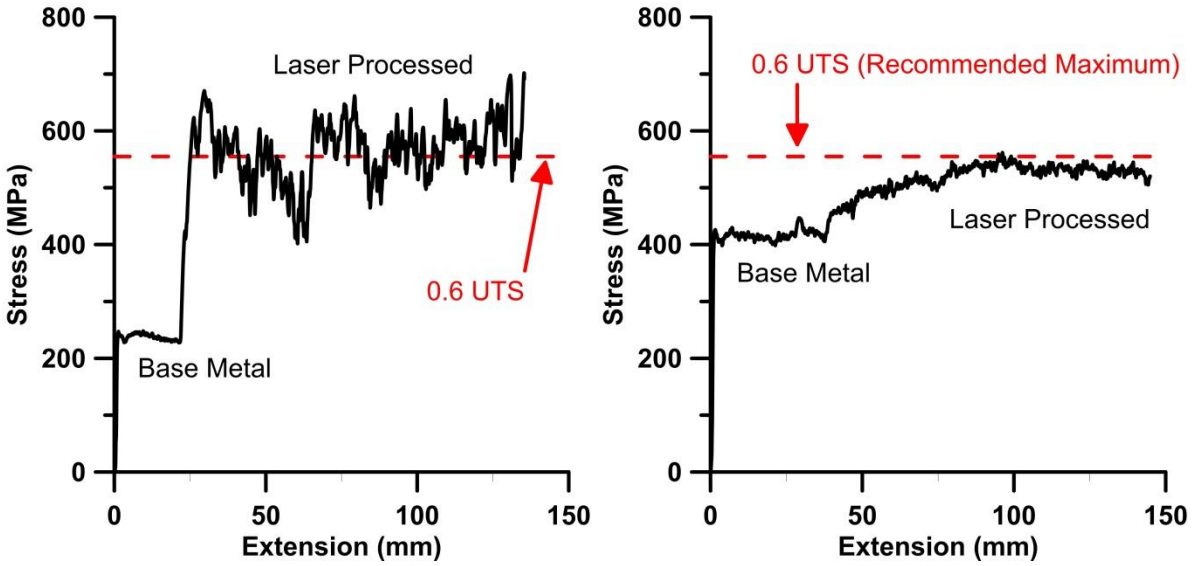

Figure 3.9: Wire drawing stress for left) first reduction after solutionization treatment, right) first reduction after inter annealing treatment

A number of defects can occur on the surface of wires including sticking, striations, and cracking [202]. It is important to avoid these defects because the surface properties of NiTi can affect the fatigue life of components [59]. This effect can become significant at smaller cross section sizes where defects become proportionally larger, and where the surface region becomes a large fraction of the cross-sectional area [59]. Figure 3.10 shows a comparison of the Furukawa,

Dynalloy flexinol and final treated laser processed NiTi wire. There are no observable differences between the flexinol and the treated laser processed NiTi, and no defects observed in either surface. The Furukawa surface was etched with acid by the manufacturer.

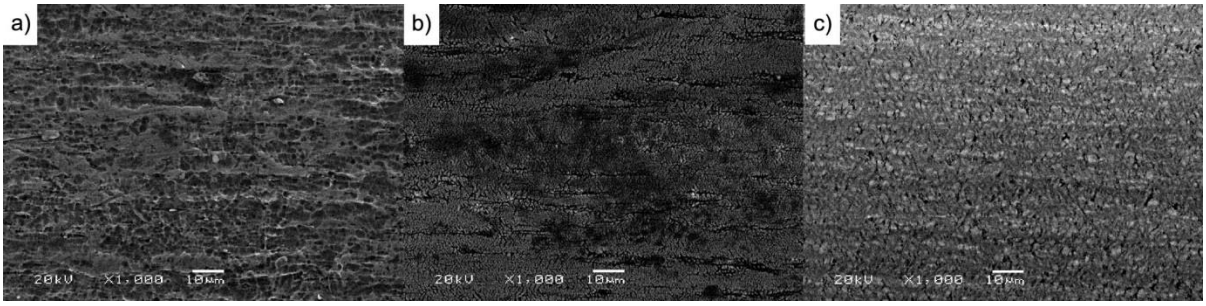

Figure 3.10: SEM analysis of the surface of the a) Furukawa base metal, b) Dynalloy flexinol base metal, c) treated laser processed NiTi. Comparison of different oxides

Micrographs of the cross sections of the treated base metal, and the treated laser processed NiTi are shown in Figure 3.11. The cross sections are free from surface defects, centreburts or any non-uniformities across the cross section [202]. The wire drawing process that the author designed for this work produced defect free wires that are suitable for characterization in the following chapters.

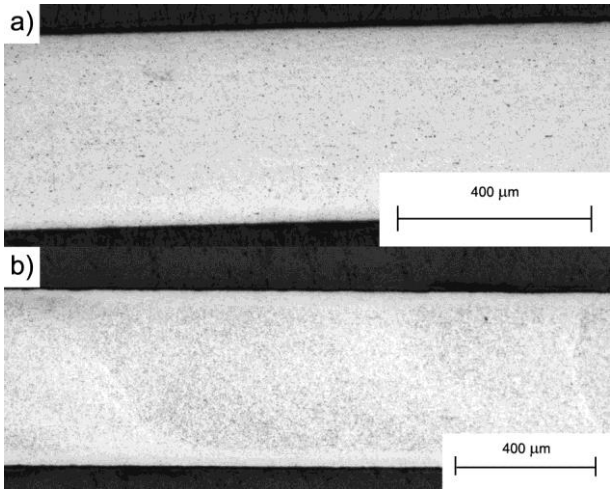

Figure 3.11: Cross sections after wire drawing; free of defects associated with wire drawing

3.2.3 Phase Analysis

The microstructure of the NiTi was analysed using a number of methods. Optical microscopy was performed using an Olympus BX51M optical microscope. The NiTi microstructures were characterized using scanning and transmission electron microscopy (STEM / TEM). A JEOL 2010F TEM/STEM field emission microscope operating at 200 kV and a Phillips CM12 analytical TEM operating at 120 kV were used. Prior to analysis the thin film samples were prepared using focused ion beam milling (FIB) on wires that had been cold mounted in epoxy and prepared with a final polish of colloidal silica. Cold mounting of the wires was required to ensure no significant alteration to the sensitive microstructure, which can be significantly altered by the hot mounting process.

The composition of the base metal and laser processed NiTi was measured using micro-particle induced X-ray emission (micro-PIXE) spectroscopy. A 3 MeV, 4 nA photon beam was scanned across 20 x 20 μm area of the centre of each laser processed spot. Homogeneity of the overall laser spot was confirmed by taking measurements in multiple regions of the single laser pulsed spot. The X-ray intensities were determined using a least-squares-fit. These values were converted to concentrations of the measured elements using the National Institute of Standards and Technology (NIST) materials standards. The accuracy of the measurements was ±0.12 at. % Ni. The lower crystal charging from Bremsstrahlung radiation reduces the background radiation compared to X-ray spectroscopy analysis, which provides the higher accuracy of micro-PIXE. This high accuracy is required for measuring NiTi because a 0.1 at.% Ni can result in a 10 K change in the M_s transformation temperature of the material [69].

A Thermal Analysis Q2000 system, equipped with a refrigerated cooling system was used for differential scanning calorimetry (DSC) analysis.

3.2.4 Tensile and Shape Memory Properties

Tensile tests were performed using an Instron model 5548 micro-tensile tester equipped with an environmental chamber. The testing protocol followed the ASTM F216-07 protocol, with a gauge length of 20 mm, at a strain rate of 0.04 mm $mm^{-1}min^{-1}$ and a measurement accuracy of +- 0.5 μm. Pneumatic grips with knurled faces were used to clamp the wires. Tests were performed

below the M_f (i.e. -26 °C) with the environmental using liquid nitrogen as the cooling medium. Tests were also performed, above the A_f of the materials and above the M_d temperatures to compare the materials in their martensitic, pseudoelastic austenitic, and stable austenitic phases. Tests performed on 2 memory actuators were performed with the gauge length being half one material and half the other material.

3.2.5 Thermomechanical Fatigue of Laser Processed NiTi

The transformation temperatures compared in this section were measured using a TA Instruments, Discovery DSC. The tensile testing was performed at room temperature using an a strain rate of 0.04 mm $mm^{-1}min^{-1}$ and a gauge length of 25.1 mm were used to test specimens. This change was made to match the gauge length of the specimens tested in the fatigue tester.

Thermomechanical fatigue was performed using a custom setup as shown in Figure 3.12. Lead weights were used to apply a constant load shown in Table 3.2 that was equivalent to a 600 MPa, when the stress is calculated using the nominal wire diameter. A gauge length of 25.1 mm was used for testing. The grips were faced with sacrificial pieces of ceramic, ensuring no heat sync effect on the wire. The current was delivered by speaker posts shown in Figure 3.12. The heating was performed at currents suggested by the Dynalloy Inc. manufacturer for wires of these diameters as shown in Table 3.2. These currents were determined according to the recommended currents by Dynalloy Inc. for wires of these diameters. The current for the laser processed NiTi was determined by extrapolation via a polynomial fit of the data provided by Dynalloy Inc. Heating was controlled to specific strains, and thermally cycled until failure. Cooling was performed using a vortex tube that was turned on when the current was turned off. The setup measured the load using an Omega LCMFD 500 N load sensor, and the displacement using a MT 2571 Heidenhain displacement sensor with a measurement sensitivity of ±0.2 μm. A NI PXI-1031 DAQ from National Instruments was used to monitor the sensors and control the power supply. The currents were kept constant by a constant current control set by a Sorensen XG 33-25 power supply.

Table 3.2: Wire diameter, constant loads and currents used in the thermomechanical fatigue testing

Wire	Laser Processed NiTi	Treated Laser Processed NiTi	Flexinol
Nominal Diameter (μm)	700	460	381
Constant Load (N)	241	100	68
Current (A)	7.43	3.27	2.25

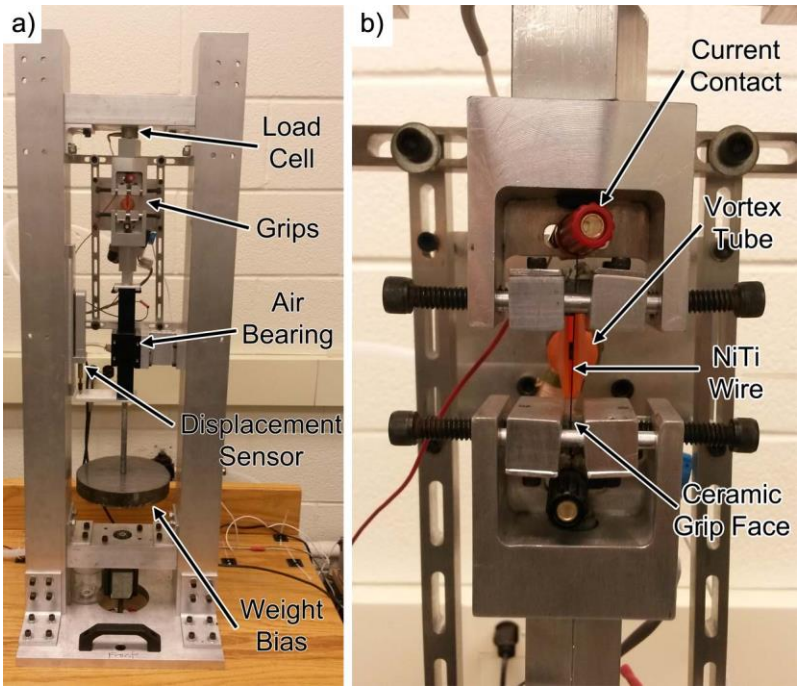

Figure 3.12: a) Thermomechanical fatigue tester in constant load configuration, b) close-up view of grips with wire specimen

3.3 Development of a Stable, High Stress Self-Biasing Actuator

3.3.1 Material and Processing

The material used was the 700 μm diameter Ni-rich NiTi wire (NT-E9) manufactured by the Furukawa Electric Co. The laser processing parameters used had an energy of 15 J. Individual wire specimens of 80 mm length for use as test actuators were cut from the supplied material and then processed as described in the previous section. One half (i.e. 40 mm) of each wire specimen was laser processed to exhibit shape memory effect properties while the other half retained the

base metal pseudoelastic properties (Figure 3.13). The laser processing enabled control of the properties of the shape memory effect portion of the actuator to allow for the synergistic coupling with the pseudoelastic portion. Additional specimens were processed and subjected to a series of thermomechanical treatments designed to improve their properties. These treatments were the same as those described in the previous section. The different regions of the thermomechanically treated wire are referred to as treated base metal and treated laser processed regions. The combination base metal and laser processed actuator are referred to as the untreated actuator, and the thermomechanically treated pair will be referred to as the treated actuator.

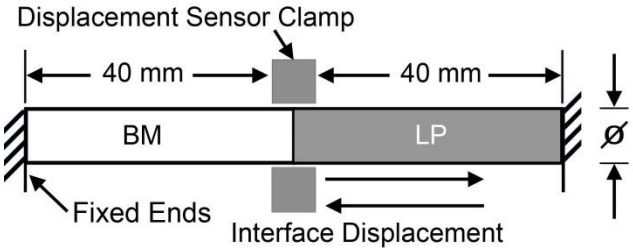

Figure 3.13: Schematic of self-biasing laser processed linear actuator, with the base metal (BM) on the left and laser processed NiTi (LP) on the right

3.3.2 Tensile and Shape Memory Properties

An Instron model 5548 micro-tensile tester with a measurement accuracy of ±0.5 μm and an ASTM F216-07 testing protocol with a strain rate of 0.04 mm $mm^{-1}min^{-1}$ were used to test specimens. The materials were tested separately with a gauge length of 20 mm. The untreated and treated actuators were pulled with half of the gauge length being base metal and half being laser processed NiTi. Tests were performed at room temperature (22 °C) and 10 °C above the A_f temperature of the laser processed (LP) or laser processed and thermomechanically treated (TMLP) sample, these test temperatures were also used for the biasing base metal and thermomechanically treated base metal.

A custom setup was built to characterize the self-biasing laser processed linear actuator as shown in Figure 3.14. A load cell was placed in line with the actuator to measure the change in force during actuation. A pre-stress was applied to the actuator prior to actuation; measuring 400 MPa and 180 MPa for the as-processed and treated actuators respectively. After being pulled into

tension, the ends of the actuator were held fixed in place. A Heidenhain displacement sensor with a sensitivity of ±0.2 μm was attached at the interface between the base material and laser processed portions of the actuator (Figure 3.13), and was used to measure displacement during the heating and cooling of the actuator. The actuation and plastic strain were calculated as the displacement of the interface with respect to the original 40 mm length of the laser processed region.

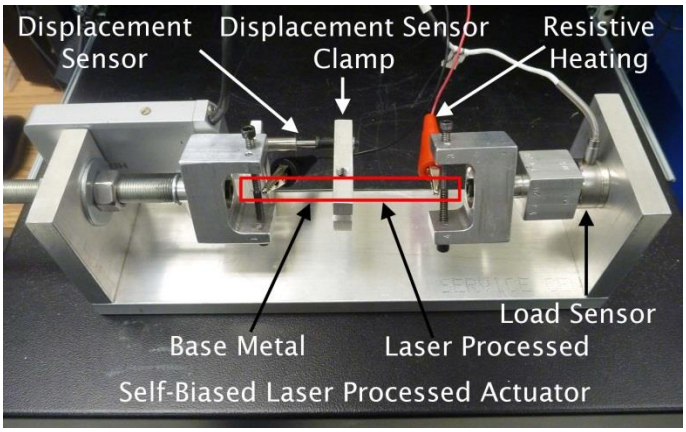

Figure 3.14: Self-biasing laser processed actuator fatigue tester with biasing base metal (BM) on the left and actuating laser processed NiTi (LP) on the right

A constant current Sorensen XG 33-25 programmable direct current (DC) power supply was used for joule heating of the actuator enabling transformation of the shape memory effect regions from martensite to austenite. The entire actuator was joule heated to prove applicability in passive as well as active situations. A fan was used to increase the convective cooling of the actuator so that the actuator could be cycled at a higher frequency (i.e. 0.04Hz). The load, displacement and current were measured using a National Instruments PXI-1031 data acquisition (DAQ) module.

4 Thermomechanical Fatigue of Laser Welded NiTi

The first investigation of the effect of laser processing on the properties of NiTi is to investigate the effect of a single laser processed spot, or a weld. This chapter investigates the effect of a bead on plate weld made in Ti-rich flexinol wire. The results reveal a significant effect of the weld on the physical and fatigue properties of the NiTi. Post-weld heat treatments improved the properties of the material by minimizing strain localization.

4.1 Microstructure

Both the welded and post-weld heat treated microstructures are shown in Figure 4.1. The low magnification optical microscopy analysis of these microstructures revealed that both the weld and post-weld heat treated samples had the coarse grained fusion zones typical of laser welded SMA wires [238]. The large reduction in grain boundary area, dislocations, precipitates and other structures that limit transformation induced plasticity make these coarse grained structures less stable than the ideal nanocrystalline NiTi base metals during thermomechanical cycling [163]. While being a small region of the wire, the substantially different properties of the welded region may have a significant effect on the performance of the welded assembly. The coarse grained structure was found to contain micron scaled dendrites when analysed at higher magnification as shown in Figure 4.1. These dendrites and the coarse grained heat affected zone did not change during the post-weld heat treatment because it was performed below the recrystallization temperature of NiTi [214, 269].

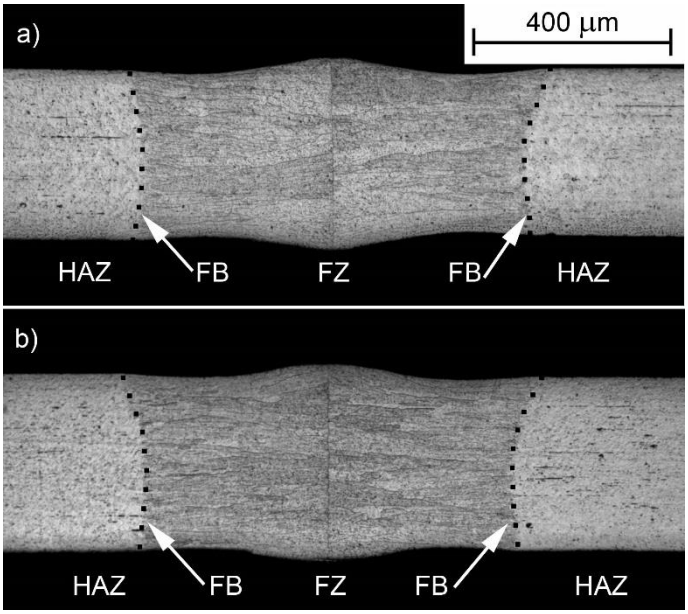

Figure 4.1: Optical micrograph of the a) welded and b) post-weld heat treated samples

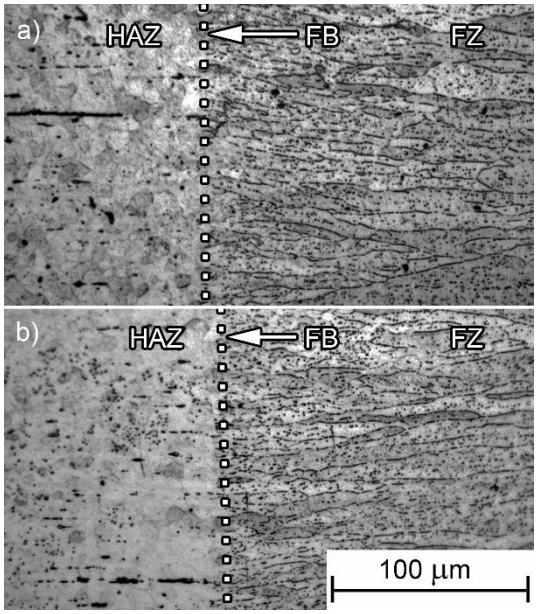

Figure 4.2: Optical micrograph of the heat affected zone and fusion zone in the a) weld and b) post-weld heat treated samples

4.2 Transformation Temperatures

The DSC analysis of the phase transformation properties of the base metal, solutionized base metal, welded and post-weld heat treated NiTi are shown in Figure 4.3 and Table 4.1. The forward austenite peak of the base metal was the amalgamation of both the martensite to R-phase and R-phase to austenite transformations. The R-phase is observed in materials that have undergone thermomechanical treatments to increase the dislocation density, form Ni-rich precipitates, or form nanocrystalline grains [39, 59, 270]. The constrictions of movement in the microstructure introduced by these features limit the strain that can be accommodated by the matrix, and leads to the intermediate R-phase transformation which has a lower strain than the austenite to martensite transformation [271, 272].

The solutionized base metal had the single stage transformation typical of large grained NiTi [190, 273]. This sample served as a reference for the heat affected zone in the welded samples. The transformation peaks of the solutionized base metal overlapped those of the welded NiTi, with these overlapping regions being related to the heat affected zone. The R-phase was not distinctly observed in the welded NiTi; however it may have been obscured in the overlapped peaks. The coarse grains, and low dislocation density would lead to single stage transformations in these regions [234]. However, oxygen pickup can lead to the formation of Ti_2Ni and Ti_2NiO phases in the fusion zone, which can induce the R-phase transformation [22]. The R-phase was observed in the post-weld heat treated wires. The grain structure of the fusion zone was not changed by the heat treatment, but the temperatures were sufficient to affect the dislocation density [196]. The change in dislocation networks, or the presence of base metal in the DSC specimen was responsible for the observed R-phase peak. Ni_4Ti_3 precipitates forming in the heat affect zones of laser welded NiTi have previously been identified as the source of the R-phase peak; however, it is unlikely that this phase formed in the current alloy [274].

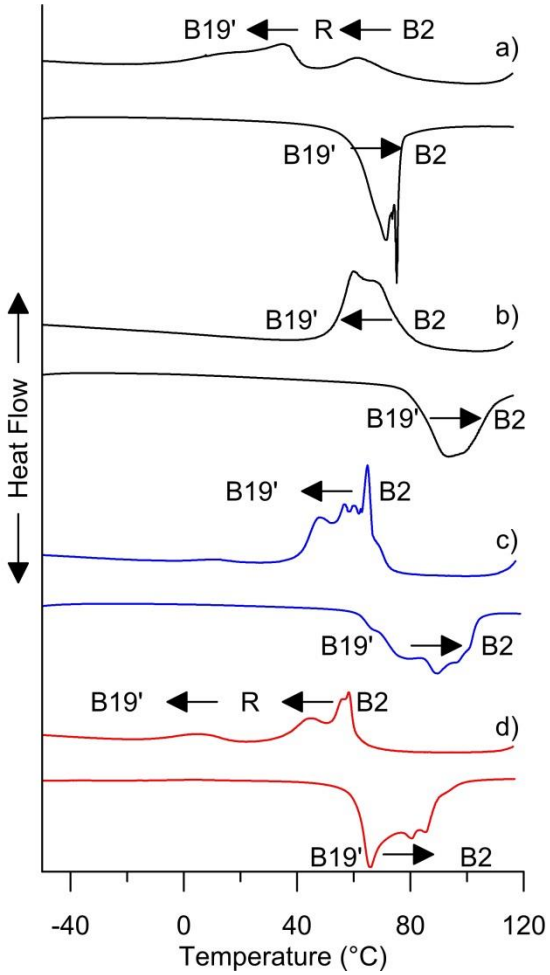

Figure 4.3: DSC of the transformation temperatures for a) base metal, b) solutionized BM, c) weld, d) post-weld heat treated samples

Table 4.1: Transformation temperatures (°C) of the base metal (BM), solutionized base metal (SOL), weld and post-weld heat treated (PWHT) samples. R_s in the PWHT sample is the beginning of the combined transformation peak and not the beginning of the R-phase transformation

	A_s	A_f	R_s	R_f	M_s	M_f
BM	58	77	74	51	41	2
SOL	81	110	N/A	N/A	80	52
Weld	61	105	N/A	N/A	73	40
PWHT	57	92	63	29	17	-16

4.3 Tensile Properties

The tensile failure properties of the base metal, weld, and post-weld heat treated samples at room temperature and 87 °C (i.e. 10 °C above the A_f of the base material) are shown in Figure 4.4. As shown in Table 4.2, at room temperature the welded samples maintained 86 % ± 1 % of the ultimate tensile strength (UTS) of the base material and had an increase in ductility. The post-weld heat treated samples had the same UTS and a further increased ductility. At 87 °C the base metal maintained 94 % ± 4 % of the base metal UTS but had a reduced ductility, while the post-weld heat treated sample maintained 78 % ± 1 % of the base metal UTS and had a slightly increased ductility. The heat affected and fusion zones of the welded samples experienced annealing temperatures which destroyed dislocations [35, 58, 196, 275], and increased grain size as shown in Figure 4.2. This coarsening of the microstructure resulted in the observed decrease in ultimate tensile strength and increase in ductility of the welded samples compared to the base metal.

Application of the post-weld heat treatment was done to the entire gauge length of the wire. No grain growth was observed in the fusion zone, and as discussed in the previous section, a change in the transformation temperatures indicated alteration of the dislocation density in the material. These phases increase the strength and decrease the ductility of the heat affect and fusion zones. This would have had minimal effect on the fusion and heat affected zones, however the remaining base material in the gauge length had a reduction in dislocation density [6, 196, 237], which contributed to the increased ductility and decreased UTS of the post-weld heat treated sample compared to the base material and welded samples. These changes in the post-weld heat treated samples also resulted in the formation of a clear martensite detwinning plateau, and a small initial R-phase plateau. The R-phase plateau was present due to the shift in transformation temperatures observed in Figure 4.3.

The localized alteration to the microstructure in the welded and post-weld heat treated samples led to necking in the wires which further contributed to the decreased properties [241]. The ductility of these wires was reduced during pseudoelastic deformation (i.e. tensile test at 87 °C) due to this strain localization, which correlated well with previous work in welded pseudoelastic wires [238]. The higher pseudoelastic stress plateau of the post-weld heat treated samples

compared to the base metal was due to the shift to a lower A_f shown in Figure 4.3. This higher plateau contributed to a greater plastic deformation in these samples compared to the base metal during the stress-induced phase transformation. Furthermore, the presence of both martensite in the weld region, and austenite in the base metal resulted in an interface between these two phases, with plastic deformation being reported to occur at these interfaces [6, 75].

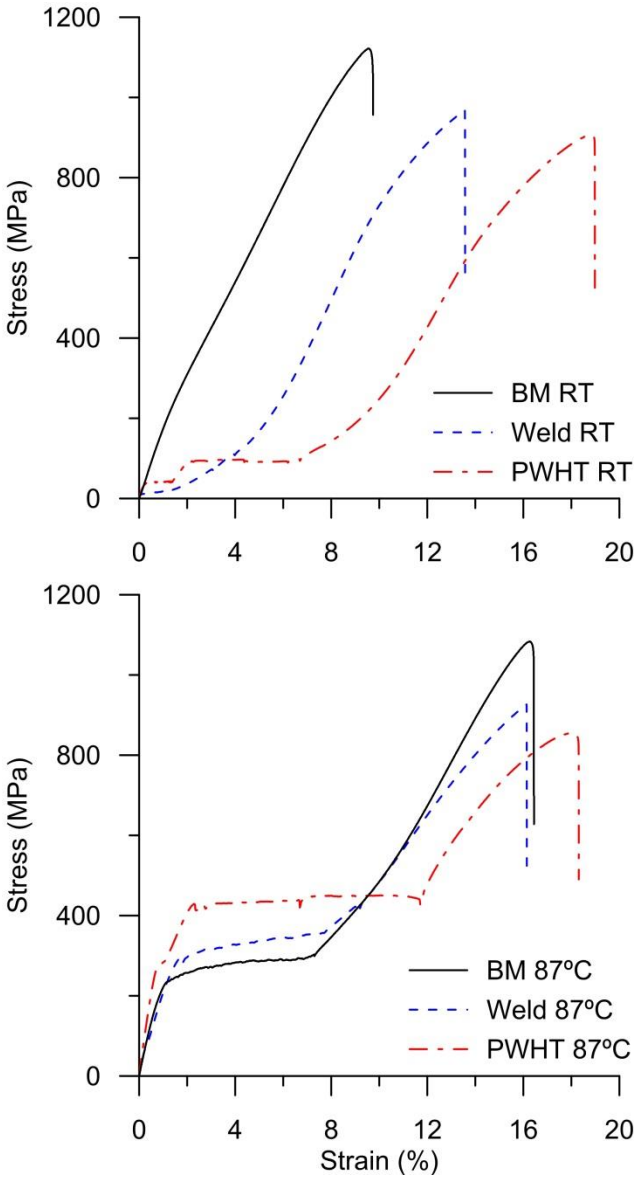

Figure 4.4: Tensile failure of the base metal (BM), weld and post-weld heat treated (PWHT) samples at room temperature (top) and 87°C (bottom)

Table 4.2: Comparison of the ultimate tensile strength (UTS) and ductility of the weld and post-weld heat treated (PWHT) to the base metal

	Room Temperature		87 °C	
	% BM UTS	% BM Ductility	% BM UTS	% BM Ductility
Weld	86 ± 1	135 ± 10	94 ± 4	86 ± 0
PWHT	86 ± 1	191 ± 3	78 ± 1	106 ± 0

4.4 Cyclic Properties

Single tensile cycles followed by the zero-load shape memory effect recovery of the base metal, welded and post-weld heat treated samples are shown in Figure 4.5. The welded and post-weld heat treated samples had lower detwinning stresses than the base metal for the previously discussed microstructural and phase reasons; however, their recoverable strain was unaffected during a single cycle. All three samples recovered their strain fully under zero-load heating. Small deflections from the linear detwinning plateaus observed in the welded and post-weld-heat treated samples were related to the detwinning of the martensite in the different regions of the material (i.e. base metal, heat affected zone, fusion zone), which have different grain sizes, with respective differences in detwinning stresses [276, 277].

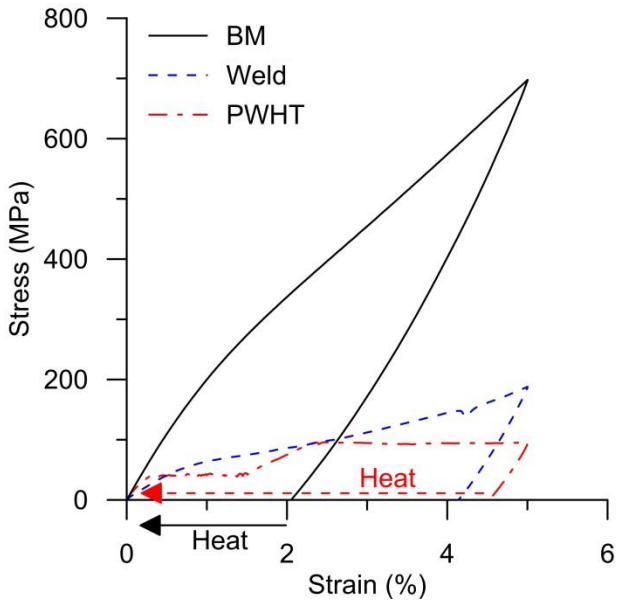

Figure 4.5: Tensile cycle followed by zero-load shape memory recovery of the base metal (BM), welded and post-weld heat treated (PWHT) samples.

Thermomechanically cycling the wires while under load resulted in a significant difference in the properties of the base metal, welded, and post-weld heat treated samples as shown in Figure 4.6. Actuation strain was measured as the change in strain between the austenitic and martensitic states of the material. The plastic strain was measured as the change in strain of the martensitic state of the material. The base metal sample had the highest number of cycles to failure, and retained the greatest amount of actuation throughout cycle life. The welded sample had a rapid reduction in actuation, high necking and low cycles to failure compared to the base material. The post-weld heat treated samples had improved cycle life and actuation stability compared to the welded samples. The reduction in actuation strain and increase in plastic strain during thermomechanical cycling were related to the creation and motion of dislocations as the habit plane passed through the material [59, 72, 74]. Reduction in transformation strain was resultant from the buildup of these dislocations which formed retained martensite that no longer transformed [278]. This same dislocation activity resulted in plastic elongation of the wires, which also contributed to the necking.

The fine-grained, cold worked and precipitation hardened modern SMAs are designed to impede plastic buildup in the material in order to maintain geometric and actuation properties [59]. Decrease of the actuation strain and increase of the plastic strain in the welded NiTi occurred because the coarse grained, dislocation lean heat affected zone and fusion zones could not impede the rapid buildup and motion of dislocations [59, 190, 279]. The post-weld heat treated samples had a reduction in dislocation density in the remaining base metal of the gauge length resulting in a gauge length with more consistent properties than the as-welded wires. This reduced the strain localization in the coarse grained region, and led to a stability of actuation strain similar to that observed in the base material. The elongation of the wires during the tests resulted in the extension of the biasing spring being reduced throughout the cycle life of the samples. This reduction in biasing load was responsible for part of the reduction in actuation strain.

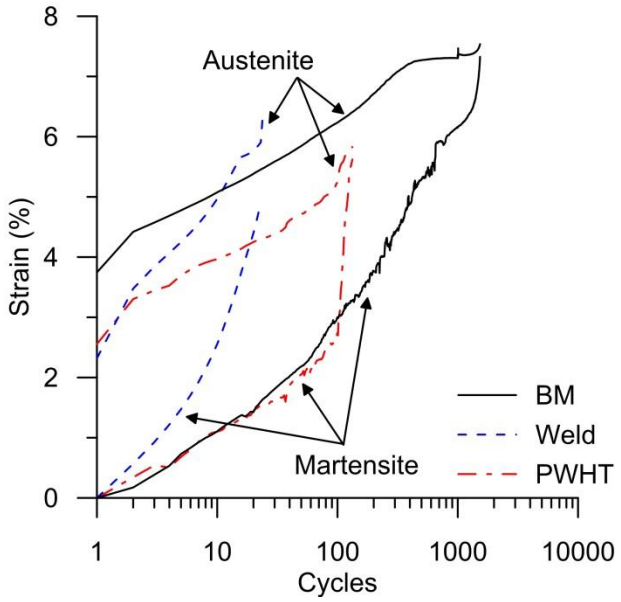

Figure 4.6: Evolution of tensile strains in the heated austenite and cooled martensite state of the base metal (BM), weld, and post-weld heat treated (PWHT) samples that were pre-loaded to 40 N (i.e. 350 MPa)

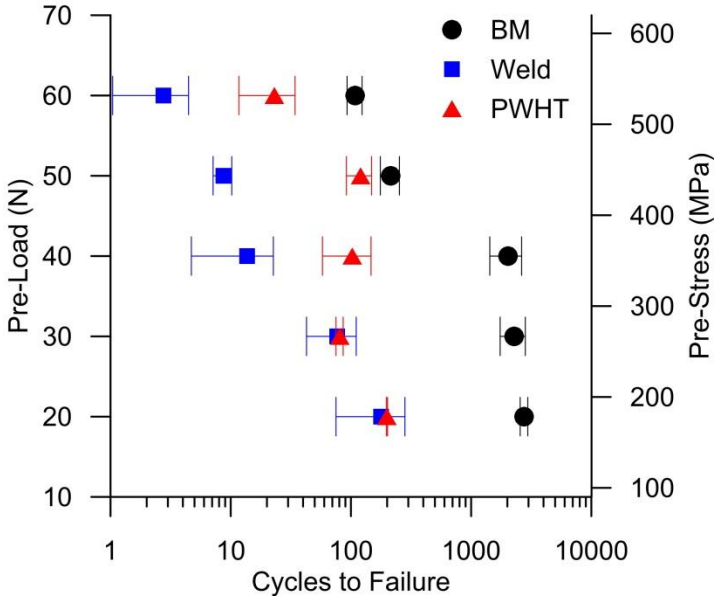

Figure 4.7: Cycle life versus pre-load of the base metal (BM), weld, and post-weld heat treated (PWHT) samples

The cycle-life of the base metal, welded and post-weld heat treated samples loaded to different pre-loads are shown in Figure 4.7. The welded and post-weld heat treated samples pre-loaded to

20 and 30 N (i.e. 186 and 279 MPa) experienced significant plastic elongation to the point where the biasing spring was fully unloaded. Unloading of the biasing spring resulted in the samples not failing via fracture; therefore, failure for these samples was defined as the cycle at which the actuation strain was less than 0.2 %. This lack of fracture resulted in little to no change in the cycle lives of the welded and post-weld heat treated samples as shown in Figure 4.7. In all other samples failure occurred by fracture. Analysis by pre-load and not stress was chosen because the stress state of the samples changed during testing due to the necking of the wires and the unloading of the biasing spring. The equivalent pre-stress was provided for reference on the right side of Figure 4.7. A non-constant biasing load was chosen to be studied as a real-world example of application instead of the standard constant load testing.

The welded samples had the lowest fatigue life compared to the base metal and post-weld heat treated samples. The coarsening of the grains, and destruction of dislocations enabled significant dislocation activity during themomechanical cycling, leading to the low fatigue life. After post-weld heat treatment the samples had a significant improvement in fatigue life. The more uniform gauge length properties contributed to the improvement in cycle life. These improvements in thermomechanical fatigue properties were similar to the improvements observed in mechanical fatigue of pseudoelastic NiTi wires [237, 238].

Low fatigue lives observed in these wires were compounded by a number of factors in the testing protocol. The high loads, and non-constant biasing stress both have been shown to reduce fatigue life [280]. The high loads were chosen to shorten testing time, which at these low test frequencies can take months or up to a year to complete, and are generally reserved for proving out real-world design [59]. The power used to heat the wire was selected to rapidly heat the wire; however, it may have contributed to overheating evidenced by oxidation of the wires, which can reduce cycle life. Overheating of the centre of the wire can occur due to heat sink effects of the grips on the ends of the wires, which can reduce cycle life [176]. The transformation temperatures of NiTi may decrease as thermomechanical cycling occurs, which can lead to more severe overheating [65, 176]. Partial transformation (i.e. lower heating), and lower loads in the actual applications would significantly reduce the plastic strain, improve retention of actuation strain and the cycle life [59, 237].

4.5 Summary

This study was the first investigation on the effects of welding, and a post-weld heat treatment on the thermomechanical fatigue of NiTi shape memory alloys. Several areas of key interest were identified:

1. The welding protocol used in this investigation achieved 86 % of the base metal ultimate tensile strength; however, this metric was not an adequate gauge for thermomechanical fatigue properties.
2. The welded wires had greater buildup of plastic strain and degradation of actuation strain than the base metal during thermomechanical cycling, with a significantly lower fatigue life.
3. The post-weld heat treated wires had similar plastic strain buildup, and actuation strain degradation to the base metal during thermomechanical cycling. This reduction in strain buildup led to an order of magnitude increase of the fatigue life compared to the welded wires.

5 Laser Processing and Thermomechanical Treatment of NiTi Wires

The previous section investigated the effect of a single laser weld on a Ti-rich wire. The laser welding process coarsened the microstructure and reduced the fatigue life by orders of magnitude compared to the base metal. A post-weld heat treatment reduced the strain localization at the weld and increased the fatigue life of the samples. If a wire is completely processed (i.e. re-melted) then this treatment would not be effective. If the wire is Ni-rich then some strengthening would be provided via Ni_4Ti_3 precipitates; however, to achieve optimal properties both cold work and heat treatment would need to be applied to take advantage of the strengthening mechanisms of grain size reduction and precipitate hardening [6]. Furthermore, precipitate strengthening was not an option because the current study focused on laser processing to create Ti-rich NiTi, in order to create two-memory actuators.

Laser processing of SMAs to control their local composition and properties was discovered in the past decade [16]. Since its inception, development has been largely focused on components with multiple pseudoelastic plateau stresses, like the orthodontic archwire 'SmartArch' [13]. This prior work included the development of thermomechanical treatments for returning pseudoelasticity to laser processed NiTi sheets. These investigations focused on single tensile and thermal cycles.

The current work has developed a method to treat laser processed wires, which are the most commonly used shape memory alloy geometry [5]. This treatment was developed with the intent of improving the physical and fatigue properties of the material. The focus of the study is on the effect of multiple tensile, and thermomechanical cycles on the response of the material. This is the first in investigation into the stability of treated laser processed SMA wires, which has produced promising results with fatigue lives of trained wires matching those of industry made wire.

5.1 Laser Processing to Change Bulk Composition

Pequegnat et al. [13], and Khan et al. [16] investigated the use of laser processing to alter the chemistry and phase transformation properties of NiTi SMA sheets. These investigations showed the repeatability of laser processing in changing the elemental content and transformation

temperatures of SMAs. Wire is the most widely used SMA geometry but there has been no published in depth study of the repeatability of laser processing with these materials. The current study investigated the effect of multiple laser pulses on a single spot on a wire. Micro-PIXE analysis of these laser processed spots revealed a consistent reduction of 0.23 at.% Ni with each successive laser pulse, as shown in Figure 5.1. The first laser pulse removed 0.40 at.% Ni, a larger amount than the average, because the wire drawn surface finish was less reflective than the laser processed surface. There was no change in rate observed from the Ni-rich to the Ti-rich regions of the phase diagram. The point at which Ni reduction no longer affects the change of transformation temperatures has been reported to be 49.7 at.% Ni [22]. Beyond this point the matrix maintains a constant composition and any excess Ti forms the brittle Ti_2Ni phase. In the current study this saturation point was reached between 4 to 5 laser pulses, as shown by the plateau in the M_s temperature in Figure 5.2. The phase transformation and composition data was used to plot the relation between Ni content and M_s temperatures, which is shown in Figure 5.3. The slope of the change in M_s with change in at.% Ni was first investigated by Tang et al. [68], but the study depended heavily on literature for experimental validation of the model derived to predict the relationship between M_s and at.% Ni. A more recent study by Frenzel et al. [22], made a series of vacuum cast specimens controlled to specific compositions, which were used to calculate a slope of -83 K / at.% Ni. In their study of laser processing of sheets Pequegnat et al. [13] calculated a slope of -72.36 K / at.% Ni, and attributed the variation from Frenzel et al.'s work to the uptake of oxygen, which is known to decrease the transformation temperature of NiTi [24]. The current study calculated a slope of -68.76 K / at.% Ni which is in the range of the value determined by Pequegnat et al. [13], due to the oxygen dissolution into the fusion zone that occurs during laser processing.

The laser processing of the tensile specimens used in the current work was designed to make a Ti-rich material for actuation above room temperature. To achieve this goal a composition in the range of 4 to 6 pulses was desired, which would be minimize Ti-saturation, thereby minimizing the formation of the brittle Ti_2Ni phase while maximizing the transformation temperature. DSC analysis presented in Figure 5.8 confirmed the desired transformation temperatures were achieved.

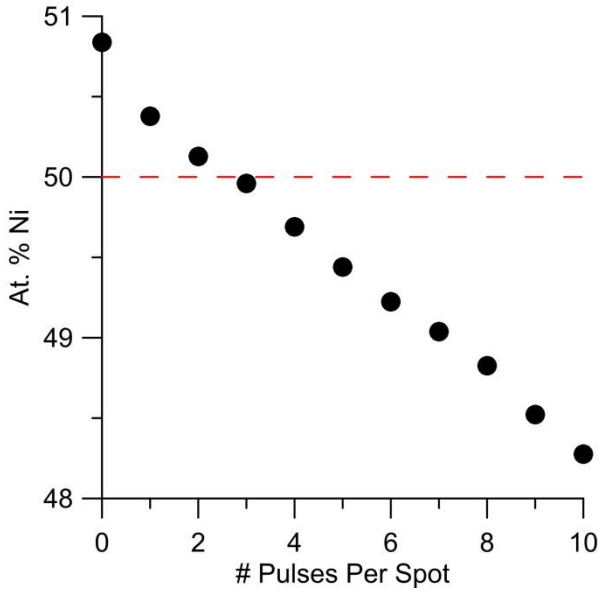

Figure 5.1: Micro-PIXE analysis of change in Ni content with number of laser pulses per spot

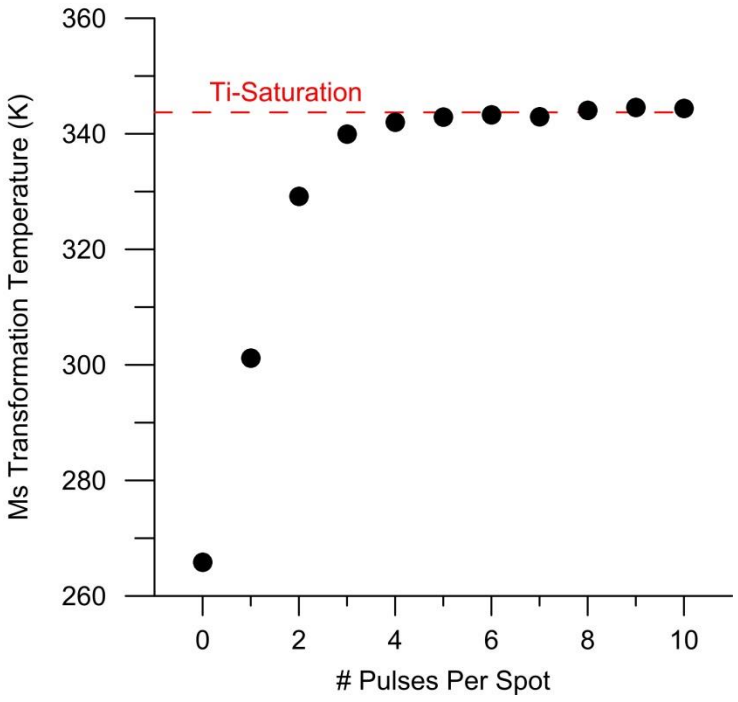

Figure 5.2: Change in M_s temperature with number of laser pulses per spot

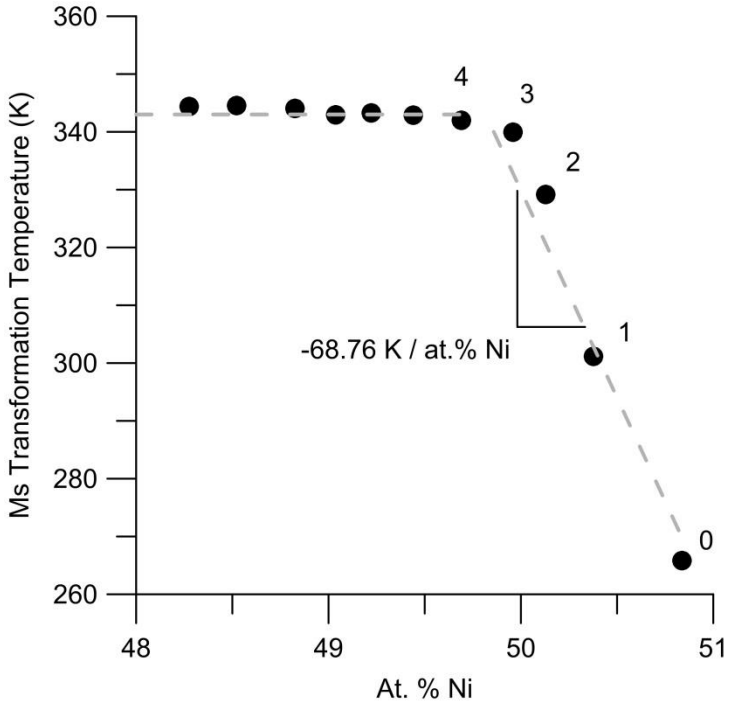

Figure 5.3: Change in M_s temperature vs at.% Ni. Number of laser pulses per spot before saturation indicated (i.e. 0, 1, 2, 3, 4)

5.2 Microstructure and Phase Analysis

TEM analysis of the base material is shown in Figure 5.4. Darkfield TEM analysis was used to measure the grain size to be 70 nm. The small scale of the grains was confirmed by the ringed diffraction pattern shown in Figure 5.4a. This grain size is desired for stability of transformation in NiTi SMAs [163]. These nanocrystalline microstructures limit the dislocation activity responsible for transformation induced plasticity during repeated cycles of either pseudoelastic or shape memory phase transformations [59, 163]. The Ni-rich material was confirmed to be B2 austenite at room temperature by SAD analysis in Figure 5.4a. High purity of NiTi is required to avoid the formation of excessive amounts of brittle oxide and carbide inclusions so that long fatigue lives can be achieved [26, 27, 29-31]. However the high reactivity of the material leads to the inevitable formation of these inclusions, with costly process controls required to avoid large amounts of these phases during the vacuum casting methods used to form and homogenize the ingots [183]. Ti_2NiO_x oxides (Figure 5.4b), and TiC carbides (Figure 5.4c) form the majority of inclusions in NiTi SMAs achieved [26, 27, 29-31]. These phases cannot be dissolved via heat treatment, but are reduced in size by being fractured during cold working and forming particle-

void-assemblies as shown in Figure 5.4b. These hard phases and their delamination with the surrounding matrix serve as mechanisms for reduction of material strength, and crack initiation points especially when they are located on the surface of the material [31]. No Ni_4Ti_3 strengthening precipitates were located; however, they may be indistinguishable from the matrix due to the nanocrystalline size, and they can be obscured in grain boundaries.

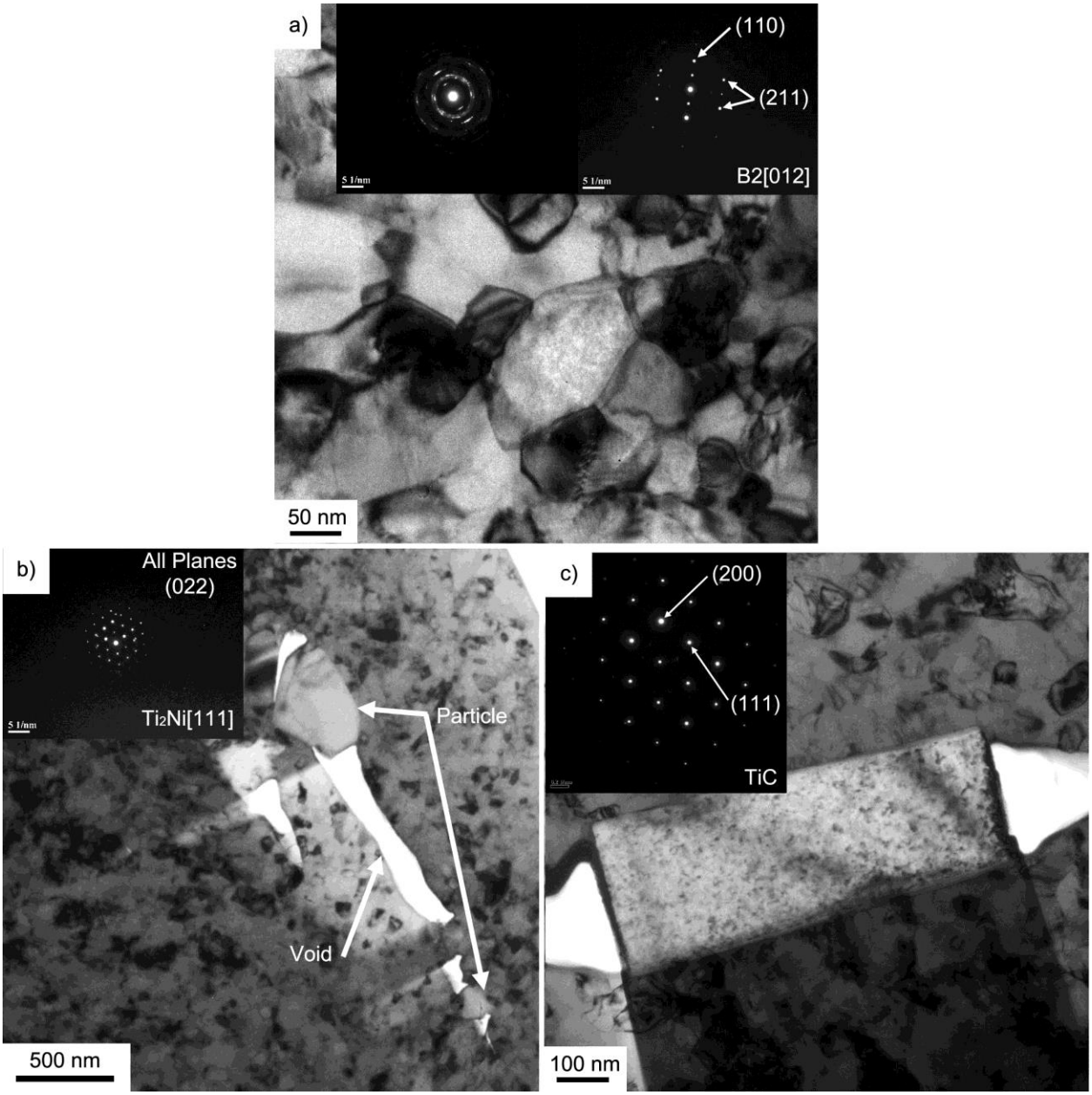

Figure 5.4: TEM analysis of a) NiTi base metal, SAED from multiple grains (left), and from a single grain (right), b) Ti_2NiO_x oxide identified as particle in image, SAED of the large particle on the left, c) Rectangular inclusion identified as TiC carbide by SAED

Laser processing of the NiTi involved the full re-melting of the material with laser energy. As discussed in the experimental section, the weak point of the weld centreline was removed by overlapping the welds 60 % in order to accommodate the wire drawing process. However, to avoid Ti saturation and large amounts of brittle Ti_2NiO_x phases, a balance of centreline and Ni removal was required. Therefore, minimal overlap was used, which resulted in part of the centreline remaining. The microstructure is shown in Figure 5.5a, with both the fusion boundaries, and the remaining centreline indicated. This fusion zone is dominated by large columnar dendrites (Figure 5.5b), which is typical of welded NiTi wires [233, 281]. There is also a small region of planar growth at the fusion boundary. The low cross sectional area of the wires limits the heat conduction away from the joint, which limits the cooling rate of the fusion zone, resulting in the planar growth at the fusion boundaries, and the columnar dendrites in the fusion zone [233, 238, 282]. Epitaxial growth is shown by the dendrites indicated in Figure 5.5b and c, which cross the fusion boundary. The microstructure of the laser processed NiTi is coarse compared to the nanocrystalline base metal, with the grains and dendrites in the micron scale. TEM analysis of the laser processed NiTi is shown in Figure 5.6. The diffraction pattern in Figure 5.6a indicates that the material was in the B19’ phase at room temperature. Figure 5.6b shows a larger amount of Ti_2NiO_x compared to the base metal, due to the saturation of Ti in the matrix. Compositional analysis was used to confirm the identity of these inclusions. The Ti_2NiO_x phase formed by microsegregation along the dendrite boundaries [283].

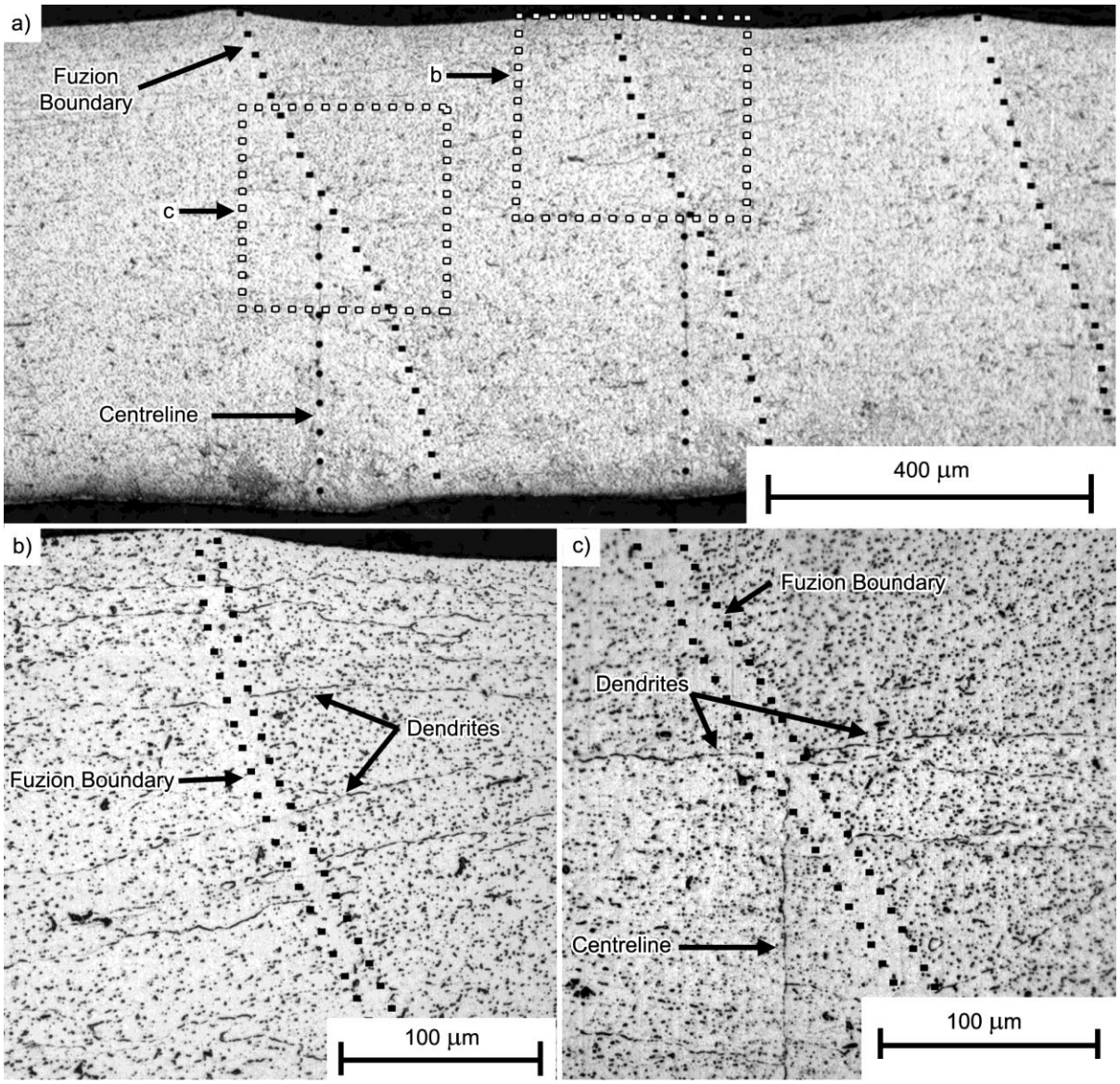

Figure 5.5: Optical micrograph of a) laser processed NiTi cross section, b) fusion boundary, c) centerline of partially overlapped fusion zone

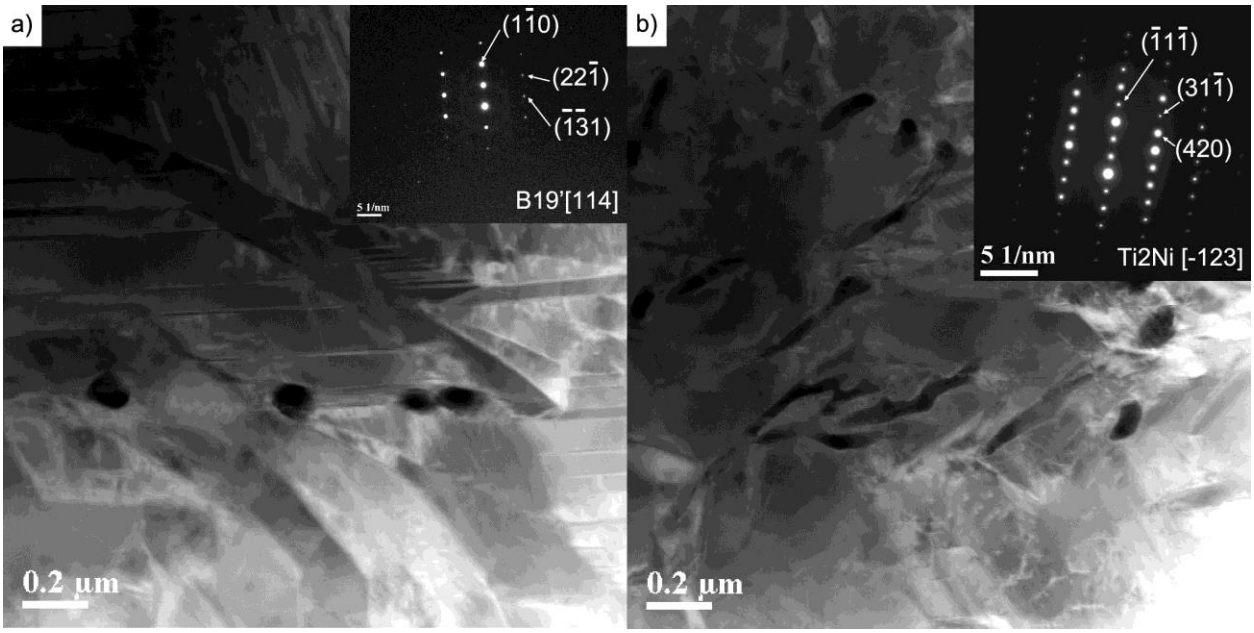

Figure 5.6: STEM of laser processed NiTi a) twinned matrix and SAED from a large region of the coarse microstructure, b) Ti_2NiO_x phase (darker) in matrix identified by SAED

TEM analysis of the microstructure of the treated laser processed NiTi is shown in Figure 5.7. The microstructure was refined to a nanograined material with an average grain size measured via dark-field imaging of 29 nm. This small grain size geometrically confined the matrix so that the constricted compound (001) twinning of nano-scaled microstructures formed (Figure 5.7a), instead of the larger length scaled type I and II twins (Figure 5.6a) of coarser microstructures that was observed in the laser processed NiTi [272]. The Ti_2NiO_x inclusions shown in Figure 5.7b were fractured and formed into particle-void-assemblies during the wire drawing process.

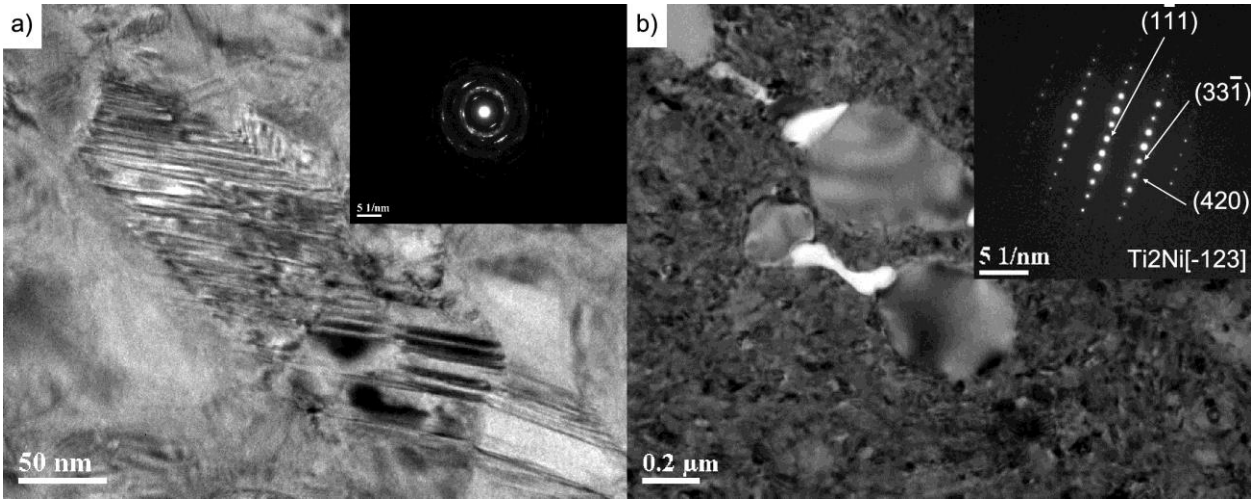

Figure 5.7: TEM of a) treated laser processed NiTi matrix with SAED of multiple grains, b) Ti_2NiO_x particle void assemblies identified by SAED

The DSC results of the phase transformations of the materials are shown in Figure 5.8. The B19' phase transformation was suppressed in the base metal, and the R-phase transformation occurred due to the nanocrystalline microstructure [284]. The presence of the R-phase in the forward and reverse transformations was due to the geometric constriction of the matrix by the grain boundaries, leading to lower strain intermediate R-phase [39].

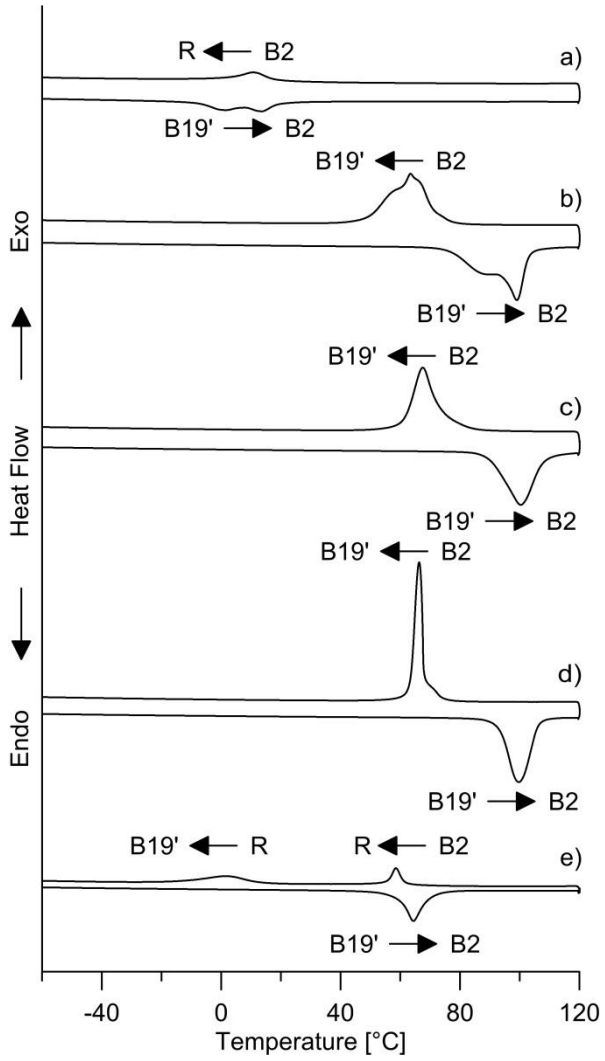

Figure 5.8: DSC analysis of transformation temperatures of a) base metal, b) laser processed NiTi, c) laser processed NiTi solutionized at 1000C, d) cold drawn to 0.62 µm and heat treated at 600 °C for 10 min, e) treated laser processed NiTi

Table 5.1: Transformation temperatures (°C) of the a) base metal (BM), b) laser processed NiTi (LP), c) laser processed NiTi solutionized at 1000 °C (LP 1000°C), d) cold drawn to 0.62 µm and heat treated at 600 °C for 10 min (LP CW 600°C), e) treated laser processed NiTi (T-LP)

Sample	M_f	M_s	R_f reverse	R_s reverse	A_s	A_f	R_s forward	R_f forward
BM	-	-	-0.10	19.12	-8.81	-	-	22.70
LP	48.62	74.18	-	-	74.86	103.20		
LP 1000°C	60.18	77.66	-	-	88.48	109.26		
LP CW 600°C	62.94	74.16	-	-	92.63	106.53	-	-
T-LP	-15.36	13.80	49.85	62.25	55.35	73.46	-	-

Laser processing coarsened the microstructure, and removed a significant amount of Ni resulting in the material being Ti-rich. The resultant transformation temperatures reached the range of the maximum potential temperatures of NiTi with an M_s of 74.18 °C as shown in Figure 5.8b. The deviation observed in the laser processed NiTi curves compared to the smooth curves of the solutionized NiTi was related to inhomogeneity across the fusion zones [16]. Solidification during welding can cause inhomogeneity across the fusion zone due to microsegregation of the alloy constituents as the solidification front grows [6, 16, 282]. Solutionization of the laser processed NiTi resulted in the homogenization of the processed regions as shown by the single smooth peak in Figure 5.8C. After cold work to 0.62 µm and inter annealing the transformation peaks narrowed due to a homogenization of the microstructutre into a uniform grain size [190].

After the final heat treatment the material had the R-phase and suppressed transformation temperatures typical of nanograined NiTi [284]. The Ti-rich material had no Ni_4Ti_3 precipitates, meaning the presence of R-phase was solely due to the geometric constriction of the grains.

5.3 Tensile Deformation

NiTi SMAs have a significant change in their tensile properties depending on their temperature and phase present [6, 59]. Lower temperatures will have martensite detwinning, while higher temperatures will have pseudoelastic deformation. Failure of the samples was compared at temperatures sufficiently above M_d (i.e. the temperature above which the stress for slip is below the stress for inducing the martensite transformation) to ensure that there were no longer any pseudoelastic properties in the material (i.e. A_f + 175 °C). This enabled comparison of the

materials without the influence of the phase transformations. The Ni-rich nanocrystalline base metal had the highest ductility and ultimate tensile strength of the three materials as shown in Figure 5.9 and Table 5.2. The coarse grained and Ti_2NiO_x embrittled laser processed NiTi achieved 71% of the base metal UTS and 40 % of the base metal ductility. The treated laser processed NiTi had a significant improvement in properties with a UTS of 95 % of the base metal and a ductility of 68 % of the base metal. Ti-rich NiTi alloys have a lower UTS and ductility than Ni-rich NiTi, due to the larger amount of brittle Ti_2NiO_x phases [6, 59]. The ductility of the treated laser processed wire was lower than the base metal due to these brittle phases, which had a stronger effect than the reduction in grain size. Change in texture of the laser processed materials may also have contributed to the loss of physical properties [4]. Other contributors to the observed difference in properties include the thermomechanical treatments applied by the manufacturer compared to those used in the current study. Further optimization of the current parameters could lead to an improvement in the properties of the treated laser processed NiTi.

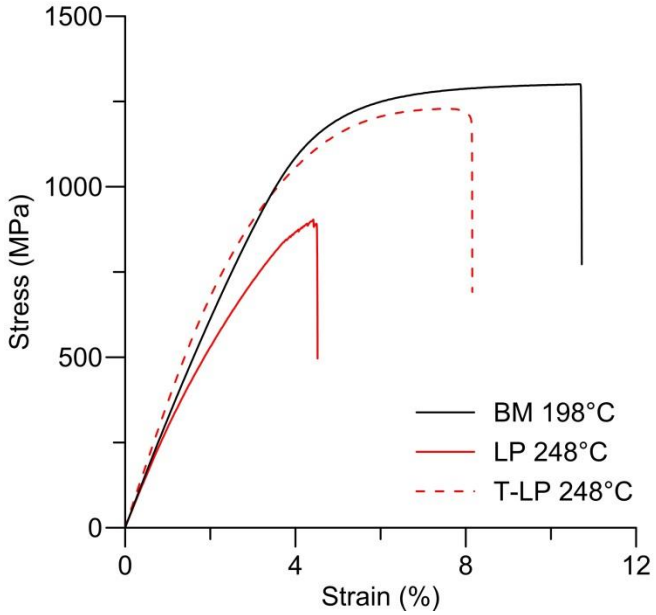

Figure 5.9: Tensile failure of the base metal (BM), laser processed NiTi (LP), and the treated laser processed NiTi (T-LP) at M_d + 175 °C

Table 5.2: Tensile properties of the base metal (BM), laser processed NiTi (LP), and treated laser processed NiTi (T-LP) at M_d + 175 °C

	Ultimate Tensile Strength (MPa)	Ductility (%)
BM	1298.61 ± 3.06	11.93 ± 1.71
LP	925.02 ± 66.76	4.76 ± 1.10
T-LP	1235.52 ± 5.98	8.08 ± 0.28

5.4 Transformation Properties

The pseudoelastic response of the base metal over 100 tensile cycles is shown in Figure 5.10, and the plastic and pseudoelastic strains at the 100th cycle are shown in Table 5.3. The increase in plastic strain observed as the cycles progressed is due to the multiplication and displacement of dislocations that occurs as the phase transformation moves through the material [59, 72]. The base metal had a low plastic strain due to the small grain size which limits transformation induced plasticity (i.e. dislocation activity) [163, 225]. The grain size of this material was designed to limit the transformation induced plasticity and ensure a stable phase transformation. The reduction in pseudoelastic stress as the tensile cycles progressed was previously theorized to be due to the reorientation of the microstructure into a preferred direction for pseudoelastic deformation, and the presence of retained martensite; however, the change in response of the material was recently proven to be due to the buildup of dislocations which alters the transformation from a propagating transformation front, to a uniform transformation the gauge length [6, 88]. This effect is also responsible for the reduction in hysteresis. The broadened peaks of the base metal transformation observed in the DSC results of Figure 5.8 indicated that the base metal had undergone a stabilization protocol [59]. This contributed to the limited plastic strain buildup and the stable pseudoelastic response.

Table 5.3: Plastic strain and pseudoelastic strain of the base metal (BM), and treated laser processed NiTi at the 100th cycle of deformation to 5 % strain at A_f + 20 °C.

	Plastic Strain %	Pseudoelastic Strain %
BM	0.73	4.23
T-LP	2.36	2.64

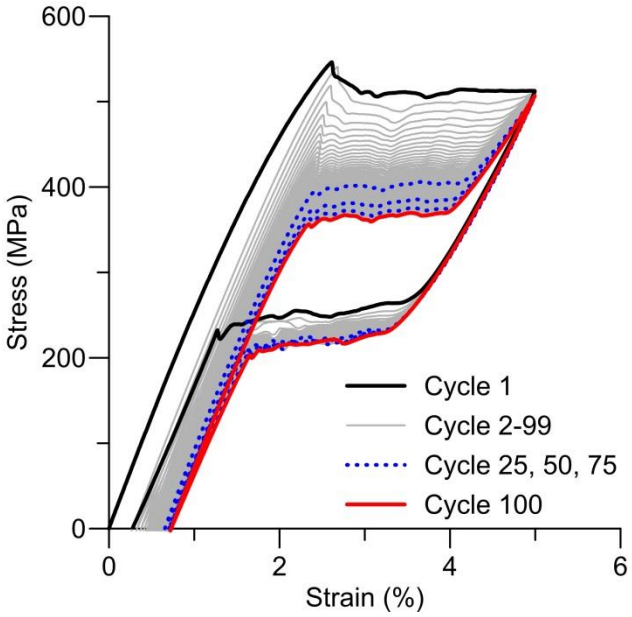

Figure 5.10: Pseudoelastic tensile response of base metal cycled to 5 % strain, at 43 °C (i.e. A_f + 20 °C)

The coarse grained laser processed NiTi had a yield stress that was lower than that required for stress-induced martensite [13]; therefore, no pseudoelastic behaviour was observed as shown in Figure 5.11. The low UTS and ductility of this material resulted in failure occurring after 17 cycles.

The treated laser processed NiTi regained the pseudoelastic effect as shown in Figure 5.12. The grain refinement served to increase the strength of the material to enable the pseudoelastic properties. However, the pseudoelastic response changed from that observed in the base metal to the response of a material with 30 nm grains [285], which achieved 62 % of the base metal pseudoelasticity. This small grain size constricted the maximum recoverable strain, resulting in the observed decrease in pseudoelastic strain, and collapse of the hysteresis [39, 285].

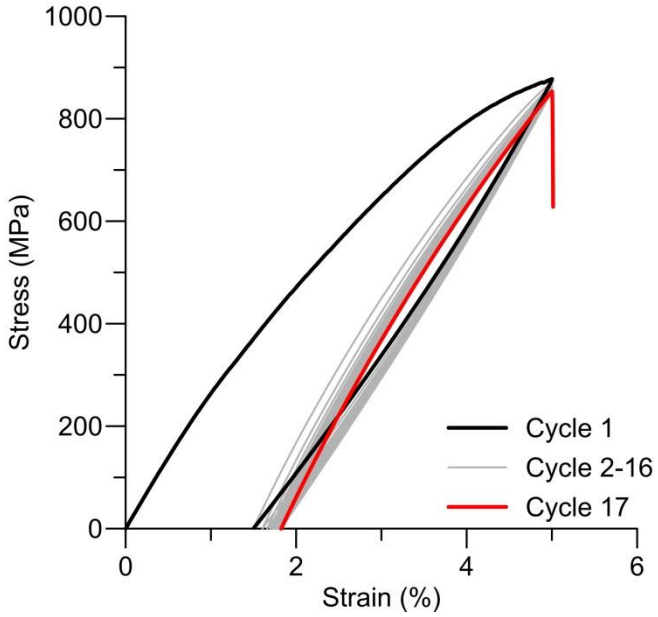

Figure 5.11: Pseudoelastic tensile response of laser processed NiTi cycled to 5 % strain, at 123 °C (i.e. A_f + 20 °C)

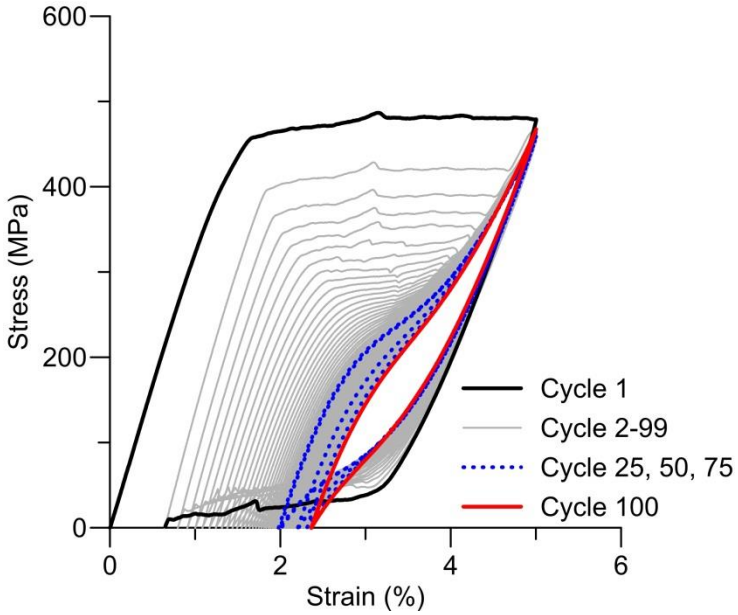

Figure 5.12: Pseudoelastic tensile response of treated laser processed NiTi cycled to 5 % strain, at 94 °C (i.e. A_f + 20 °C)

Tensile cycling and zero-load recovery of the base metal at a temperature below the R_f of the base metal are shown in Figure 5.13, and Table 5.4. The initial R-phase plateau was observed in

the tensile curve, followed by the higher stress martensite detwinning curve. Plastic deformation of the R-phase resulted in a lager plastic strain of the materials cycled in the thermal martensite phase than the cycling of pseudoelastic austenite phase. The lower stress required for detwinning the thermal martensite resulted in the shape memory effect stabilizing within a smaller number of cycles than the pseudoelastic effect [286].

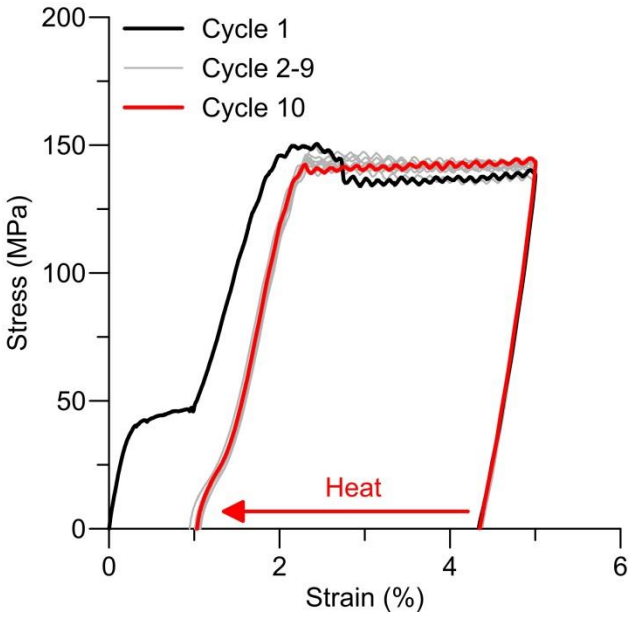

Figure 5.13: Tensile cycling to 5 % strain at -26 °C (i.e. M_f of treated laser processed NiTi -10 °C), and zero-load shape memory recovery of the base metal

Table 5.4: Plastic strain and shape memory recovery strain after 10 tensile cycles to 5 % strain at M_f – 10 °C, and zero-load shape memory recovery of the base metal (BM), laser processed NiTi (LP), and treated laser processed NiTi (T-LP)

	Plastic Strain %	Shape Memory Strain %
BM	1.03	3.36
LP	2.66	1.02
T-LP	2.52	1.81

The cyclic tensile deformation of the laser processed NiTi is shown in Figure 5.14. This coarse grained microstructure was unable to block dislocation activity so exhibited strain hardening during martensite detwinning [13], leading to 260 % of the plastic strain of the base metal, and a shape memory recovery of 30 % of the base metal.

The treated laser processed NiTi (Figure 5.15) had a shape memory recovery of 54 % of the base metal, and a plastic strain of 245 % of the base metal. The reduced grain size constricted the matrix, resulting in a lower recoverable strain [39, 225, 285]. This resulted in only a portion of the 5 % strain being recoverable, with the remainder being lost to plastic strain via permanent deformation of the grains. The larger grains of the base metal constrict the matrix less, enabling greater self-accommodation and reorientation of the twins instead of permanent deformation via slip [225].

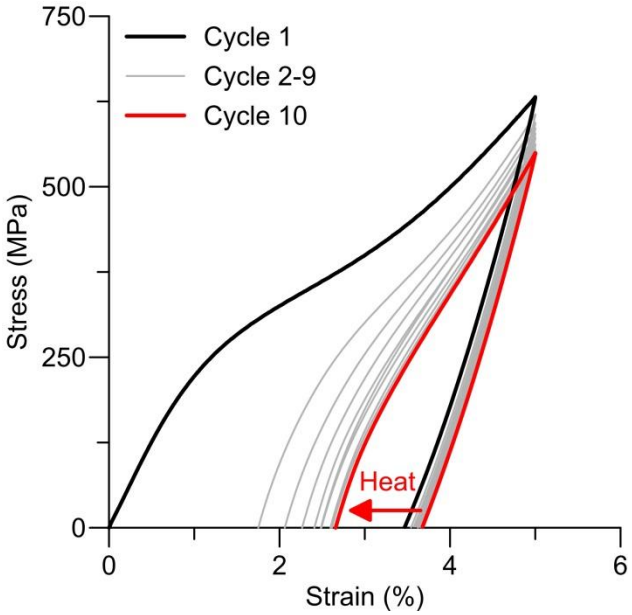

Figure 5.14: Tensile cycling to 5 % strain at 38°C (i.e. M_f -10 °C), and zero-load shape memory recovery of the laser processed NiTi

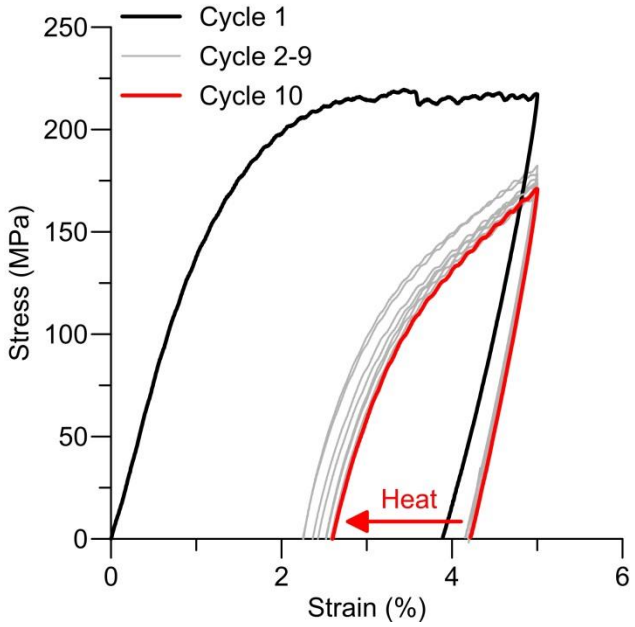

Figure 5.15: Tensile cycling to 5 % strain at -26 °C (i.e. M_f -10 °C), and zero-load shape memory recovery of the treated laser processed NiTi

5.5 Multiple Memory Actuation

Laser processing of SMAs has a wide range of revolutionary applications that the can be advantageous to multiple industries. One of these opportunities is the development of SMAs that have different transformation temperatures in a single component. Initial exploration of this concept was on coarse grained actuators that had the physical limitations explored above. With the development of the thermomechanical treatments to improve the properties of the laser processed NiTi it is now possible to create multi-memory actuators with stable responses, and potentially long lives. The tensile cycling and shape memory recovery response of both a laser processed, and a treated laser processed two-memory actuator are shown in Figure 5.16 and Figure 5.17 respectively, with key values highlighted in Table 5.5. These actuators were half base metal, and half laser processed. Significant deformation (i.e. 15 % strain) was applied in order to observe the response of both memories in these actuators. The treated actuator had 33 % less plastic strain than the untreated actuator, and 42 % greater shape memory recovery strain. The treated actuator stabilized due to the nanocrystalline microstructure, compared to the coarse

grained untreated actuator which did not stabilize. The majority of the plastic strain in the untreated actuator was in the coarse grained laser processed region. In addition to grain refinement, the transformation temperatures were closer together, which enabled less overheating of the lower temperature memory, and contributed to the higher stability [159]. The increase in actuation of the treated base metal compared to the original base metal indicates that potential texture effects contributed to the low shape memory recovery of the treated laser processed NiTi, in addition to the discussed potential grain size mechanisms [4]. Further optimization of the laser processing and thermomechanical treatments is underway which will enable less overheating, and more uniform detwinning plateaus, enabling a two memory response with a higher stability. The transformation temperatures of the current actuators are unsuitable for fatigue testing at room temperature. Furthermore, there are limited applications for this sub-zero temperature range. Current work is underway to develop actuators that have two or more memories above room temperature.

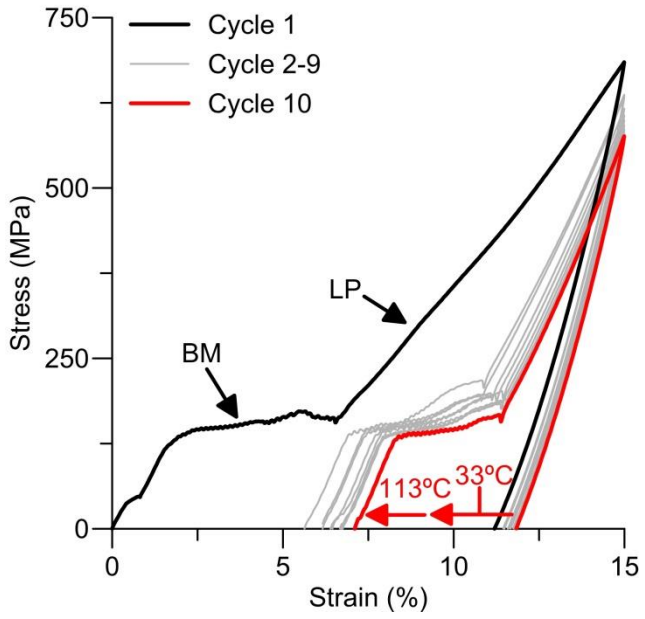

Figure 5.16: Tensile cycling to 5 % strain at -26 °C (i.e. M_f-10 °C of treated laser processed NiTi), and zero-load shape memory recovery of the base metal, of a half-base metal and half-laser processed sample heated to 33 °C and 113 °C.

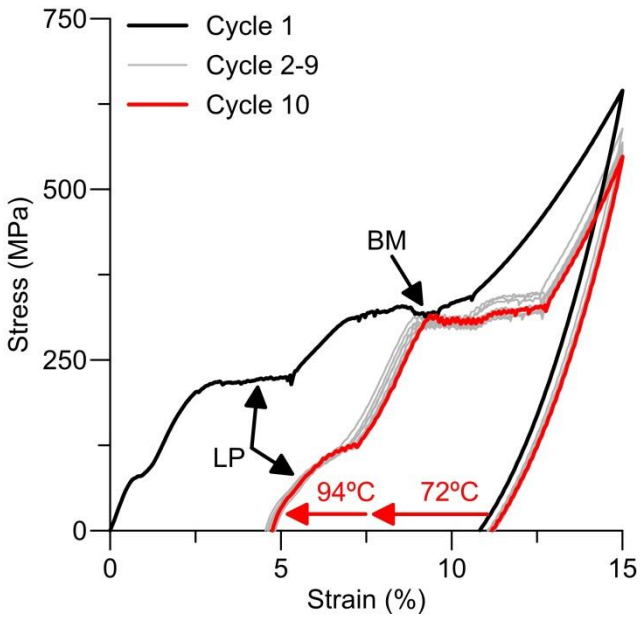

Figure 5.17: Tensile cycling to 5 % strain at -26 °C (i.e. M_f of treated laser processed NiTi -10 °C), and zero-load shape memory recovery of the base metal, of a treated half-base metal and half-laser processed sample heated to 72 °C and 94 °C.

Table 5.5: Plastic strain and shape memory recovery strain after 10 tensile cycles to 5 % strain, and zero-load shape memory recovery of the laser processed (BM-LP), and treated laser processed (T-BM-LP) two memory actuators

	Plastic Strain %	Shape Memory Strain %		
		1st Memory	2nd Memory	Total
BM-LP	7.10	3.21	1.44	4.65
T-BM-LP	4.75	3.55	3.05	6.60

5.6 Comparison of Laser Processed NiTi to Industry Standard Actuation Wire

The previous section compared the treated laser processed NiTi to a Ni-rich pseudoelastic base metal from which it was manufactured. The current section compares the treated laser processed NiTi to a Ti-rich shape memory actuation wire. This is the same material used in Chapter 4, and will be referred to as flexinol throughout the following discussion. There are numerous difference between the Ni-rich and Ti-rich wires, making comparison of two Ti-rich wires a better measure of performance metrics. This investigation revealed that the treated laser

processed NiTi achieved similar fatigue lives to the commercial flexinol wires when thermomechanically cycled at low strains.

5.6.1 Microstructure and Phase Analysis

TEM analysis of the microstructure of the flexinol is shown in Figure 5.18. The average grain size as measured by dark-field TEM was 72 nm. This is similar to the base metal of the previous section, and is typical of industrial NiTi designed for stability of actuation and long life. This Ti-rich material had no observed Ni_4Ti_3 precipitates, as these do not form in Ti-rich NiTi. The cross section was observed to contain Ti_2NiO_X and TiC inclusions which were identified by EDS analysis, however, neither of these was found in the TEM sample.

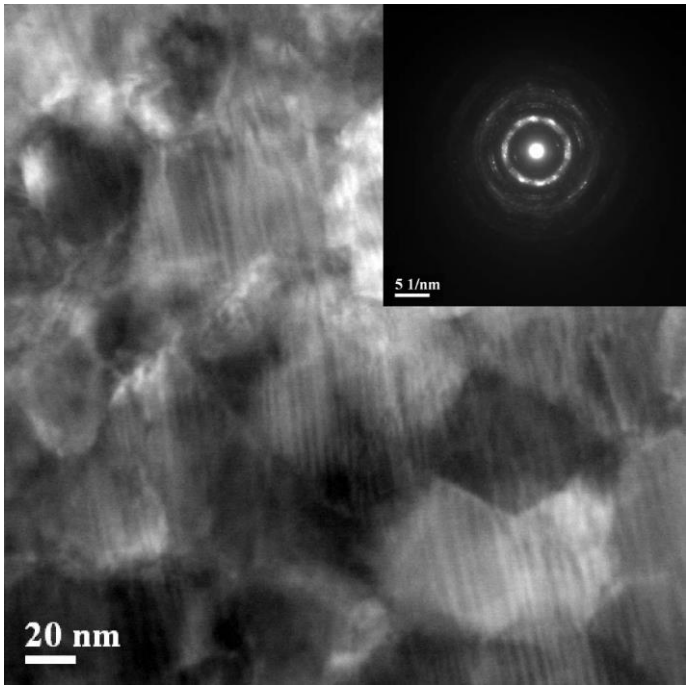

Figure 5.18: STEM of the nanocrystalline flexinol microstructure

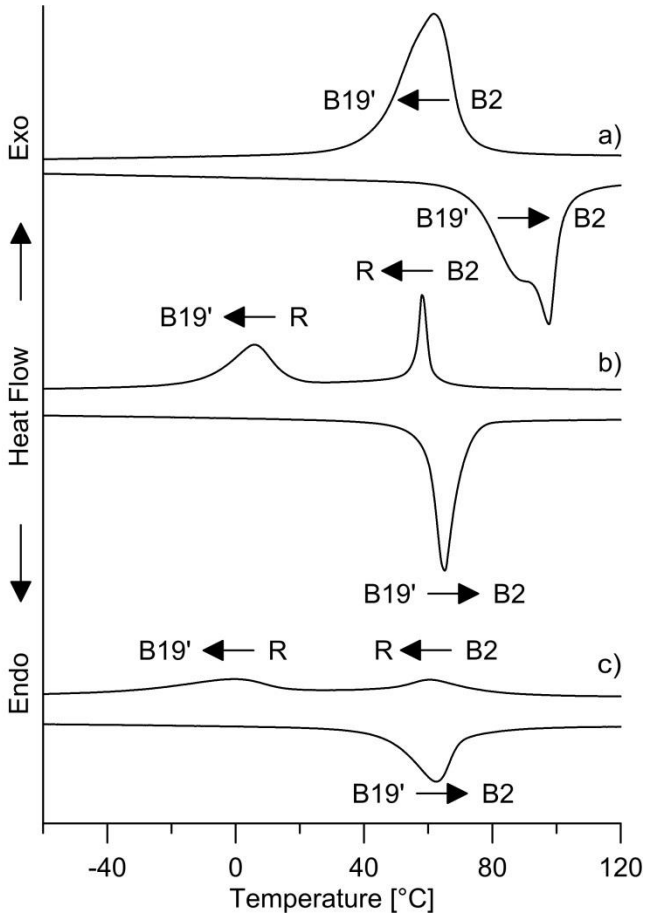

Figure 5.19: DSC analysis of a) laser processed NiTi, b) treated laser processed NiTi, and c) flexinol

The laser processed NiTi had the single phase transformations typical of a coarse grained, low dislocation density and precipitate free NiTi [6]. The treated laser processed NiTi had a similar phase transformation property to the flexinol, due to the Ni-lean composition and the small grain size. The sharp peaks indicated that the grains were dislocation lean [72].

The flexinol had a multi-stage phase transformation of a nanograined microstructure which geometrically constrained the martensite, reducing the maximum transformation strain, leading to the lower strain transformation of the R-phase [39]. The peaks of both materials are in similar positions, indicating that they have similar compositions, and microstructures, which is confirmed by the microscopy and composition analysis discussed in previous sections. The broad peaks of the flexinol phase transformations indicate that the flexinol had undergone a training by

the manufacturer to stabilize the microstructure by introducing dislocations to create networks [166, 167].

5.6.2 Tensile Properties

As discussed in the previous sections the laser processed NiTi had a coarse grained microstructure which led to a lower UTS and ductility compared to the nanocrystalline treated laser processed NiTi. The treated laser processed NiTi and the flexinol had equal UTS, while the treated laser processed NiTi had a 34 % greater ductility than the flexinol, due to the smaller grain size [286].

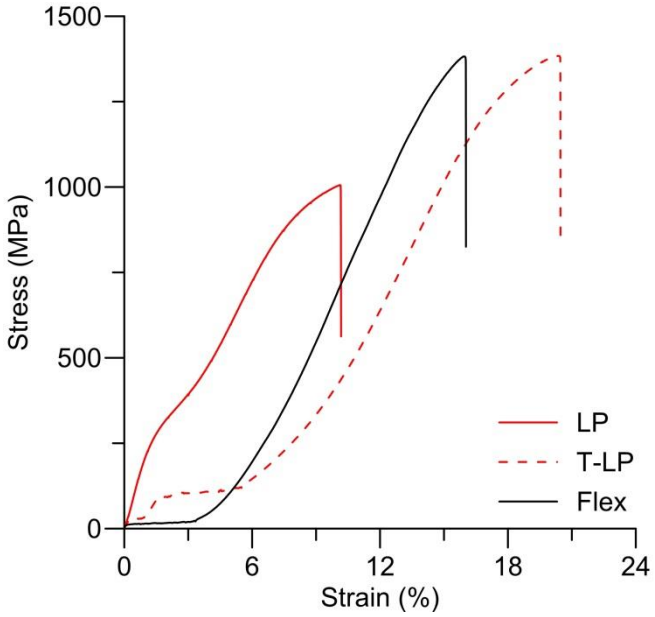

Figure 5.20: Tensile failure of the laser processed NiTi (LP), the treated laser processed NiTi (T-LP) and the flexinol (flex) at room temperature

Table 5.6: Tensile properties of the laser processed NiTi (LP), the treated laser processed NiTi (T-LP), and the flexinol (flex) at room temperature

	Ultimate Tensile Strength (MPa)	Ductility (%)
LP	1017.64 ± 28.24	10.48 ± 0.44
T-LP	1303.38 ± 69.83	20.39 ± 0.09
Flex	1311.22 ± 61.85	15.25 ± 0.75

The materials were tensile cycled to a load of 600 MPa and then thermally cycled at zero stress to recover shape memory strain as shown in Figure 5.21-23. The coarse grained laser processed NiTi had a significant plastic strain, and the resultant plastic deformation resulted in a shape memory strain of 18 % of flexinol after 10 cycles. The treated laser processed NiTi had an increase in plastic strain compared to the laser processed NiTi, but maintained significant shape memory strain equal to that of the flexinol. The smaller grains enabled a larger deformation to occur than the coarse laser processed NiTi, but a large part of this deformation was not recoverable due to the constriction of the matrix [88, 225]. The flexinol wire had 22 % of the plastic strain buildup of the treated laser processed NiTi, and a similar shape memory strain. The training that the flexinol had undergone was used to build a dislocation network that ensured that it had a more stable initial deformation than the virgin treated laser processed NiTi, which was dislocation lean as indicated by the DSC curves in Figure 5.19.

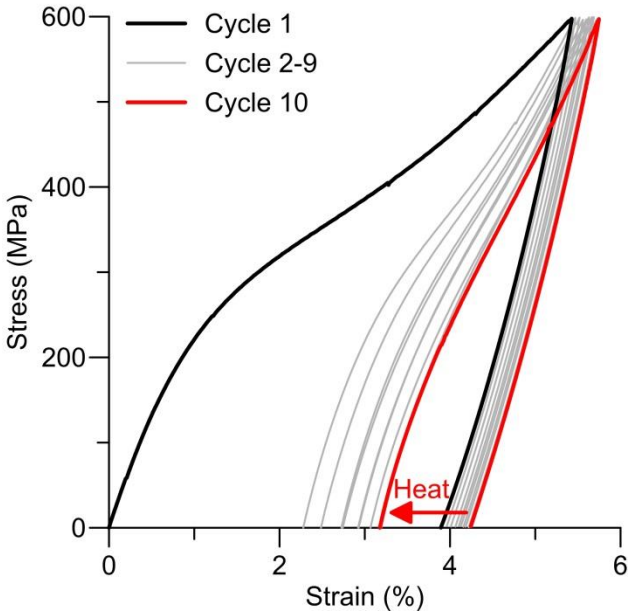

Figure 5.21: Tensile cycling to 600 MPa at room temperature, and zero-load shape memory recovery of the laser processed NiTi

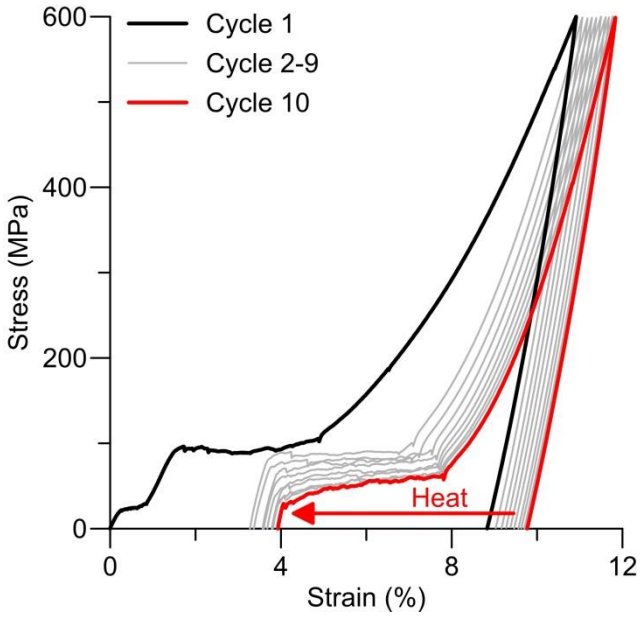

Figure 5.22: Tensile cycling to 600 MPa at room temperature, and zero-load shape memory recovery of the treated laser processed NiTi

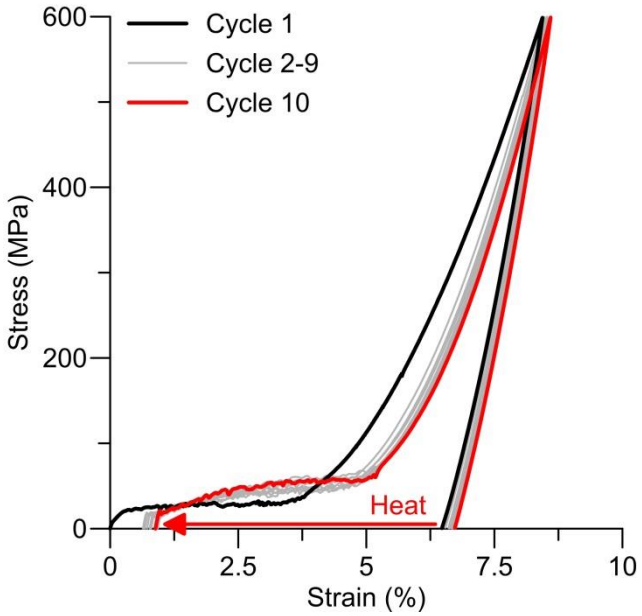

Figure 5.23: Tensile cycling to 600 MPa at room temperature, and zero-load shape memory recovery of the flexinol

Table 5.7: Plastic strain and shape memory strain after 10 tensile cycles to 600 MPa at room temperature, and zero-load shape memory recovery of the laser processed NiTi (LP), treated laser processed NiTi (T-LP), and flexinol

	Plastic Strain %	Shape Memory Strain %
LP	3.18	1.08
T-LP	3.93	5.94
Flex	0.88	5.99

5.6.3 Thermomechanical Fatigue Properties

Comparison of the fatigue lives of the laser processed NiTi, treated laser processed NiTi, and the flexinol are shown in Figure 5.24. The wires were loaded to 600 MPa and thermally cycled to controlled strains until failure. The coarse grained laser processed NiTi was previously shown to have high plastic buildup and low shape memory strain which resulted in very low fatigue lives compared to the treated laser processed NiTi and the flexinol. The thermomechanical fatigue life of NiTi is related to the maximum achievable strain [59, 163]. The lower the percentage of the maximum strain used, the greater the fatigue life achievable. The maximum strains for 1 cycle at a load of 600 MPa are indicated on the strain axis (i.e. Y-axis) of Figure 5.24. The optimized microstructure of flexinol enabled the maximum recoverable strain, followed by the more restrictive, smaller grained treated laser processed, and finally the coarse grained laser processed NiTi. At lower percentages of the maximum strain the treated laser processed NiTi and flexinol had fatigue lives in the same order of magnitude.

The treated laser processed NiTi had a substantial increase in both achievable strains and fatigue life at these higher strains compared to the laser processed NiTi. The flexinol had a further increase in both achievable strain and fatigue life due to the more optimized grain size [163], and the training that it underwent by the manufacturer [166, 167]. A training of 20 cycles at 4 % strain was applied to the treated laser processed NiTi and resulted in an increase in the fatigue life at 2 % strain from 21474 cycles to 33043 cycles, bringing it close to parity with the flexinol which had an average cycle life of 36022 cycles as shown in Figure 5.24. The stability of the microstructure ensured that progression of dislocations, and crack growth was slowed in the trained treated laser processed NiTi, leading to the longer fatigue life [59, 163].

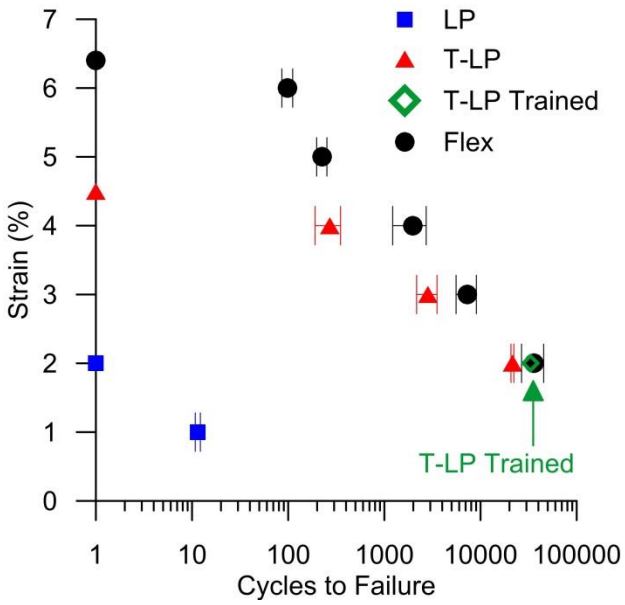

Figure 5.24: Cycles to failure of laser processed NiTi (LP), treated laser processed NiTi (T-LP), trained treated laser processed NiTi (T-LP Trained), and flexinol (flex) loaded to a constant 600 MPa and cycled to the indicated strains

5.7 Summary

A consistent reduction in Ni content of 0.23 at.% Ni was observed with each laser pulse. The change in M_s temperature with at.% was measured to be -68.76 K / at.% Ni. This value is consistent with a previous investigation of laser processing of NiTi sheets.

The Ni-rich base metal had an average grain size of 70 nm that was optimized for a stable pseudoelastic response. The Ti-rich laser processed NiTi had a coarse grained, columnar dendritic microstructure that had 71% of the base metal ultimate tensile strength (UTS) and 40 % of the base metal ductility, when tested above the M_d temperature. This coarse grained material was refined to a nanocrystalline microstructure through application of a thermomechanical treatment. This refined material had 95 % of the base metal UTS and 68 % of the base metal ductility, when tested above the M_d temperature.

The laser processed NiTi had a yield stress lower than that required for the pseudoelastic effect, and only 30 % of the shape memory recovery strain of the base metal after 10 cycles. The nanocrystalline treated laser processed NiTi had 62 % of the base metal pseudoelasticity after 100 cycles, and 54 % of the shape memory recovery strain of the base metal after 10 cycles. The

smaller grain size of the treated laser processed NiTi constricted the maximum achievable strain, contributing to the reduced transformation strain.

An untreated and a treated two memory actuator were cycled 10 times and recovered the shape memory strain at two distinct temperatures. The treated two memory actuator had a decrease in plastic strain of 33 % and an increase of shape memory recovery of 42 % compared to the untreated two memory actuator. Future work is underway in the development of treated actuators that have multiple memories above room temperature.

The treated laser processed NiTi had the same UTS as flexinol and 34 % greater ductility due to the smaller grain size. The treated laser processed NiTi had the same shape memory recovery strain as flexinol when cycled to 600 MPa and thermally recovered at zero-load. The treated laser processed NiTi had 347 % greater plastic strain than the flexinol. The training of the flexinol by the manufacturer, and the less constrictive microstructure of the flexinol ensured lower permanent deformation compared to the treated laser processed NiTi.

When loaded to 600 MPa the coarse grained and embrittled laser processed NiTi had 1/3 of the recoverable strain of flexinol and fatigue lives orders of magnitudes smaller. The treated laser processed NiTi had 2/3 of the maximum achievable strain of the flexinol, and fatigue lives in the same order of magnitude as flexinol at lower strains. The smaller grain size of the treated laser processed NiTi limited the achievable strain. Training of the treated laser processed NiTi increased the fatigue life to parity with the flexinol at 2 % strain. Future work is underway to further optimize the processing and training for superior fatigue properties.

6 Development of a Stable, High Stress Self-Biasing Actuator

SMA actuators that can move on both heating and cooling without an external bias would reduce complexity, weight and space compared to standard one-way SMA actuators. Industry would require these self-biasing actuators to maintain their properties over thousands of cycles. This benchmark has thus far not been met by other technologies. This chapter presents the development of a stable laser processed self-biasing actuator.

6.1 Multiple Memory Material Enabled Self-Biasing Actuation

Laser based vaporization technologies use a high intensity energy source to locally alter composition and microstructure of shape memory alloys; controlling their properties with greater accuracy and repeatability than other processes [16]. In NiTi SMAs the process increases local transformation temperatures through the preferential vaporization of Ni [16]. Control of local properties was used in this study to make a monolithic SMA with both shape memory effect and pseudoelastic properties enabling a novel self-biasing actuation mechanism. A simplified self-biasing linear actuator is shown experiencing a heating and cooling cycle in Figure 6.1. The laser processed NiTi shape memory effect region acted as the actuator and the base metal pseudoelastic region acted as the internal bias, removing the requirement for an external spring or weight bias. A pre-stress was applied by extending the actuator, to detwin the martensite in the laser processed NiTi and cause stress-induced martensite to form in the austenite base metal (Figure 6.1a). After this initial strain was applied, the ends of the actuator were held fixed in place, and the middle of the actuator moved during thermal cycling as shown in Figure 6.1. Heating the actuator (Figure 6.1 a-b) resulted in the detwinned martensite transforming to austenite and recovering some of its original length by extending the base metal. The limited strain applied to the base metal only partially transformed this region into stress-induced martensite. Upon cooling (Figure 6.1 b-c-d) the laser processed NiTi transformed back into martensite and was detwinned by the base metal. This moved the interface between the two regions back to the original position. When the laser processed NiTi was detwinned the strain in the base metal reduced and the stress-induced martensite transformed back into austenite. It should be noted that step c) of Figure 6.1 is shown for clarification however, steps c) and d) occur simultaneously.

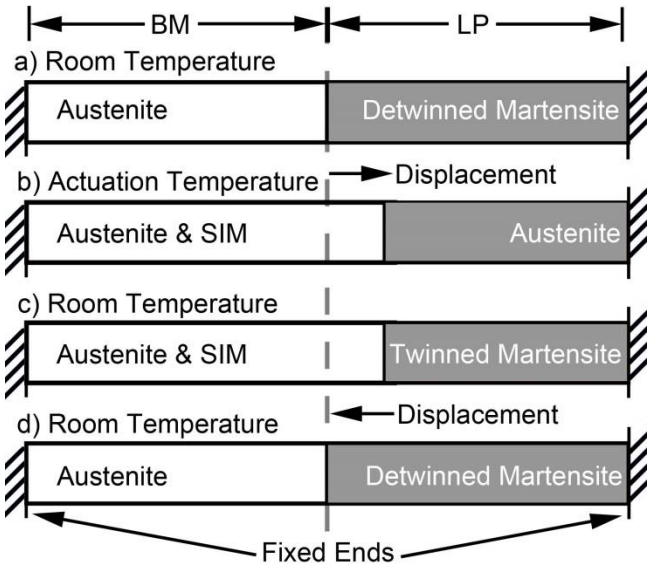

Figure 6.1: A simplified schematic of self-biasing laser processed actuator being thermally cycled, left) biasing base metal (BM), right) actuating laser processed NiTi (LP). Stress-induced martensite (SIM)

Successful design of SMA actuators must account for the dependence of SMA material properties on temperature [35]. When the actuator is heated, the detwinning stresses of the laser processed NiTi will decrease due to thermal effects on twin boundary motion [35]. The stress for stress-induced martensite of both the base metal and austenitic laser processed NiTi increase with temperature due to stabilization of the austenite phase, following a Clausius-Clapeyron relationship [84]. Furthermore, pre-stressing the actuator and the dynamic actuation of both laser processed NiTi and base metal can affect the strains and stresses exhibited by the actuator [287]. These effects are accounted for in the design of standard SMA actuators, which have proper matching between the biasing loads (e.g. spring, weight) and the actuating NiTi. Similarly the self-biasing actuator of the current application required careful matching of properties for both biasing base metal and actuating laser processed NiTi.

6.2 Microstructural Refinement

Successful matching of the base metal and laser processed NiTi properties was dependent on the composition and microstructure of the two materials. It is known that the physical and shape memory properties of NiTi are improved in nanocrystalline structures, so fine grained materials

have become an industry standard. The original base metal had a nanocrystalline microstructure, as shown through TEM analysis in Figure 6.2a. In comparison, the re-solidified laser processed NiTi consisted of a coarse grained microstructure (Figure 6.2c) as described in previous studies on laser melted NiTi wires [233, 281]. Using dark field TEM imaging the average grain size of the base metal was measured to be 70 nm, which was orders of magnitude smaller than the coarse grained laser processed NiTi. Standard single memory NiTi SMAs with a nano-scaled microstructure have high actuation stability and long fatigue lives [163]. It was hypothesized that similar benefits would occur if the microstructure of the untreated actuator could be refined; however, the effects of cold-drawing on a multi-phase component were unknown. Cold-drawing of the half austenitic and half martensitic wire revealed similar deformation properties to single phase NiTi. This resulted in a uniform, nanocrystalline microstructure throughout both regions of the actuator as shown in Figure 6.2 b and d. Using dark field TEM imaging the average grain size of the base metal and laser processed regions of the treated actuator were measured to be 27 nm and 29 nm respectively.

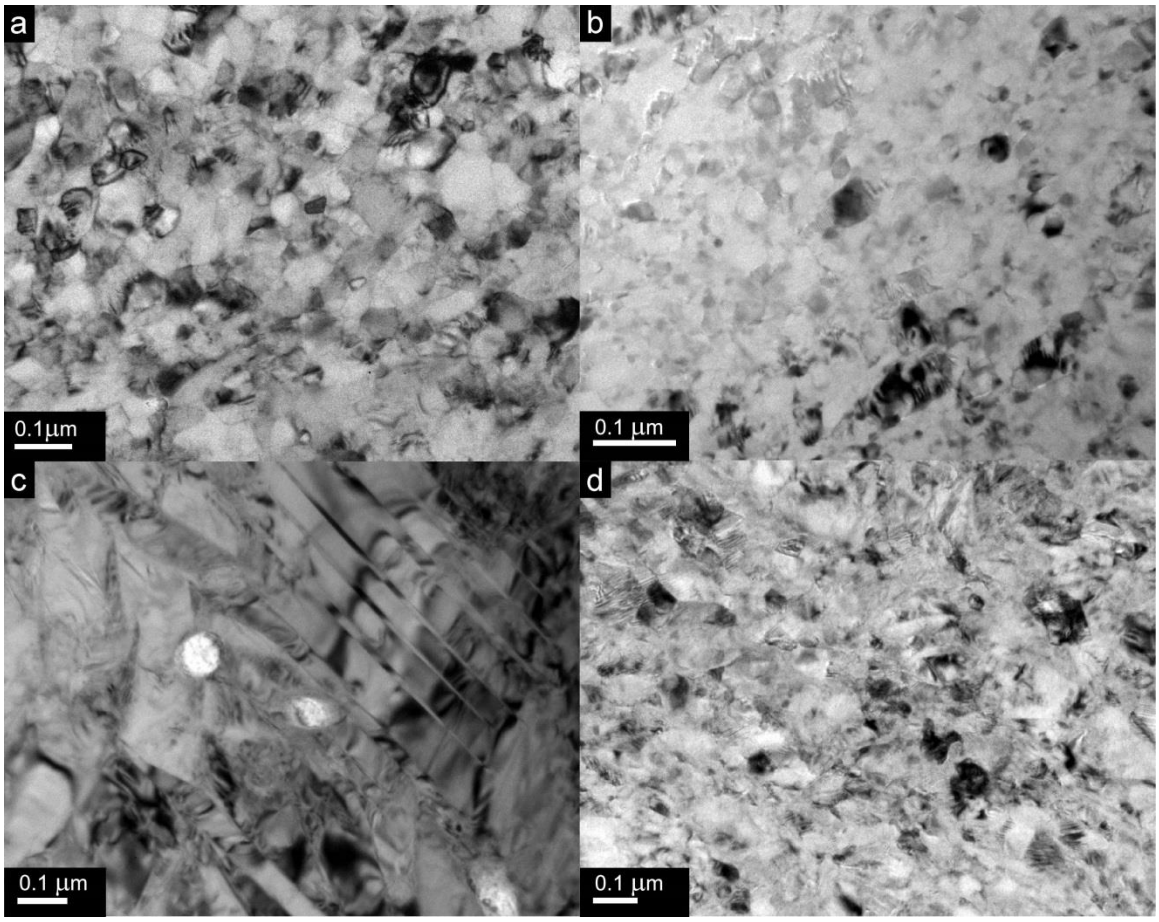

Figure 6.2: TEM images of a) untreated base metal, b) treated base metal, c) laser processed NiTi, d) treated laser processed NiTi

6.3 Transformation Temperatures

Microstructural and compositional change was used to control the NiTi mechanical and thermal properties following previous work [13, 191]. Ideal pairing of the transformation temperatures would avoid overheating the biasing component and ensure maximum stability [288]. Transformation temperatures and DSC curves of the four materials are shown in Table 6.1 and Figure 6.3, respectively. The untreated base metal (Figure 6.3a) had a single stage forward transformation that was the amalgamation of the martensite to R-phase, and the R-phase to austenite transformations. Constriction of the matrix by the grain boundaries in the nano-scaled grains limited the strain that could be accommodated for the martensite transformation, resulting

in the lower strain intermediate R-phase transformation occurring [284]. The B19' transformation was completely suppressed in the finer grained treated base metal which only had the lower strain R-phase transformation as shown in Figure 6.3b [284]. This suppression of the martensite transformation was responsible for the missing return peak in Figure 6.3a. The increase in transformation temperature that followed the decrease in grain size from untreated to treated base metal (Figure 6.3b) has been previously observed; however, no valid explanation has been given for this relation to-date [289].

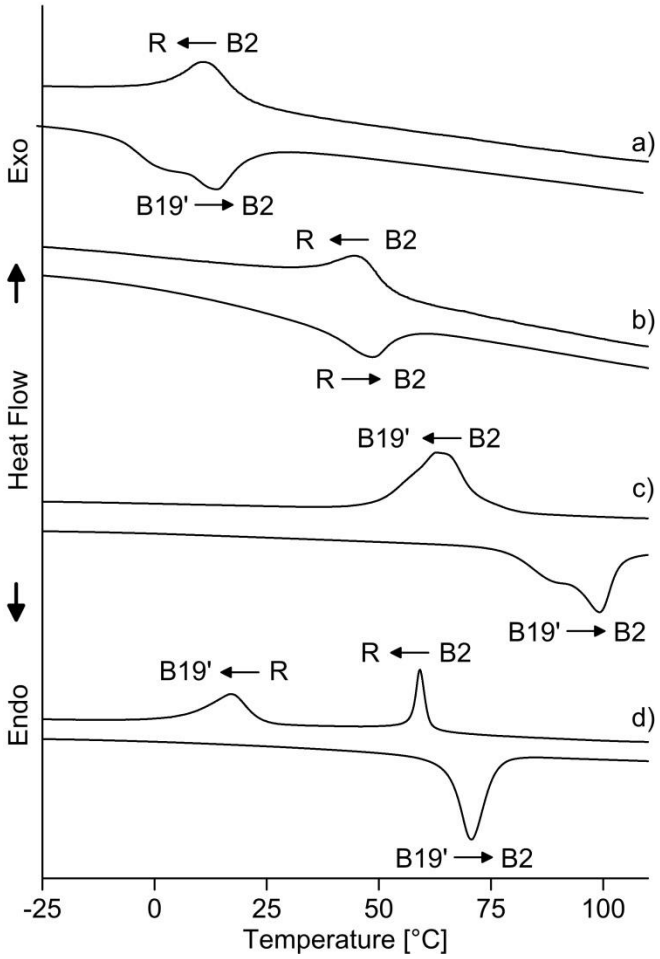

Figure 6.3: DSC results of a) untreated base metal, b) treated base metal, c) laser processed NiTi, and d) treated laser processed NiTi

Table 6.1: Phase transformation temperatures (°C) of the untreated and treated base metal and laser processed NiTi.

	R_s	R_f	M_s	M_f	A_s	A_f
Untreated NiTi	21.0	1.6	-	-	-8.2	29.5
Treated NiTi	53.9	32.5	-	-	48.4	61.6
Laser Processed NiTi	-	-	73.0	49.2	99.5	105.2
Treated Laser Processed NiTi	61.3	55.7	24.4	5.7	58.8	75.1

Laser processing of the base metal dramatically increased the transformation temperature due to nickel depletion and grain growth [13, 16]. This large change in grain size led to a lack of R-phase as shown in Figure 6.3c. Increase in the grain size altered the martensite morphology from the constricted compound (001) twinning of nano-scaled microstructures to the larger length scaled (Figure 6.2c) type I and II twins of coarser microstructures [272]. Finally, non-uniformity observed in the forward transformation peak in Figure 6.3c was due to inhomogeneity from microsegregation that occurs in laser welded materials [6, 16].

Thermomechanical treatments applied to the laser processed NiTi significantly refined the grain size, as described in the previous section. Figure 6.3d showed a depression of the transformation temperature and the formation of R-phase in the treated laser processed NiTi. Geometric constriction imposed by the nanocrystalline grain boundaries increased the driving force required for the martensite transformation and caused these shifts in transformation properties [284]. The applied thermomechanical treatment changed the transformation temperatures to a more ideal pairing of austenite finish temperatures that reduced the aforementioned risk of overheating the biasing treated base metal, as compared to the untreated actuator.

6.4 Tensile Failure Properties

The mechanical properties of SMAs can be controlled by the alteration of microstructure and composition designed through laser processing and thermo-mechanical treatment [13, 190]. Tensile failure results for the untreated, treated and laser processed materials are shown in Figure 6.4. The nano-grained base metal exhibited a flat stress-induced martensite plateau, a high ultimate tensile strength (UTS) and high elongation. Grain size reduction from the untreated to treated base metal increased the UTS and elongation. The significant increase in elongation may

have been due in part to grain boundary sliding which can occur in similar scaled nano grained metals [290, 291]. The increase in plateau stress of the treated base metal was due to the previously discussed suppression of the martensite transformation that accompanies the reduction in grain size [292]. Compared to the nano-grained base metal, the coarse grained and solidification embrittled [283] laser processed NiTi had a significantly lower UTS and elongation. Grain refinement of the treated laser processed NiTi restored the UTS and elongation (Figure 6.4).

The tensile failure of the untreated and treated actuators is shown in Figure 6.5. The thermal martensite detwinning plateau of the laser processed NiTi and the stress-induced martensite plateau of the base metal were observed in the tensile curves of both the untreated and treated actuators. The failure stress of the untreated actuator was limited by the coarse grained laser processed NiTi region, but the overall ductility was greater than that of the laser processed NiTi because of the stress-induced martensite transformation in the base metal region. The failure stress and ductility of the treated actuator was much greater than the untreated actuator due to the refined microstructure.

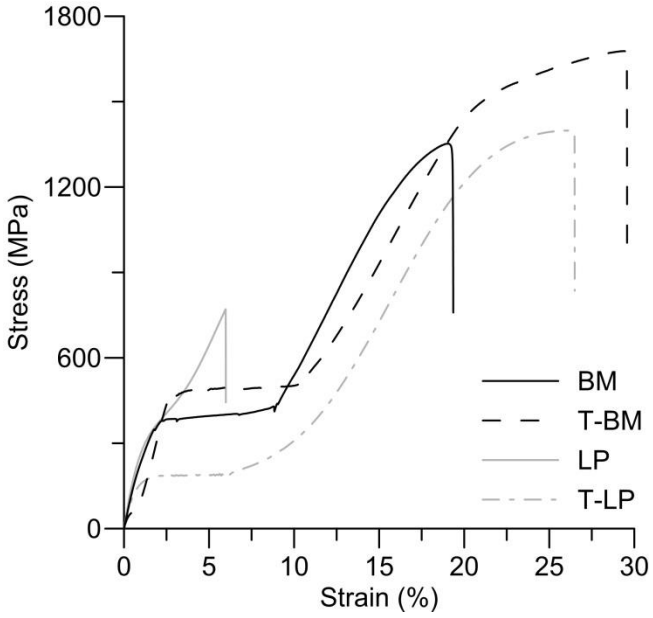

Figure 6.4: Tensile failure of the untreated base metal (BM), treated base metal (T-BM), laser processed NiTi (LP), and treated laser processed NiTi (T-LP) at room temperature

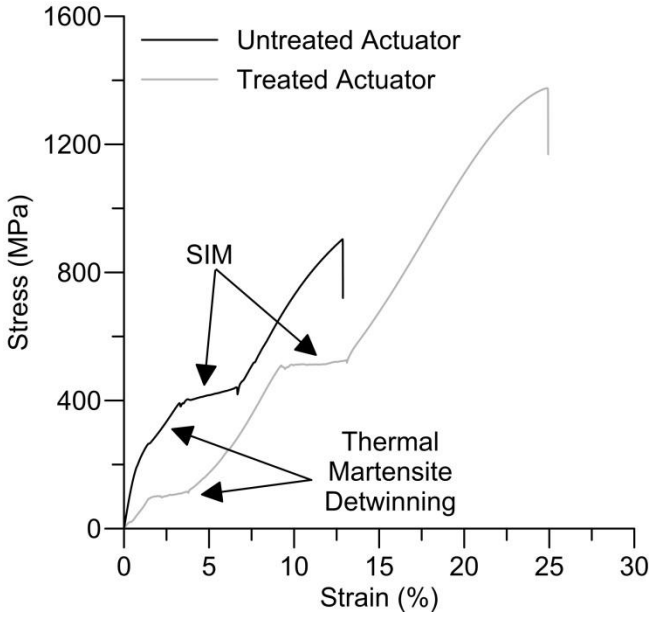

Figure 6.5: Tensile failure of the untreated and treated actuators, with labeled stress-induced martensite (SIM), and thermal martensite detwinning plateaus

6.5 Cycled Tensile Properties

Tensile cycling results for the untreated materials up to 5 % strain at room temperature and 115 °C are shown in Figure 6.6. At room temperature, the untreated base metal exhibited less than 1 % plastic strain, which is typical for nanocrystalline NiTi [286]. At 115 °C, which is 10 °C above the laser processed NiTi A_f, the untreated base metal was no longer pseudoelastic and did not recover from deformation. The shape memory effect of the laser processed NiTi recovered 2 % strain after being strained to 5 %, as indicated by the arrow in Figure 6.6. No detwinning plateau was observed for the martensite phase at room temperature as the coarse microstructure yielded before the onset of detwinning [13]. Plastic deformation that occurred during the detwinning resulted in the observed limited shape recovery. The laser processed NiTi did not exhibit pseudoelasticity above its A_f temperature due to the flow stress being below the stress required for stress-induced martensite of the coarse grain microstructure [13]. These properties of the base metal and laser processed regions were designed to function synergistically as a self-biasing actuation system, with martensite detwinning stresses of the shape memory effect region

and the stress-induced martensite plateau of the PE region coinciding. These complementary properties assisted the cyclic self-biasing actuation.

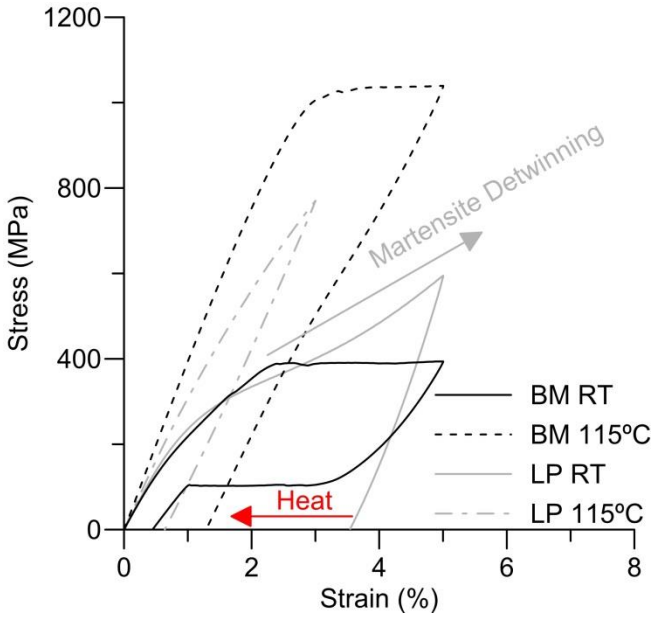

Figure 6.6: Cyclic tensile properties of the untreated base metal (BM) and laser processed NiTi (LP) at room temperature and 10 °C above the austenite finish temperature of the laser processed NiTi

Tensile cycling of the treated material is shown in Figure 6.7. The treated base metal revealed the R-phase plateau, as expected from the transformation temperatures (Figure 6.3). The apparent greater residual strain compared to the untreated base metal, was partially recovered by heating to transform the R-phase to austenite [84]. The A_f of the treated laser processed NiTi and base metal exhibited a better overlay when compared to the untreated material in Figure 6.3. This allowed the treated base metal to retain its pseudoelasticity above the A_f of the treated laser processed NiTi. After cycling to 5% strain at room temperature the treated laser processed NiTi wire recovered 2 % strain as shown in Figure 6.7. Limited actuation was due to grain refinement of the treated laser processed NiTi suppressing martensite transformation so that only R-phase transformation occurred above room temperature [163]. The increase in strength brought about by the grain refinement ensured minimal plasticity during detwinning of the martensite and formation of stress-induced martensite, with both deformation mechanisms having relatively flat plateaus (Figure 6.7).

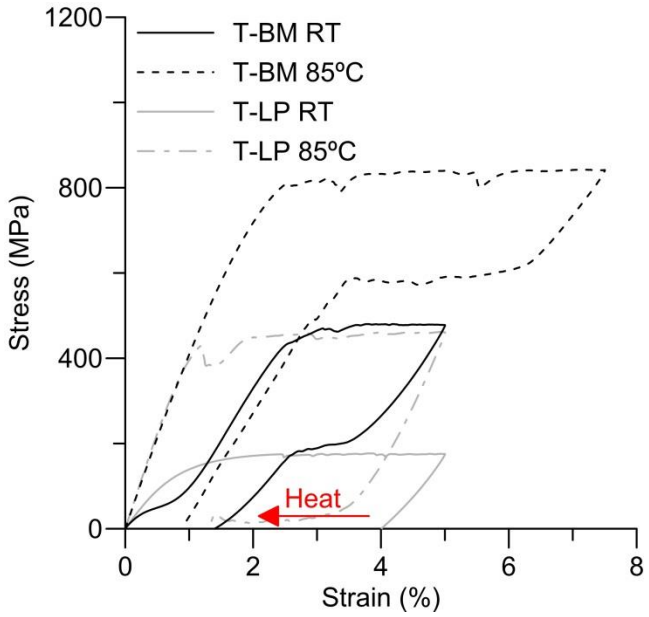

Figure 6.7: Cyclic tensile properties of the treated base metal (T-BM) and treated laser processed NiTi (T-LP) at room temperature and 10 °C above the austenite finish temperature of the treated laser processed NiTi

Tensile cycling and zero-load shape memory effect recovery of the untreated and treated actuators are shown in Figure 6.8 and 11 respectively. The coarse grained laser processed NiTi of the untreated actuator was unable to impede dislocation activity, so the plastic strain increased and the shape memory effect recovery reduced as shown in Figure 6.8 [163]. In contrast, the nanocrystalline base metal impeded dislocation motion and maintained the pseudoelastic properties [163]. The hardening of the stress-induced martensite plateaus was due to the increase in dislocation density that occurs with mechanical cycling, which reduced the transformation temperature further below the test temperature and increased the required driving force (i.e. stress) for the stress-induced martensite to transform [59, 72, 75]. The treated actuator had significant initial plastic deformation, but had a greater stability than the untreated actuator during the ten cycles as shown in Figure 6.9. The stability of the shape memory effect and pseudoelastic was due to the nanocrystalline microstructure impeding dislocation activity during the cyclic phase transformations [59]. The stress-induced martensite plateau and the martensite detwinning plateau of the treated actuator softened due to dislocation accumulation which reduced the transformation temperatures [72], bringing them closer to the test temperature, and thus reducing both the driving force required for stress-induced martensite, and the detwinning

stress of martensite [35, 75]. The discovery that both the shape memory and pseudoelastic properties in the treated actuator stabilized, and did not negatively impact one another is of great import to the understanding of multi-phase SMA components.

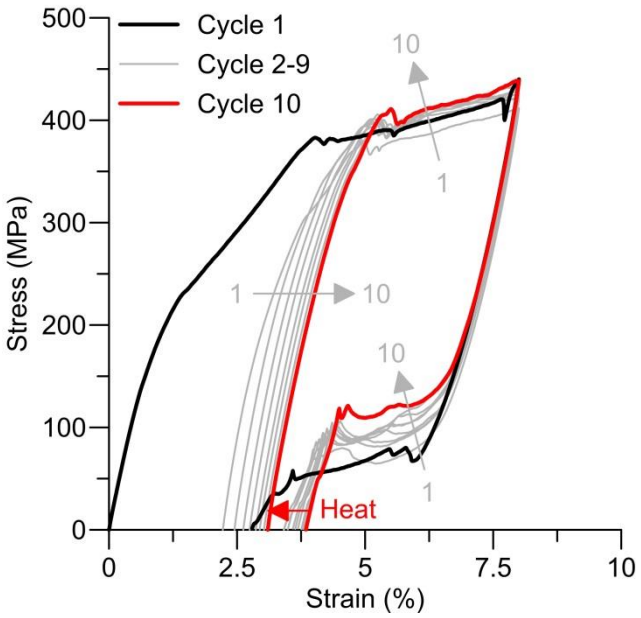

Figure 6.8: Ten tensile cycles and zero-load thermal recovery of the untreated actuator

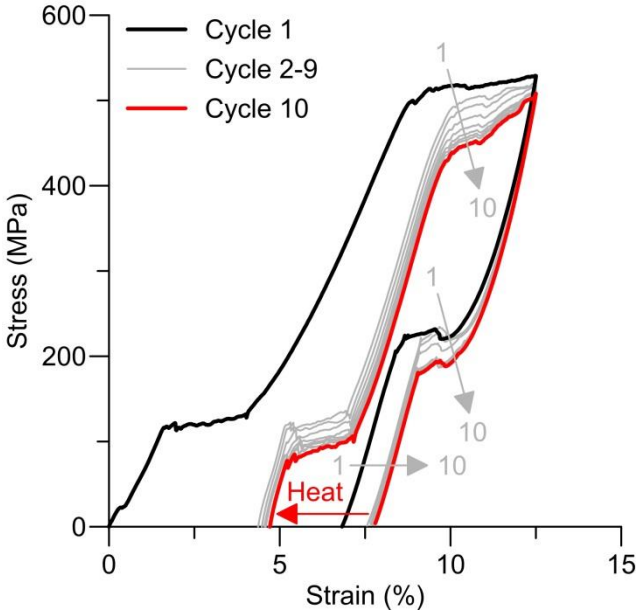

Figure 6.9: Ten tensile cycles and zero-load thermal recovery of the treated actuator

6.6 Self-Biasing Actuation Properties

Characterization of the separate base metal and laser processed NiTi regions was used to design the combined untreated and treated self-biasing actuators. The evolution of the actuation and plastic strain in the self-biasing untreated and treated actuators are shown in Figure 6.10. Both of the actuators completed 6,000 self-biased actuation cycles without failure. A pre-stress was applied to these actuators, after which they were held fixed at both ends and the displacement was measured in the middle of the actuator at the interface between the base metal and laser processed regions. During thermomechanical testing the untreated actuator cycled between 175 and 400 MPa, due to the phase transformations in the different regions of the wire. Actuation strain reduced from 0.9 % to below 0.5 % strain by 1000 cycles and further decreased to below 0.4 % by 6000 cycles. The plastic strain did not stabilize and increased above 1.1 %. This decrease in actuation and increase in plastic strain resulted from the coarse microstructure of the laser processed NiTi being unable to impede dislocation formation, motion and buildup during thermal cycling (i.e. transformation induced plasticity) [75].

The homogeneous nanocrystalline structure of the treated actuator limited plastic strain at 6000 cycles to 0.11 % [163]. This limited plastic strain was achieved despite the larger stress and strain experienced by the treated actuator, which cycled between 150 and 600 MPa. Actuation strain decreased from 1.2 % to 0.6 % by 1000 cycles and this actuation was maintained past 6000 cycles. The lower detwinning stress of the treated laser processed NiTi, and the more ideal pairing of transformation temperatures also contributed to the increased stability of the treated actuator. The discovery that different transformation properties (i.e. pseudoelastic and shape memory effect) contained in a single component can stabilize and remain consistent for a significant number of cycles is a vital contribution to the rapidly expanding field of multi-phase SMAs.

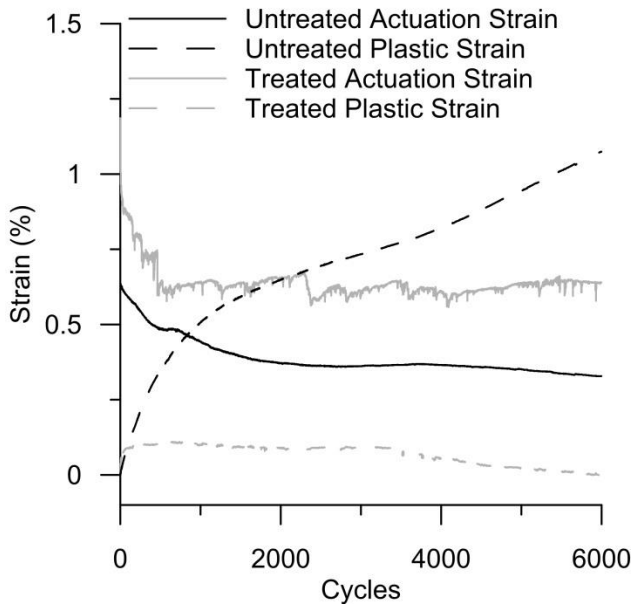

Figure 6.10: Evolution of the actuation and plastic strain during thermomechanical cycling of the untreated and treated actuators.

Compared to other methods of inducing a two-way shape memory effect in SMAs, the actuators prototyped in this work have unparalleled stability due to their refined microstructure. The stability of the treated actuator was similar to a standard untrained NiTi SMA [163]. Training of the treated actuator would further improve the stability [293]. A number of routes are available for further improving the performance of these actuators. The limited actuation stroke of the current prototypes can be improved by optimizing the shape memory effect properties for the application specific temperatures; thereby using the full martensite transformation, and not the low-strain R-phase transformation. Optimization of the shape memory effect and pseudoelastic pairing can further improve the actuator properties. Immediate improvement of the current actuator stroke can be achieved by using different geometries, such as coiling the wire into a spring. This would provide the design freedom necessary to enable larger actuation strains from the shape memory effect region and balance the biasing stress from the pseudoelastic region. This would also enable biasing to occur at stresses near the detwinning stress of the shape memory effect region, greatly increasing the fatigue life and stability of the actuator.

6.7 Summary

A self-biasing actuator was created using a laser based vaporization method that altered the bulk composition of one half of a NiTi wire. The laser processed region was martensitic at room temperature serving as the actuator. The unprocessed base metal region served as an internal bias that detwinned the martensite after an actuation cycle was completed. It was discovered that the laser processed region of the actuator had significant increase in plastic strain and decrease in actuation strain during high stress thermomechanical cycling due to the coarse grained microstructure.

Investigation of cold working to strengthen the microstructure revealed that the half martensitic and half austenitic actuator had similar deformation properties to single phase shape memory alloys. Due to these consistent deformation characteristics, the cold-worked actuator had a uniform nanocrystalline microstructure along its entire length. High stress thermomechanical cycling of this nanocrystalline self-biasing actuator revealed that it had the same stabilization behaviour as a single memory actuator, with minimal plastic strain buildup after thousands of cycles. This important discovery proves that separate shape memory properties existing in a single component can evolve stable transformation characteristics.

Other self-biasing technologies are unable to attain the stability of these self-biasing actuators, and as such are unsuitable for real-world applications. The stable self-biasing shape memory alloy (SMA) prototypes developed in this study can be readily adopted by industry to achieve reduction in weight, cost and complexity of current SMA designs. Work is currently underway to develop a self-biasing spring actuator. Significant improvement of the actuation stroke, stability and cycle life could be achieved by forming the self-biasing actuator into a spring. Optimized actuator-bias matching would be possible by tailoring the spring geometry of the different regions.

7 Conclusions and Future Work

7.1 Thermomechanical Fatigue of Laser Welded NiTi

The investigation of the thermomechanical fatigue of laser welded NiTi showed that weld strength was not an indicator of stability or cycle life. Despite maintaining 86 % of the base metal strength, during thermomechanical cycling the welded wire had a greater buildup of plastic strain and degradation of actuation strain than the base metal. This resulted in a significantly lower fatigue life. Application of a post-weld heat treatment reduced strain localization at the weld. During thermomechanical cycling the heat treated wires had similar plastic strain build-up and actuation strain to the base metal, resulting in an order of magnitude improvement of the fatigue life compared to the welded wires. This work highlighted that post weld heat treatments would be insufficient to return the properties of laser processed NiTi, which would not be subject to strain localization.

7.2 Laser Processing

The laser processing of NiTi wires had a consistent reduction of 0.23 at.% Ni with each laser pulse. A Ni-rich base metal was laser processed to be a Ti-rich composition. The base metal had an average grain size of 70 nm, while the laser processed NiTi had a coarse grained columnar dendritic structure that was embrittled by Ti_2NiO_x inclusions. This coarse grained embrittled laser processed NiTi had 71 % of the base metal ultimate tensile strength (UTS) and 40 % of the base metal ductility, when tested above the M_d temperature. The laser processed NiTi had a yield stress lower than that required for the pseudoelastic effect. The microstructure was unable to resist dislocation motion, resulting in large plastic strain buildup, and only 30 % of the shape memory recovery strain of the base metal after 10 cycles. The laser processed NiTi was compared to flexinol in thermomechanical fatigue tests with a constant stress of 600 MPa. The coarse grained and embrittled laser processed NiTi had 1/3 of the recoverable strain of flexinol and fatigue lives orders of magnitudes smaller due to the inability of the microstructure to inhibit dislocation activity.

The coarse grained material of the laser processed NiTi was refined to a nanocrystalline microstructure through application of a thermomechanical treatment. This reduction in grain size

resulted in the treated laser processed NiTi having 95 % of the base metal UTS and 68 % of the base metal ductility, when tested above the M_d temperature. Improvements were also realized in the shape memory properties with the treated laser processed NiTi having 62 % of the base metal pseudoelasticity after 100 cycles, and 54 % of the shape memory recovery strain of the base metal after 10 cycles. The grain size of the treated laser processed NiTi was less than half that of the base metal, which resulted in a constriction of the twins, and a reduction in the maximum achievable transformation strain compared to the base metal. This smaller grain size resulted in the treated laser processed NiTi having the same UTS as flexinol and 34 % greater ductility. When cycled to 600 MPa and thermally recovered at zero-load the treated laser processed NiTi had the same shape memory recovery strain as flexinol. The treated laser processed NiTi had 347 % greater plastic strain than the flexinol, due to permanent deformation of the grains, and a lack of training compared to the trained flexinol. The treated laser processed NiTi had 2/3 of the maximum achievable strain of the flexinol due to the smaller grain size, and fatigue lives in the same order of magnitude as flexinol at lower strains. Training of the treated laser processed NiTi increased the fatigue life to parity with the flexinol at 2 % strain.

The laser processing and thermomechanical treatments were used to make an untreated and a treated two memory actuator. These actuators were cycled to 15 % strain and recovered the shape memory strain at two distinct temperatures 10 times. The untreated actuator did not stabilize in plastic strain or shape memory recovery. The treated two memory actuator had a decrease in plastic strain of 33 % that stabilized within 10 cycles, and an increase of shape memory recovery of 42 % compared to the untreated two memory actuator.

7.3 Self-Biased Actuator

A self-biasing actuator was created using the laser processing and thermomechanical treatments developed in this work. Half of the wire actuator was austenitic at room temperature, while the other half was martensitic. The austenitic region was a pseudoelastic bias, and the martensitic region was the shape memory actuator. The laser processed self-biasing actuator had a buildup of 1.1 % plastic strain and decrease of actuation strain to 0.4 % at 6000 thermomechanical cycles because the coarse microstructure could not inhibit dislocation activity. Treating the actuator to refine the microstructure successfully created a homogenous microstructure in both regions. This

nanocrystalline microstructure enabled self-biasing of high stress actuation. This self-biasing actuator had similar stabilization behaviour to standard one-memory after thermomechanical cycling, with minimal plastic buildup of 0.11 % after 6000 cycles, and 50 % greater strain than the untreated actuator despite being cycled to a 50 % larger stress. This proves that multiple memory NiTi components can evolve stable transformation characteristics, making them viable for real-world application. This is not possible with the other self-biasing mechanisms developed to date.

7.4 Future Opportunities

7.4.1 Welding and Joining of NiTi

The first part of this work was the first investigation to be published on the effect of welding on the thermomechanical fatigue of SMAs. Future work in this area includes investigating methods to improve the properties of the welded region.

- The NiTiCu alloy has lower stresses required for thermomechanical cycling, and lower plastic deformation during cycling, so may have an advantage over NiTi in the fatigue of welds [153, 154].
- Alloy elements could be added to the fusion zone to refine the grains [294, 295], however this would not address the coarsened heat affected zone (HAZ).
- The NiTiHf alloy has great potential for post weld heat treatments due to their dense network of strengthening precipitates that form, which could strengthen both the fusion zone and HAZ [296].
- The investigation of dissimilar welds and their fatigue is the ultimate goal of these studies. Many applications and revolutionary designs can be realized if joints of NiTi-based SMAs with dissimilar materials could achieve high cycle fatigue lives.
- The functionality of these designs would be further increased by the joining of multiple memory SMAs to dissimilar materials.

7.4.2 Laser Processing Shape Memory Alloys for Many Memories

Future work is underway in the development of actuators that have multiple memories above room temperature. This work is focusing on the development of new laser processing methods

that can increase the resolution of the current process by reducing the amount of Ni removed per laser pulse. Numerical modeling of the laser process [254, 255, 297], would enable a better fundamental understanding of the process, and enable faster development of new processes.

7.4.3 Treatment of Laser Processed NiTi for Optimized Performance

Parallel work is being performed on the optimization of the post-laser processing thermomechanical treatments to optimize the properties of the material so that the initial base metal properties can be fully recovered. The development of finer wire diameter actuators, training to improve stability, and control of actuation are all being pursued by research collaborators.

7.4.4 Laser Processing of other Shape Memory Alloys

Other SMA systems have benefits compared to NiTi including lower cost, higher temperatures, and smaller transformation hysteresis [298-300]. Successful laser processing of these other SMA alloys would lead to a wide range of beneficial multiple memory SMA applications. Initial studies have been performed, including the study of a lower cost CuAlMn SMA alloy by the author [301].

7.4.5 Modeling of Laser Processed Shape Memory Alloys

The modeling of these multiple memory NiTi components is important for both gaining a fundamental understanding of the deformation of these materials, and to improve efficiency in the initial design stages for products. The manufacturing methods developed in the current work were used to make multiple memory wires that had their tensile response modelled in the published work of Michael et al. [302]. Future work is being pursued to investigate more complicated models that are being developed for use with new medical devices.

7.4.6 Self-Biasing Springs and other Geometries

The proposed work of a self-biasing spring is currently being investigated. The strains and stresses of actuation in springs are lower than linear actuators, which would increase the stability of actuation, and fatigue life [106, 156]. Other methods of using geometry to exploit these methods have been explored and could be applied using sheets, tubes, or ring.

8 Contributions

8.1.1 Accepted/Published in Peer Reviewed Journal Publications

J1 **PhD**	M.L. Kuntz, **B. Panton,** S. Wasiur-Rahman, S.F. Corbin, and Y.N. Zhou, "An Experimental Study of Transient Liquid-Phase Bonding of the Ternary Ag-Au-Cu System Using Differential Scanning Calorimetry", Metallurgical and Materials Transactions A, 2013, 44(8), 3708-3720
J2 **PhD**	**B. Panton,** A. Pequegnat, Y.N. Zhou, "Dissimilar Laser Joining of NiTi SMA and MP35N Wires", Metallurgical and Materials Transactions A, 2014, 45(8), 3533-3544
J3 **PhD**	Z. Zeng, **B. Panton*,** J.P. Oliveira, A. Han, Y.N. Zhou, (2015) "Dissimilar laser welding of NiTi shape memory alloy and copper". Smart Materials and Structures, 2015, 24, 125036 (8pp) ***corresponding author**
J4 **PhD**	J. P. Oliveira, **B. Panton**, Z. Zeng, T. Omori, Y.N. Zhou, R. M. Miranda, F. M. Braz Fernandes, "Laser welded superelastic Cu-Al-Mn shape memory alloy wires", Materials and Design, 2016, 90, 122-128
J5 **PhD**	A. Pequegnat, **B. Panton,** Y.N. Zhou, M.I. Khan, "Local Composition and Microstructure Control for Multiple Pseudoelastic Plateau and Hybrid Self-Biasing Shape Memory Alloys", Materials and Design, 2016, 92, 802-813
J6 **PhD**	J. P. Oliveira, **B. Panton**, Z. Zeng, C. M. Andrei , Y.N. Zhou, R. M. Miranda, F. M. Braz Fernandes, "Laser welding of NiTi to Ti6Al4V with a niobium interlayer", Acta Materialia, 2016, 105, 9-15

8.1.2 Submitted to Peer Reviewed Journal Publications

JS1 **Thesis**	**B. Panton,** Y.N. Zhou, M.I. Khan, "A High Stress Two-Way Shape Memory Effect Actuator", Responded to reviewers of Acta Materialia [Dec 12, 2015]
JS2 **Thesis**	**B. Panton,** J.P. Oliveira, Z. Zeng, Y.N. Zhou, M.I. Khan, "Thermomechanical fatigue of post-weld heat treated NiTi shape memory alloy wires", Submitted to International Journal of Fatigue [Dec 14, 2015]

8.1.3 In Progress Journal Publications

JX1 **Thesis**	**B. Panton,** M. Daly, Y.N. Zhou, M.I. Khan, "Re-orienting the crystallographic texture of laser processed NiTi wires", To submit to Acta Materialia [Apr 2016]
JX2 **Thesis**	**B. Panton,** G. Seviora Y.N. Zhou, M.I. Khan, "Thermomechanical fatigue of laser processed NiTi wires", To submit to Material Science and Engineering A [May 2016]

8.1.4 Peer Reviewed Conference Publications (* = Presenter)

JC1	**B. Panton*,** Z. Zeng, Y.N. Zhou, M.I. Khan, "The effect of laser welds on the thermomechanical fatigue of NiTi shape memory alloys", Proceedings of the ASME 2014 Conference on Smart Materials, Adaptive Structure and Intelligent Systems, SMASIS2014, September 8-10, Newport, Rhode Island, USA

JC2	**B. Panton***, A. Michael, A. Pequegnat, M. Daly, Y.N. Zhou, M.I. Khan, "An innovative laser-processed NiTi self-biasing linear actuator", Proceedings of the ASME 2013 Conference on Smart Materials, Adaptive Structures and Intelligent Systems, SMASIS2013, September 16-18, Snowbird, Utah, USA
JC3	A. Moon*, **B. Panton**, H.F.M. Van der Loos, E.A. Croft, "Using Hesitation Gestures for Safe and Ethical Human-Robot Interaction", IEEE ICRA'10 Workshop on Interactive Communication for Autonomous Intelligent Robots, Anchorage, USA, May 2010.

8.1.5 Conference Presentations (* = Presenter)

CP1	**B. Panton***, Z. Zeng, Y.N. Zhou, "Laser Welding of NiTi and Copper", European Congress and Exhibition on Advanced Materials and Processes Warsaw, Poland, September 20-24 2015
CP2	**B. Panton*,** Z. Zeng, Y.N. Zhou, M.I. Khan, "Thermomechanical fatigue of laser welded NiTi shape memory alloys", International Workshop on Advanced Materials Joining and Processing, Centre for Advanced Materials Joining, University of Waterloo, Waterloo, ON, Canada, 2014
CP3	**B. Panton***, A. Pequegnat, Y.N. Zhou, "Dissimilar Laser Joining of NiTi shape memory alloy wire and MP35N alloy wire", International Workshop on Advanced Materials Joining and Processing, Centre for Advanced Materials Joining, University of Waterloo, Waterloo, ON, Canada, 2013
CP4	B. Tam, B. **Panton***, A. Pequegnat, M.I. Khan, M. Daly, J. Wang, Y.N. Zhou, "Laser Microwelding of NiTi Shape Memory Alloy Wires", Materials Science and Technology 2012 Conference and Exhibition (MS&T'12), Pittsburgh, Pennsylvania, USA
CP5	M. Daly, **B. Panton*, A.** Pequegnat, J. Wang, Y.N. Zhou, M.I. Khan, (2012) "Modification of NiTi Shape Memory Alloy Functional Properties Via Laser Processing: Proof of Concept", Materials Science and Technology 2012 Conference and Exhibition (MS&T'12), Pittsburgh, Pennsylvania, USA

8.1.6 Technical Reports and Presentations

TP1	**B. Panton**, Y.N. Zhou, Technical presentation on dissimilar laser welding of stainless steel and platinum-iridium, presented to Baylis Medical Inc. as part of an NSERC Engage project (2015)
TR1	**B. Panton**, Y.N. Zhou, Technical report on high performance sapphire joint development, submitted to Suretech Development Limited as part of an NSERC Engage project (2015)
TR2	**B. Panton**, A. Pequegnat, Y.N. Zhou, Technical report on dissimilar joining of NiTi submitted to Emcara Gas Development Inc. as part of Industry Academia Collaboration Program Technical Problem Solving project (2012)

9 References

[1] L. C. Chang and T. A. Read, "Plastic Deformation and Diffusionless Phase Changes in Metals-The Gold-Cadmium Beta Phase," *Journal of Metals,* vol. 3, pp. 47-52, 1951.

[2] M. W. Burkart and T. A. Read, "Diffusionless phase change in the Indium-Thallium system," *American Institutre of Mining and Metallurgical Engineers,* vol. 197, pp. 1516-1524, 1954.

[3] W. J. Buehler, J. V. Gilfrich and R. C. Wiley, "Effect of Low-Temperature Phase Changes on the Mechanical Properties of Alloys near Composition TiNi," *Journal of Applied Physics,* vol. 34, pp. 1475-1477, 1963.

[4] T. Saburi, M. Yoshida and S. Nenno, "Deformation behavior of shape memory Ti Ni alloy crystals," *Scripta Metallurgica,* vol. 18, pp. 363-366, 1984.

[5] J. Mohd Jani, M. Leary, A. Subic and M. A. Gibson, "A review of shape memory alloy research, applications and opportunities," *Materials and Design,* vol. 56, pp. 1078-1113, 2014.

[6] K. Otsuka and X. Ren, "Physical metallurgy of Ti–Ni-based shape memory alloys," *Progress in Materials Science,* vol. 50, pp. 511-678, 2005.

[7] D. J. Hartl and D. C. Lagoudas, "Aerospace applications of shape memory alloys," *Proc. of the Institution of Mechanical Engineers, Part G: Journal of Aerospace Engineering,* vol. 221, pp. 535–552, 2007.

[8] Y. Fu, W. Huang, H. Du, X. Huang, J. Tan and X. Gao, "Characterization of TiNi shape-memory alloy thin films for MEMS applications," *Surface and Coatings Technology,* vol. 145, pp. 107-112, 2001.

[9] T. Duerig, A. Pelton and D. Stöckel, "An overview of nitinol medical applications," *Materials Science and Engineering: A,* vol. 273-275, pp. 149-160, 1999.

[10] F. Butera, "Shape Memory Actuators for Automotive Applications," *Advanced Materials & Processes,* vol. 166, pp. 37–40, 2008.

[11] K. Yamauchi, *Shape Memory and Superelastic Alloys : Technologies and Applications.* Cambridge, UK;: Woodhead Pub, 2011.

[12] D. C. Lagoudas, *Shape Memory Alloys: Modeling and Engineering Applications.* New York: Springer Science Business Media, 2008.

[13] A. Pequegnat, B. Panton, M. I. Khan and Y. N. Zhou, "Local Composition and Microstructure Control for Multiple Pseudoelastic Plateau and Hybrid Self-Biasing Shape Memory Alloys," *Materials and Design,* vol. 92, pp. 802-813, 2015.

[14] M. Daly, A. Pequegnat, Y. Zhou and M. Khan, "Fabrication of a novel laser-processed NiTi shape memory microgripper with enhanced thermomechanical functionality," *Journal of Intelligent Material Systems and Structures,* vol. 24, pp. 984-990, 2013.

[15] B. Panton, A. Michael, A. Pequegnat, M. Daly, Y. N. Zhou and M. I. Khan, "An innovative laser-processed NITI self-biasing linear actuator," in *Proceedings of the ASME 2013 Conference on Smart Materials, Adaptive Structures and Intelligent Systems, SMASIS2013, September 16-18,* Snowbird, Utah, USA, 2013, .

[16] M. I. Khan, A. Pequegnat and Y. N. Zhou, "Multiple Memory Shape Memory Alloys," *Advanced Engineering Materials,* vol. 15, pp. 386-394, 2013.

[17] A. Y. N. Sofla, D. M. Elzey and H. N. G. Wadley, "Cyclic degradation of antagonistic shape memory actuated structures," *Smart Materials and Structures,* vol. 17, pp. 1-6, 2008.

[18] X. Wang, Y. Bellouard and J. J. Vlassak, "Laser annealing of amorphous NiTi shape memory alloy thin films to locally induce shape memory properties," *Acta Materialia,* vol. 53, pp. 4955-4961, 2005.

[19] K. Wada and Y. Liu, "On the two-way shape memory behavior in NiTi alloy-An experimental analysis," *Acta Materialia,* vol. 56, pp. 3266-3277, 2008.

[20] A. Pequegnat, M. Daly, J. Wang, Y. Zhou and M. I. Khan, "Dynamic actuation of a novel laser-processed NiTi linear actuator," *Smart Materials and Structures,* vol. 21, pp. 094004, 2012.

[21] M. Daly, A. Peuqegnat, Y. Zhou and M. I. Khan, "Enhanced thermomechanical functionality of a laser processed hybrid NiTi–NiTiCu shape memory alloy," *Smart Materials and Structures,* vol. 21, 2012.

[22] J. Frenzel, E. P. George, A. Dlouhy, C. Somsen, M. F. X. Wagner and G. Eggeler, "Influence of Ni on martensitic phase transformations in NiTi shape memory alloys," *Acta Materialia,* vol. 58, pp. 3444-3458, 2010.

[23] Y. T. Hsu, Y. R. Wang, S. K. Wu and C. Chen, "Effect of CO2 Laser Welding on the Shape-Memory and Corrosion Characteristics of TiNi Alloys," *Metallurgical and Materials Transactions A,* vol. 32, pp. 569-576, 2001.

[24] J. Frenzel, Z. Zhang, C. Somsen, K. Neuking and G. Eggeler, "Influence of carbon on martensitic phase transformations in NiTi shape memory alloys," *Acta Materialia,* vol. 55, pp. 1331-1341, 2007.

[25] W. Kurz, *Fundamentals of Solidification.* Aedermannsdorf, Switzerland: Trans Tech Publications, 1989.

[26] F. Sczerzenie, G. Paul and C. Belden, "Comparison of Inclusions in Cold Drawn Wire and Precursor Hot-Rolled Rod Coil in VIM-VAR Nickel-Titanium Alloy," *Journal of Materials Engineering and Performance,* vol. 20, pp. 752-756, 2011.

[27] F. Sczerzenie, R. M. Manjeri, C. Belden and R. LaFond, "The effect of alloy formulation, cold work and inclusion content on micro-void formation in NiTi alloys," in *The International Conference on Shape Memory and Superelastic Technologies (SMST) may 12–16,* Pacific Grove, California, USA, 2014, pp. 17.

[28] Z. Zhang, J. Frenzel, K. Neuking and G. Eggeler, "On the reaction between NiTi melts and crucible graphite during vacuum induction melting of NiTi shape memory alloys," *Acta Materialia,* vol. 53, pp. 3971-3985, 2005.

[29] B. Reinholz and S. Brinckmann, "Phase transformations in the proximity of TiC precipitates in a NiTi matrix during fatigue," *International Journal of Fatigue,* vol. 41, pp. 72-82, 2012.

[30] S. K. Sadrnezhaad and S. B. Raz, "Effect of Microstructure on Rolling Behavior of NiTi Memory Alloy," *Materials Manufacturing Processes,* vol. 23, pp. 646-650, 2008.

[31] A. Toro, F. Zhou, M. Wu, W. Geertruyden and W. Misiolek, "Characterization of Non-Metallic Inclusions in Superelastic NiTi Tubes," *Journal of Materials Engineering and Performance,* vol. 18, pp. 448-458, 2009.

[32] T. B. Massalski, H. Okamoto, P. R. Subramanian and L. Kacprzak, Eds., *Binary Alloy Phase Diagrams.* Materials Park, OH: ASM International, 1990.

[33] M. Nishida, C. Wayman and T. Honma, "Precipitation processes in near-equiatomic TiNi shape memory alloys," *Metallurgical Transactions A,* vol. 17, pp. 1505-1515, 1986.

[34] T. Saburi, T. Tatsumi and S. Nenno, "Effects of Heat Treatment on Mechanical Behavior of Ti-Ni Alloys," *Journal De Physique Colloques,* vol. 43, pp. C4-261-C4-266, 1982.

[35] S. Miyazaki, Y. Ohmi, K. Otsuka and Y. Suzuki, "Characteristics of deformation and transformation pseudoelasticity in Ti-Ni alloys," *Journal De Physique,* vol. 43, pp. C4–255, 1982.

[36] G. Fan, W. Chen, S. Yang, J. Zhu, X. Ren and K. Otsuka, "Origin of abnormal multi-stage martensitic transformation behavior in aged Ni-rich Ti–Ni shape memory alloys," *Acta Materialia,* vol. 52, pp. 4351-4362, 2004.

[37] K. Otsuka, T. Sawamura and K. Shimizu, "Crystal structure and internal defects of equiatomic TiNi martensite," *Physica Status Solidi,* vol. 5, pp. 457-470, 1971.

[38] T. V. Philip and P. A. Beck, "CsCl-type ordered structures in binary alloys of transition elements," *Transactions AIME,* vol. 209, pp. 1269-1271, 1957.

[39] T. Waitz, T. Antretter, F. D. Fischer and H. P. Karnthaler, "Size effects on martensitic phase transformations in nanocrystalline NiTi shape memory alloys," *Materials Science and Technology,* vol. 24, pp. 934-940, 2008.

[40] S. Miyazaki, "Martensitic transformation in TiNi alloys," in *Thin Film Shape Memory Alloys: Fundamentals and Device Applications,* S. Miyazaki, Y. Q. Fu and W. M. Huang, Eds. Cambridge University Press & Science Press, 2009, pp. 73-87.

[41] S. Miyazaki, S. Kimura and K. Otsuka, "Shape-memory effect and pseudoelasticity associated with the R-phase transition in Ti-50·5 at.% Ni single crystals ," *Philosophical Magazine A, Philos Mag A,* vol. 57, pp. 467-478, 1988.

[42] E. R. Petty, Ed., *Martensite.* Great Britain: Longman, 1970.

[43] K. Otsuka and C. M. Waymann, *Shape Memory Materials.* Cambridge: Cambridge Univ. Press, 1998.

[44] K. Bhattacharya, *Microstructure of Martensite: Why it Forms and how it Gives Rise to the Shape-Memory Effect.* New York: Oxford University Press, 2003.

[45] S. Zhang, H. Braasch and P. G. McCormick, "FEM Simulation of the Martensitic Transformation in NiTi Alloys," *Journal De Physique IV,* vol. 7, pp. 537-542, 1997.

[46] S. Miyazaki, K. Otsuka and C. M. Wayman, "The shape memory mechanism associated with the martensitic transformation in Ti Ni alloys-I. Self-accommodation," *Acta Metallurgica,* vol. 37, pp. 1873-1884, 1989.

[47] R. A. Varin and M. B. Winnicka, "Plasticity of structural intermetallic compounds," *Materials Science & Engineering A,* vol. 137, pp. 93-103, 1991.

[48] T. W. Duerig, "Some unsolved aspects of Nitinol," *Materials Science & Engineering A,* vol. 438-440, pp. 69-74, 2006.

[49] T. Ezaz, J. Wang and H. M. Sehitoglu H.J., "Plastic deformation of NiTi shape memory alloys," *Acta Materialia,* vol. 61, pp. 67-78, 2013.

[50] I. V. Belova and G. E. Murch, "Diffusion in substitutionally disordered B2 intermetallics," *Journal of Physics: Condensed Matter,* vol. 14, pp. 9563-9577, 2002.

[51] A. M. Russell, "Ductility in Intermetallic Compounds," *Advanced Engineering Materials,* vol. 5, pp. 629-639, 2003.

[52] P. Nagpal and I. Baker, "Effect of cooling rate on hardness of FeAl and NiAl," *Metallurgical Transactions A,* vol. 21, pp. 2281-2282, 1990.

[53] M. H. Mueller and H. W. Knott, "The Crystal Structure of Ti2Cu, Ti2Ni, Ti4Ni2O, and Ti4Cu2O," *Transactions of the Metallurgical Society of AIME,* vol. 227, pp. 674-679, 1963.

[54] F. Takei, T. Miura, S. Miyazaki, S. Kimura, K. Otsuka and Y. Suzuki, "Stress-Induced Martensitic Transformation in a Ti-Ni Single Crystal," *Scripta Metallurgica,* vol. 17, pp. 987-992, 1983.

[55] S. Miyazaki, Y. Kohiyama, K. Otsuka and T. W. Duerig, "Effects of Several Factors on the Ductility of the Ti-Ni Alloy," *Materials Science Forum,* vol. 56-58, pp. 765-770, 1990.

[56] S. Miyazaki, T. Kawai and K. Otsuka, "On the origin of intergranular fracture in ß phase shape memory alloys," *Scripta Metallurgica,* vol. 16, pp. 431-436, 1982.

[57] S. Miyazaki, Y. Kohiyama and K. Otsuka, *Proc Int Symp on Intermetallic Compounds,* Sendai, 1991, pp. 691.

[58] A. R. Pelton, J. DiCello and S. Miyazaki, "Optimization of processing and properties of medical-grade Nitinol wire," *Minimally Invasive Therapy & Allied Technologies,* vol. 9, pp. 107-118, 2000.

[59] S. W. Robertson, A. R. Pelton and R. O. Ritchie, "Mechanical fatigue and fracture of Nitinol," *International Materials Reviews,* vol. 57, pp. 1-37, 2012.

[60] K. M. Knowles and D. A. Smith, "The crystallography of the martensitic transformation in equiatomic nickel-titanium," *Acta Metallurgica,* vol. 29, pp. 101-110, 1981.

[61] O. Matsumoto, S. Miyazaki, K. Otsuka and H. Tamura, "Crystallography of martensitic transformation in Ti Ni single crystals," *Acta Metallurgica,* vol. 35, pp. 2137-2144, 1987.

[62] S. Miyazaki, K. Otsuka and C. M. Wayman, "The shape memory mechanism associated with the martensitic transformation in Ti-Ni alloys-I. Self-accommodation," *Acta Metallurgica,* vol. 37, pp. 1873-1884, 1989.

[63] M. Pohl, C. Heßing and J. Frenzel, "Electrolytic processing of NiTi shape memory alloys," *Materials Science and Engineering: A,* vol. 378, pp. 191-199, 2004.

[64] E. Hornbogen and G. Eggeler, "Surface Aspects in Fatigue of Shape Memory Alloys (SMA)," *Materialwissenschaft Und Werkstofftechnik,* vol. 35, pp. 255-259, 2004.

[65] S. Miyazaki, Y. Igo and K. Otsuka, "Effect of thermal cycling on the transformation temperatures of Ti Ni alloys," *Acta Metallurgica,* vol. 34, pp. 2045-2051, 1986.

[66] G. Fan, W. Chen, S. Yang, J. Zhu, X. Ren and K. Otsuka, "Origin of abnormal multi-stage martensitic transformation behavior in aged Ni-rich Ti–Ni shape memory alloys," *Acta Materialia,* vol. 52, pp. 4351-4362, 8/16, 2004.

[67] W. Tang, "Thermodynamic study of the low-temperature phase B19' and the martensitic transformation in near-equiatomic Ti-Ni shape memory alloys," *Metallurgical and Materials Transactions A,* vol. 28, pp. 537–544, 1997.

[68] W. Tang, B. Sundman, R. Sandström and C. Qiu, "New modelling of the B2 phase and its associated martensitic transformation in the Ti–Ni system," *Acta Materialia,* vol. 47, pp. 3457-3468, 1999.

[69] M. H. Elahinia, M. Hashemi, M. Tabesh and S. B. Bhaduri, "Manufacturing and processing of NiTi implants: A review," *Progress in Materials Science,* vol. 57, pp. 911-946, 2012.

[70] S. Miyazaki and K. Otsuka, "Deformation and Transition Behavior Associated with the R-Phase in Ti-Ni Alloys," *Metallurgical Transactions A,* vol. 17, pp. 53-63, 1986.

[71] R. F. Hamilton, H. Sehitoglu, Y. Chumlyakov and H. J. Maier, "Stress dependence of the hysteresis in single crystal NiTi alloys," *Acta Materialia,* vol. 52, pp. 3383-3402, 2004.

[72] A. R. Pelton, G. H. Huang, P. Moine and R. Sinclair, "Effects of thermal cycling on microstructure and properties in Nitinol," *Materials Science & Engineering A,* vol. 532, pp. 130-138, 2012.

[73] A. Ahadi and E. Rezaei, "Microstructure and Phase Transformation Behavior of a Stress-Assisted Heat-Treated Ti-Rich NiTi Shape Memory Alloy," *Journal of Materials Engineering and Performance,* vol. 21, pp. 1806-1812, 2012.

[74] T. Simon, A. Kröger, C. Somsen, A. Dlouhy and G. Eggeler, "On the multiplication of dislocations during martensitic transformations in NiTi shape memory alloys," *Acta Materialia,* vol. 58, pp. 1850-1860, 2010.

[75] A. Pelton, "Nitinol Fatigue: A Review of Microstructures and Mechanisms," *Journal of Materials Engineering and Performance,* vol. 20, pp. 613-617, 2011.

[76] C. Urbina, S. De la Flor and F. Ferrando, "Effect of thermal cycling on the thermomechanical behaviour of NiTi shape memory alloys," *Materials Science & Engineering A,* vol. 501, pp. 197-206, 2009.

[77] D. Stoeckel, "The Shape Memory Effect - Phenomenon, Alloys and Applications," *Proceedings: Shape Memory Alloys for Power Systems EPRI,* pp. 1-13, 1995.

[78] J. A. Shaw and S. Kyriakides, "On the nucleation and propagation of phase transformation fronts in a NiTi alloy," *Acta Materialia,* vol. 45, pp. 683-700, 1997.

[79] P. Sittner, Y. Liu and V. Novak, "On the origin of Luders-like deformation of NiTi shape memory alloys," *Journal of the Mechanics and Physics of Solids,* vol. 53, pp. 1719-1746, 2005.

[80] K. Otsuka and K. Shimizu, "Pseudoelasticity and shape memory effects in alloys," *International Metals Reviews,* vol. 31, pp. 93-114, 1986.

[81] S. Miyazaki, K. Otsuka and Y. Suzuki, "Transformation pseudoelasticity and deformation behavior in a Ti-50.6at%Ni alloy," *Scripta Metallurgica,* vol. 15, pp. 287-292, 1981.

[82] J. R. Patel and M. Cohen, "Criterion for the action of applied stress in the martensitic transformation," *Acta Metallurgica,* vol. 1, pp. 531-538, 1953.

[83] H. Yin and Q. Sun, "Temperature Variation in NiTi Shape Memory Alloy During Cyclic Phase Transition," *Journal of Materials Engineering and Performance,* vol. 21, pp. 2505-2508, 2012.

[84] S. Miyazaki and K. Otsuka, "Deformation and transition behavior associated with the R-phase in Ti-Ni alloys," *Metallurgical Transactions A,* vol. 17, pp. 53-63, 1986.

[85] S. Eucken and T. Duerig, "The effects of pseudoelastic prestraining on the tensile behaviour and two-way shape memory effect in aged NiTi," *Acta Metallurgica,* vol. 37, pp. 2245-2252, 1989.

[86] S. Miyazaki, T. Imai, Y. Igo and K. Otsuka, "Effect of cyclic deformation on the pseudoelasticity characteristics of Ti-Ni alloys," *Metallurgical Transactions A,* vol. 17, pp. 115-120, 1986.

[87] J. M. McNaney, V. Imbeni, Y. Jung, P. Papadopoulos and R. O. Ritchie, "An experimental study of the superelastic effect in a shape-memory Nitinol alloy under biaxial loading," *Mechanics of Materials,* vol. 35, pp. 969-986, 2003.

[88] E. Polatidis, N. Zotov, E. Bischoff and E. J. Mittemeijer, "The effect of cyclic tensile loading on the stress-induced transformation mechanism in superelastic NiTi alloys: an in-situ X-ray diffraction study," *Scripta Materialia,* vol. 100, pp. 59-62, 2015.

[89] H. Scherngell and A. C. Kneissl, "Generation, development and degradation of the intrinsic two-way shape memory effect in different alloy systems," *Acta Materialia,* vol. 50, pp. 327-341, 2002.

[90] J. Pfetzing-Micklich, R. Ghisleni, T. Simon, C. Somsen, J. Michler and G. Eggeler, "Orientation dependence of stress-induced phase transformation and dislocation plasticity in NiTi shape memory alloys on the micro scale," *Materials Science and Engineering: A,* vol. 538, pp. 265-271, 2012.

[91] T. Buchheit and J. Wert, "Modeling the effects of stress state and crystal orientation on the stress-induced transformation of NiTi single crystals," *Metallurgical and Materials Transactions A,* vol. 25, pp. 2383-2389, 1994.

[92] T. Buchheit and J. Wert, "Predicting the orientation-dependent stress-induced transformation and detwinning response of shape memory alloy single crystals," *Metallurgical and Materials Transactions A,* vol. 27, pp. 269-279, 1996.

[93] S. Miyazaki, T. Kawai and K. Otsuka, "On the origin of intergranular fracture in ß phase shape memory alloys," *Scripta Metallurgica,* vol. 16, pp. 431-436, 1982.

[94] K. Takezawa, T. Izumi, H. Chiba and S. Sato, "Coherency of the transformation strain at the grain boundary and fracture in Cu-Zn-Al alloy," *Journal De Physique Colloques,* vol. 43, pp. 819-824, 1982.

[95] S. Gao and S. Yi, "Experimental study on the anisotropic behavior of textured NiTi pseudoelastic shape memory alloys," *Materials Science and Engineering: A,* vol. 362, pp. 107-111, 2003.

[96] Y. Liu, Z. L. Xie, J. Van Humbeeck and L. Delaey, "Effect of texture orientation on the martensite deformation of NiTi shape memory alloy sheet," *Acta Materialia,* vol. 47, pp. 645-660, 1999.

[97] N. Ono and A. Sato, "Plastic Deformation Governed by the Stres Induced Martensitic Transformation in Polycrystals," *Transactions of the Japan Institute of Metals,* vol. 29, pp. 267-273, 1988.

[98] N. Ono, A. Satoh and H. Ohta, "A Discussion on the Mechanical Porperties of Shape Memory Alloys Based on a Polycrystal Model," *Materials Transactions,* vol. 30, pp. 756-764, 1989.

[99] K. Gall and H. Sehitoglu, "The role of texture in tension–compression asymmetry in polycrystalline NiTi," *International Journal of Plasticity,* vol. 15, pp. 69-92, 1999.

[100] K. Gall, H. Sehitoglu, Y. I. Chumlyakov and I. V. Kireeva, "Tension–compression asymmetry of the stress–strain response in aged single crystal and polycrystalline NiTi," *Acta Materialia,* vol. 47, pp. 1203-1217, 1999.

[101] Y. Liu, Z. Xie, J. Van Humbeeck and L. Delaey, "Asymmetry of stress–strain curves under tension and compression for NiTi shape memory alloys," *Acta Materialia,* vol. 46, pp. 4325-4338, 1998.

[102] S. W. Robertson, X. Y. Gong and R. O. Ritchie, "Effect of product form and heat treatment on the crystallographic texture of austenitic Nitinol," *Journal of Materials Science,* vol. 41, pp. 621-630, 2006.

[103] M. M. Barney, D. Xu, S. W. Robertson, V. Schroeder, R. O. Ritchie, A. R. Pelton and A. Mehta, "Impact of thermomechanical texture on the superelastic response of Nitinol implants," *Journal of the Mechanical Behavior of Biomedical Materials,* vol. 4, pp. 1431-1439, 2011.

[104] K. Yamauchi, M. Nishida, I. Itai, K. Kitamura and A. Chiba, "Specimen Preparation for Transmission Electron Microscopy of Twins in B19' Martensite of Ti-Ni Shape Memory Alloys," *The Japan Institute of Metals,* vol. 37, pp. 210-217, 1996.

[105] H. Ling and K. Roy, "Stress-Induced Shape Changes and Shape Memory in the R and Martensite Transformations in Equiatomic NiTi," *Metallurgical Transactions A,* vol. 12, pp. 2101-2111, 1981.

[106] T. W. Duerig, *Engineering Aspects of Shape Memory Alloys.* London: Butterworth-Heinemann, 1990.

[107] N. B. Morgan and C. M. Friend, "A review of shape memory stability in NiTi alloys," *Journal De Physique IV,* vol. 11, pp. 325-332, 2001.

[108] E. Hornbogen, "Review Thermo-mechanical fatigue of shape memory alloys," *Journal of Materials Science,* vol. 39, pp. 385-399, 2004.

[109] A. Mehta, X. Y. Gong, V. Imbeni, A. R. Pelton and R. O. Ritchie, "Understanding the Deformation and Fracture of Nitinol Endovascular Stents Using In Situ Synchrotron X-Ray Microdiffraction," *Advanced Materials,* vol. 19, pp. 1183-1186, 2007.

[110] D. Norwich and A. Fasching, "A Study of the Effect of Diameter on the Fatigue Properties of NiTi Wire," *Journal of Materials Engineering and Performance,* vol. 18, pp. 558-562, 2009.

[111] A. R. Pelton, V. Schroeder, M. R. Mitchell, X. Y. Gong, M. Barney and S. W. Robertson, "Fatigue and durability of Nitinol stents," *Journal of the Mechanical Behavior of Biomedical Materials,* vol. 1, pp. 153-164, 2008.

[112] D. Tolomeo, S. Davidson and M. Santinoranont, "Cyclic properties of superelastic nitinol: Design implications," in *SMST-2000: Proceedings of the International Conference on Shape Memory and Superelastic Technologies,* 2000, pp. 471-475.

[113] R. M. Tabanli, N. K. Simha and B. T. Berg, "Mean strain effects on the fatigue properties of superelastic NiTi," *Metallurgical and Materials Transactions A,* vol. 32, pp. 1866-1869, 2001.

[114] N. B. Morgan, J. Painter and A. J. Moffat, "Mean strain effects and microstructural observation during in-vitro fatigue testing of NiTi," in *Proceedings of the International Conference on Shape Memory and Superelastic Technologies,* Monterey, USA, 2003, pp. 303-310.

[115] S. W. Robertson and R. O. Ritchie, "In vitro fatigue-crack growth and fracture toughness behavior of thin-walled superelastic Nitinol tube for endovascular stents: A basis for defining the effect of crack-like defects," *Biomaterials,* vol. 28, pp. 700-709, 2007.

[116] G. Plotino, N. M. Grande, M. Cordaro, L. Testarelli and G. Gambarini, "A Review of Cyclic Fatigue Testing of Nickel-Titanium Rotary Instruments," *Journal of Endodontics,* vol. 35, pp. 1469-1476, 2009.

[117] (2014). *Dynalloy, Inc.* Available: http://www.dynalloy.com/.

[118] A. Tuissi, P. Bassani, A. Mngioni, L. Toia and F. Butera, "Fabrication process and characterization of NiTi wires for actuators," SAES Getters, Milano, Italy, 2004.

[119] L. Fumagalli, F. Butera and A. Coda, "SmartFlex® NiTi Wires for Shape Memory Actuators," *Journal of Materials Engineering and Performance,* vol. 18, pp. 691-695, 2009.

[120] E. Macherauch, "Praktikum in werkstoffkunde," *Wiesbaden*, vol. Friedrich Vieweg & Sohn Verlagsgesellschaft, 2002.

[121] K. Melton and O. Mercier, "Fatigue of NiTi thermoelastic martensites," *Acta Metallurgica*, vol. 27, pp. 137-144, 1979.

[122] S. Miyazaki, Y. Sugaya and K. Otsuka, "Effects of various factors on fatigue life of Ti–Ni alloys," in *Proc. MRS Int. Meet. on 'Advanced Materials',* Tokyo, Japan, 1988, pp. Vol. 9, 251–256.

[123] K. N. Melton and O. Mercier, "The effect of the martensitic phase transformation on the low cycle fatigue behaviour of polycrystalline Ni Ti and Cu Zn Al alloys," *Materials Science and Engineering*, vol. 40, pp. 81-87, 1979.

[124] L. C. Brinson, I. Schmidt and R. Lammering, "Stress-induced transformation behavior of a polycrystalline NiTi shape memory alloy: micro and macromechanical investigations via in situ optical microscopy," *Journal of the Mechanics and Physics of Solids*, vol. 52, pp. 1549-1571, 2004.

[125] D. M. Norfleet, P. M. Sarosi, S. Manchiraju, M. F. X. Wagner, M. D. Uchic, P. M. Anderson and M. J. Mills, "Transformation-induced plasticity during pseudoelastic deformation in Ni–Ti microcrystals," *Acta Materialia*, vol. 57, pp. 3549-3561, 2009.

[126] M. Reinoehl, D. Bradley, R. Bouthot and J. Proft, "The influence of melt practice on final fatigue properties of superelastic NiTi wires," in *Proc. Int. Conf. on SMST*, Pacific Grove, CA, USA, April–May 2000, pp. 397-403.

[127] A. Wick, X. Y. Gong, J. Fino, J. Sheriff and A. R. Pelton, "Bending fatigue characteristics of nitinol," in *Proc. ASM Materials & Processes for Medical Devices Conf.* Minneapolis, MN, USA, August 2004, pp. 15-20.

[128] S. Miyazaki, K. Mizukoshi, T. Ueki, T. Sakuma and Y. Liu, "Fatigue life of Ti–50 at% Ni and Ti–40Ni–10 Cu at.% shape memory alloy wires," *Materials Science and Engineering A*, vol. A273-A275, pp. 658-663, 1999.

[129] R. M. Tabanli, N. K. Simha and B. T. Berg, "Mean stress effects on fatigue of NiTi," *Materials Science and Engineering: A*, vol. 273-275, pp. 644-648, 1999.

[130] L. F. Coffin and J. F. Tavernelli, "The Cyclic Straining and Fatigue of Metals," *Transactions of the American Institute of Mining and Metallurgical Engineers*, vol. 215, pp. 794-807, 1959.

[131] S. S. Manson, *Thermal Stress and Low Cycle Fatigue*Anonymous McGraw-Hill, 1966, pp. 125-192.

[132] T. W. Duerig, D. E. Tolomeo and M. Wholey, "An overview of superelastic stent design," *Minimally Invasive Therapy & Allied Technologies*, vol. 9, pp. 235-246, 2000.

[133] T. W. Duerig, "The Use of Superelasticity in Modern Medicine," *Materials Science Journal Bulletin*, vol. 27, pp. 101-104, 2002.

[134] M. R. Mitchell, "Fundamentals of modern fatigue analysis for design," in *ASM Handbook, Fatigue and Fracture*Anonymous Materials Park, OH: ASM International, 1996, pp. 227-262.

[135] S. Suresh, *Fatigue of Materials.* Cambridge: Cambridge University Press, 1998.

[136] A. Runciman, D. Xu, A. R. Pelton and R. O. Ritchie, "An equivalent strain/Coffin–Manson approach to multiaxial fatigue and life prediction in superelastic Nitinol medical devices," *Biomaterials,* vol. 32, pp. 4987-4993, 2011.

[137] S. Kari, "Design, Analysis, and Simulated Testing of a Surrogate Nitinol Fatigue Specimen," *Journal of Materials Engineering and Performance,* vol. 20, pp. 584-590, 2011.

[138] S. W. Robertson and R. O. Ritchie, "A fracture-mechanics-based approach to fracture control in biomedical devices manufactured from superelastic Nitinol tube," *Journal of Biomedical Materials Research,* vol. 84B, pp. 26-33, 2008.

[139] R. H. Dauskardt, T. W. Duerig and R. O. Ritchie, "Effects of IN SITU Phase Transformation on Fatigue Crack Propagation in Titanium Nickel Shape Memory Alloys," *MRS Shape Memory Materials,* vol. 9, pp. 243-249, 1989.

[140] R. L. Holtz, K. Sadananda and M. A. Imam, "Fatigue thresholds of Ni-Ti alloy near the shape memory transition temperature," *International Journal of Fatigue,* vol. 21, pp. 137-145, 1999.

[141] A. L. McKelvey and R. O. Ritchie, "Fatigue-crack growth behavior in the superelastic and shape-memory alloy nitinol," *Metallurgical and Materials Transactions A,* vol. 32, pp. 731-743, 2001.

[142] A. Ohta, N. Suzuki and T. Mawari, "Effect of Young's modulus on basic crack propagation properties near the fatigue threshold," *International Journal of Fatigue,* vol. 14, pp. 224-226, 1992.

[143] K. Gall, J. Tyber, G. Wilkesanders, S. W. Robertson, R. O. Ritchie and H. J. Maier, "Effect of microstructure on the fatigue of hot-rolled and cold-drawn NiTi shape memory alloys," *Materials Science & Engineering A,* vol. 486, pp. 389-403, 2008.

[144] S. W. Robertson, A. Mehta, A. R. Pelton and R. O. Ritchie, "Evolution of crack-tip transformation zones in superelastic Nitinol subjected to in situ fatigue: A fracture mechanics and synchrotron X-ray microdiffraction analysis," *Acta Materialia,* vol. 55, pp. 6198-6207, 2007.

[145] R. Vaidyanathan, D. C. Dunand and U. Ramamurty, "Fatigue crack-growth in shape-memory NiTi and NiTi–TiC composites," *Materials Science and Engineering A,* vol. 289, pp. 208-216, 2000.

[146] J. Y. He, K. W. Gao, Y. J. Su, L. J. Qiao and W. Y. Chu, "The role of hydride, martensite and atomic hydrogen in hydrogen-induced delayed fracture of TiNi alloy," *Materials Science and Engineering: A,* vol. 364, pp. 333-338, 2004.

[147] S. Gollerthan, D. Herberg, A. Baruj and G. Eggeler, "Compact tension testing of martensitic/pseudoplastic NiTi shape memory alloys," *Materials Science & Engineering A,* vol. 481-482, pp. 156-159, 2008.

[148] S. Gollerthan, M. L. Young, A. Baruj, J. Frenzel, W. W. Schmahl and G. Eggeler, "Fracture mechanics and microstructure in NiTi shape memory alloys," *Acta Materialia,* vol. 57, pp. 1015-1025, 2009.

[149] C. Maletta, L. Bruno, P. Corigliano, V. Crupi and E. Guglielmino, "Crack-tip thermal and mechanical hysteresis in Shape Memory Alloys under fatigue loading," *Materials Science & Engineering A,* vol. 616, pp. 281-287, 2014.

[150] A. L. McKelvey and R. O. Ritchie, "Fatigue-crack propagation in Nitinol, a shape-memory and superelastic endovascular stent material," *Journal of Biomedical Materials Research,* vol. 47, pp. 301-308, 1999.

[151] J. M. Stankiewicz, S. W. Robertson and R. O. Ritchie, "Fatigue-crack growth properties of thin-walled superelastic austenitic Nitinol tube for endovascular stents," *Journal of Biomedical Materials Research,* vol. 81A, pp. 685-691, 2007.

[152] G. Eggeler, E. Hornbogen, A. Yawny, A. Heckmann and M. Wagner, "Structural and functional fatigue of NiTi shape memory alloys," *Materials Science and Engineering: A,* vol. 378, pp. 24-33, 2004.

[153] D. C. Lagoudas, C. Li, D. A. Miller and L. Rong, "Thermomechanical transformation fatigue of SMA actuators," in *In Smart Structures and Materials 2000: Active Materials: Behavior and Mechanics, Proceedings of SPIE,* .

[154] D. C. Lagoudas, O. W. Bertacchini and E. Patoor, "Surface crack development in transformation induced fatigue of SMA actuators," in *Residual Stress and its Effects on Fatigue and Fracture*, A. G. Youtsos, Ed. Springer, 2006, pp. 209-222.

[155] D. A. Miller and D. C. Lagoudas, "Thermomechanical characterization of NiTiCu and NiTi SMA actuators: influence of plastic strains," *Smart Materials and Structures,* vol. 9, pp. 640-652, 2000.

[156] J. L. McNichols and P. C. Brooks, "NiTi fatigue behavior," *Journal of Applied Physics,* vol. 52, pp. 7442-7444, 1981.

[157] X. Wu, K. Kutschej and A. C. Kneissi, "Study on the thermal fatigue of NiTi wires," *Zeitschrit Fur Metallkunde,* vol. 94, pp. 122-126, 2003.

[158] O. W. Bertacchinia, D. C. Lagoudas, T. C. Calkins and J. H. Mabe, "Thermomechanical cyclic loading and fatigue life characterization of nickel rich NiTi shape-memory alloy actuators," in *Behavior and Mechanics of Multifunctional and Composite Materialsm, Proc. of SPIE,* 2008, .

[159] S. K. Bhaumik, K. V. Ramaiah and C. N. Saikrishna, "Nickel–Titanium shape memory alloy wires for thermal actuators," in *Micro and Smart Devices and Systems*, K. J. Vinoy, Ed. Springer India, 2014, pp. 181-198.

[160] B. Kockar, I. Karaman, J. I. Kim, Y. I. Chumlyakov, J. Sharp and C. J. Yu, "Thermomechanical cyclic response of an ultrafine-grained NiTi shape memory alloy," *Acta Materialia,* vol. 56, pp. 3630-3646, 2008.

[161] C. N. Saikrishna, K. V. Ramaiah, J. Bhagyaraj, Gouthama , and S. K. Bhaumik, "Influence of stored elastic strain energy on fatigue behaviour of NiTi shape memory alloy thermal actuator wire," *Materials Science & Engineering A,* vol. 587, pp. 65-71, 2013.

[162] D. Wurzel, "Effects of different thermomechanical treatments on fatigue of NiTi shape memory alloys," *Journal De Physique IV,* vol. 11, pp. Pr8-535-Pr8-540, 2001.

[163] J. Frenzel, J. A. Burow, E. J. Payton, S. Rezanka and G. Eggeler, "Improvement of NiTi Shape Memory Actuator Performance Through Ultra-Fine Grained and Nanocrystalline Microstructures," *Advanced Engineering Materials,* vol. 13, pp. 256-268, 2011.

[164] C. Saikrishna, K. Ramaiah, S. Allam Prabhu and S. Bhaumik, "On stability of NiTi wire during thermo-mechanical cycling," *Bulletin of Materials Science,* vol. 32, pp. 343-352, 2009.

[165] K. N. Melton, "Ni-ti based shape memory alloys," in *Engineering Aspects of Shape Memory Alloys*Anonymous London: Butterworth-Heinemann, 1990, pp. 21-35.

[166] C. N. Saikrishna, K. V. Ramaiah and S. K. Bhaumik, "Effects of thermo-mechanical cycling on the strain response of Ni-Ti-Cu shape memory alloy wire actuator," *Materials Science & Engineering A,* vol. 428, pp. 217-224, 2006.

[167] B. Erbstoeszer, B. Armstrong, M. Taya and K. Inoue, "Stabilization of the shape memory effect in NiTi: an experimental investigation," *Scripta Materialia,* vol. 42, pp. 1145-1150, 2000.

[168] M. Nafari Q. and S. Abbasi, "Influence of Composition and Thermomechanical Training Process on the Transformation Behavior and Shape Memory Properties of NiTi Based Alloys," *Transactions of the Indian Institute of Metals,* vol. 66, pp. 239-245, 2013.

[169] B. Ye, B. S. Majumdar and I. Dutta, "Texture development and strain hysteresis in a NiTi shape-memory alloy during thermal cycling under load," *Acta Materialia,* vol. 57, pp. 2403-2417, 2009.

[170] L. Contardo and G. Guenin, "Training and two-way memory effect in Cu-Zn-Al alloy," *Acta Metallurgica Et Materialia,* vol. 38, pp. 1267-1272, 1990.

[171] J. Perkins and R. O. Sponholz, "Stress-Induced Martensitic Transformation Cycling and Two-Way Shape Memory Training in Cu-Zn-AI Alloys," *Metallurgical Transactions A,* vol. 15A, pp. 313-321, 1984.

[172] C. Saikrishna, K. Ramaiah, B. Vidyashankar and S. Bhaumik, "Effect of Intermittent Overload Cycles on Thermomechanical Fatigue Life of NiTi Shape Memory Alloy Wire," *Metallurgical and Materials Transactions A,* vol. 44, pp. 5-8, 2013.

[173] D. C. Lagoudas, D. A. Miller, L. Rong and P. K. Kumar, "Thermomechanical fatigue of shape memory alloys," *Smart Materials and Structures,* vol. 18, pp. 1-12, 2009.

[174] S. Belyaev, N. Resnina and A. Sibirev, "Peculiarities of residual strain accumulation during thermal cycling of TiNi alloy," *Journal of Alloys and Compounds,* vol. 542, pp. 37-42, 2012.

[175] N. Ma, G. Song and H. J. Lee, "Position control of shape memory alloy actuators with internal electrical resistance feedback using neural networks," *Smart Materials and Structures,* vol. 13, pp. 777-783, 2004.

[176] H. Meier, A. Czechowicz, C. Haberland and S. Langbein, "Smart Control Systems for Smart Materials," *Journal of Materials Engineering and Performance,* vol. 20, pp. 559-563, 2011.

[177] R. Casati and A. Tuissi, "Effect of Current Pulses on Fatigue of Thin NiTi Wires for Shape Memory Actuators," *Journal of Materials Engineering and Performance,* vol. 21, pp. 2633-2637, 2012.

[178] A. Bhattacharyya, E. Dervishi, B. Berry, T. Viswanathan, S. Bourdo, H. Kim, R. Sproles and M. K. Hudson, "Energy efficient graphite–polyurethane electrically conductive coatings for thermally actuated smart materials," *Smart Materials and Structures,* vol. 16, pp. S187-S195, 2007.

[179] K. V. Ramaiah, C. N. Saikrishna, V. R. Ranganath, V. Buravalla and S. K. Bhaumik, "Fracture of thermally activated NiTi shape memory alloy wires," *Materials Science & Engineering A,* vol. 528, pp. 5502-5510, 2011.

[180] G. Scirè Mammano and E. Dragoni, "Functional fatigue of Ni–Ti shape memory wires under various loading conditions," *International Journal of Fatigue,* vol. 69, pp. 71-83, 2014.

[181] D. Hodgson and S. Russell, "Nitinol melting, manufacture and fabrication," *Minimally Invasive Therapy & Allied Technologies,* vol. 9, pp. 61-65, 2000.

[182] N. Morgan, A. Wick, J. Dicello and R. Graham, "Carbon and oxygen levels in nitinol alloys and the implications for medical device manufacture and durability," in *Proceedings of the International Conference on Shape Memory and Superelastic Technologies,* Pacific Grove, California, 2006, pp. 821-828.

[183] J. Frenzel, Z. Zhang, K. Neuking and G. Eggeler, "High quality vacuum induction melting of small quantities of NiTi shape memory alloys in graphite crucibles," *Journal of Alloys and Compounds,* vol. 385, pp. 214-223, 2004.

[184] C. Grossmann, J. Frenzel, V. Sampath, T. Depka, A. Oppenkowski, C. Somsen, K. Neuking, W. Theisen and G. Eggeler, "Processing and property assessment of NiTi and NiTiCu shape memory actuator springs," *Mat. -Wiss. U. Werkstofftech.,* vol. 39, pp. 499-510, 2008.

[185] Anonymous "Cleanest nitinol worldwide: NiTi-ELI," EUROFLEX, Pforzheim, Germany, .

[186] M. M. Patel, D. L. Plumley, R. J. Bouthot and J. L. Proft, "The significance of melt practice on fatigue properties of superelastic NiTi fine diameter wire," in *International Conference on Shape Memory and Superelastic Technologies (SMST). Fort Wayne Metals Resarch Products Corp.* Pacific Grove, CA, 2006, .

[187] J. Otubo, O. D. Rigo, C. M. Neto, M. J. Kaufman and P. R. Mei, "Scale up of NiTi shape memory alloy production by EBM," *Journal De Physique IV,* vol. 112, pp. 873, 2003.

[188] J. Otubo, O. D. Rigo, C. M. Neto, M. J. Kaufman and P. R. Mei, "Low Carbon Content NiTi Shape Memory Alloy Produced by Electron Beam Melting," *Materials Research,* vol. 7, pp. 263-267, 2004.

[189] J. Otubo, O. D. Rigo, C. M. Neto and P. R. Mei, "The effects of vacuum induction melting and electron beam melting techniques on the purity of NiTi shape memory alloys," *Materials Science & Engineering A,* vol. 438-440, pp. 679-682, 2006.

[190] C. P. Frick, A. M. Ortega, J. Tyber, K. Gall and H. J. Maier, "Multiscale structure and properties of cast and deformation processed polycrystalline NiTi shape-memory alloys," *Metallurgical and Materials Transactions A,* vol. 35, pp. 2013-2025, 2004.

[191] C. P. Frick, A. M. Ortega, J. Tyber, A. E. M. Maksound, H. J. Maier, Y. Liu and K. Gall, "Thermal processing of polycrystalline NiTi shape memory alloys," *Materials Science & Engineering A,* vol. 405, pp. 34-49, 2005.

[192] J. Frenzel, J. Pfetzing, K. Neuking and G. Eggeler, "On the influence of thermomechanical treatments on the microstructure and phase transformation behavior of Ni-Ti-Fe shape memory alloys," *Materials Science & Engineering A,* vol. 481-482, pp. 635-638, 2008.

[193] R. Kocich, I. Szurman, M. Kursa and J. Fiala, "Investigation of influence of preparation and heat treatment on deformation behaviour of the alloy NiTi after ECAE," *Materials Science & Engineering A,* vol. 512, pp. 100-104, 2009.

[194] H. Mirzadeh and M. H. Parsa, "Hot deformation and dynamic recrystallization of NiTi intermetallic compound," *Journal of Alloys and Compounds,* vol. 61, pp. 56-59, 2014.

[195] M. H. Wu, "Fabrication of nitinol materials and components," in *Proceedings of Conference SMST –SMM 2001,* pp. 285-291.

[196] S. D. Prokoshkin, I. Y. Khmelevskaya, V. Brailovski, F. Trochu, S. Turenne and V. Y. Turilina, "Thermomechanical Treatments and Their Influence on the Microstructure and Stress/Strain Diagrams of NiTi Shape Memory Alloys," *Canadian Metallurgical Quarterly,* vol. 43, pp. 95-108, 2004.

[197] Z. Lekston, M. Zubko, K. Prusik and D. Stróz, "Microstructure, Phase Transformations, and Properties of Hot-Extruded Ni-Rich NiTi Shape Memory Alloy," *Journal of Materials Engineering and Performance,* vol. 23, pp. 2362-2367, 2014.

[198] E. Hornbogen, "Ausforming of NiTi," *Journal of Materials Science,* vol. 34, pp. 599-606, 1999.

[199] D. Treppman and E. Hornbogen, "On the Influence of Thermomechanical Treatments on Shape Memory Alloys," *Journal De Physique IV,* vol. 7, pp. C5-211-C5-220, 1997.

[200] R. Kocich, I. Szurman and M. Kursa, "Ch 2: The methods of preparation of ti-ni-X alloys and their forming," in *Shape Memory Alloys - Processing, Characterization and Applications,* F. Manuel, Ed. 2013, pp. 27-52.

[201] J. C. Ewert, I. Böhm, R. Peter and F. Haider, "The role of the martensite transformation for the mechanical amorphisation of NiTi," *Acta Materialia,* vol. 45, pp. 2197-2206, 1997.

[202] R. N. Wright, *WIRE TECHNOLOGY PROCESS ENGINEERING AND METALLURGY*. Burlington, MA: Butterworth-Heinemann, 2011.

[203] W. A. Backofen, "Deformation Processing," *Metallurgical Transactions,* vol. 4, pp. 2679-2699, 1973.

[204] R. N. Wright, *Wire Technology,* vol. 6, pp. 131, 1978.

[205] R. N. Wright, *Wire Journal International,* vol. 30, pp. 88, 1997.

[206] G. J. Baker, "Workpiece Wear Mechanisms in the Drawing of Copper Wire," *Ph. D Thesis, Rensselaer Polytechnic Institute,* 1994.

[207] J. G. Wistreich, *Metallurgical Reviews,* vol. 3, pp. 97, 1958.

[208] R. N. Wright, "Center bursts - A review of criteria," in *Conference Proceedings,Wire Association International, Inc.* Guilford, CT, 2008, pp. 15.

[209] J. G. Wistreich, *Proceedings of the Institution of Mechanical Engineers,* London, UK, 1955, pp. 169.

[210] R. N. Wright and A. T. Male, *ASME Transactions, Journal for Lubrication Engineering, Series F,* vol. 97, pp. 134, 1975.

[211] R. N. Wright, *Metal Progress,* vol. 114, pp. 49, 1978.

[212] H. C. Lin, S. K. Wu and Y. C. Yen, "A study on the wire drawing of TiNi shape memory alloys," *Materials Science and Engineering: A,* vol. 215, pp. 113-119, 1996.

[213] J. Schaffer and D. Plumley, "Fatigue Performance of Nitinol Round Wire with Varying Cold Work Reductions," *Journal of Materials Engineering and Performance,* vol. 18, pp. 563-568, 2009.

[214] D. A. Miller and D. C. Lagoudas, "Influence of cold work and heat treatment on the shape memory effect and plastic strain development of NiTi," *Materials Science & Engineering A,* vol. 308, pp. 161-175, 2001.

[215] X. Lei, W. Rui and L. Yong, "The optimization of annealing and cold-drawing in the manufacture of the Ni–Ti shape memory alloy ultra-thin wire," *The International Journal of Advanced Manufacturing Technology,* vol. 55, pp. 905-910, 2011.

[216] S. K. Wu, H. C. Lin, Y. C. Yen and J. C. Chen, "Wire drawing conducted in the R-phase of TiNi shape memory alloys," *Materials Letters,* vol. 46, pp. 175-180, 2000.

[217] H. Aaronson, Y. Lee and K. Russell, "Precipitation processes in solids," in *The Minerals, Metals & Materials Society, American Institute of Mining, Metallurgical, and Petroleum Engineers,* K. C. Russell and H. I. Aaronson, Eds. Warrendale, PA: 1978, pp. 31-86.

[218] A. Santos Paula, K. Mahesh and F. Braz Fernandes, "Stability in Phase Transformation After Multiple Steps of Marforming in Ti-Rich Ni-Ti Shape Memory Alloy," *Journal of Materials Engineering and Performance,* vol. 20, pp. 771-775, 2011.

[219] A. S. Paula, K. K. Mahesh, C. M. L. dos Santos, F. M. Braz Fernandes and C. S. da Costa Viana, "Thermomechanical behavior of Ti-rich NiTi shape memory alloys," *Materials Science & Engineering A,* vol. 481-482, pp. 146-150, 2008.

[220] Y. Motemani, M. Nili-Ahmadabadi, M. J. Tan, M. Bornapour and S. Rayagan, "Effect of cooling rate on the phase transformation behavior and mechanical properties of Ni-rich NiTi shape memory alloy," *Journal of Alloys and Compounds,* vol. 469, pp. 164-168, 2009.

[221] J. Khalil-Allafi, A. Dlouhy and G. Eggeler, "Ni4Ti3-precipitation during aging of NiTi shape memory alloys and its influence on martensitic phase transformations," *Acta Materialia,* vol. 50, pp. 4255-4274, 2002.

[222] W. Guo, I. Steinbach, C. Somsen and G. Eggeler, "On the effect of superimposed external stresses on the nucleation and growth of Ni4Ti3 particles: A parametric phase field study," *Acta Materialia,* vol. 59, pp. 3287-3296, 2011.

[223] R. F. Zhu, J. N. Liu, G. Y. Tang, S. Q. Shi, M. W. Fu, T. Zion and T. Ho, "The improved superelasticity of NiTi alloy via electropulsing treatment for minutes," *Journal of Alloys and Compounds,* vol. 584, pp. 225-231, 2014.

[224] B. Malard, J. Pilch, P. Sittner, R. Delville and C. Curfs, "In situ investigation of the fast microstructure evolution during electropulse treatment of cold drawn NiTi wires," *Acta Materialia,* vol. 59, pp. 1542-1556, 2011.

[225] R. Delville, B. Malard, J. Pilch, P. Sittner and D. Schryvers, "Microstructure changes during non-conventional heat treatment of thin Ni–Ti wires by pulsed electric current studied by transmission electron microscopy," *Acta Materialia,* vol. 58, pp. 4503-4515, 2010.

[226] M. A. Polinsky, D. W. Norwich and M. H. Wu, "A study of the effects of surface modifications and process on the fatigue properties of NiTi wire," in *Proceedings, SMST-2006, Pacific Grove, California,* .

[227] M. Rahim, J. Frenzel, M. Frotscher, J. Pfetzing-Micklich, R. Steegmüller, M. Wohlschlögel, H. Mughrabi and G. Eggeler, "Impurity levels and fatigue lives of pseudoelastic NiTi shape memory alloys," *Acta Materialia,* vol. 61, pp. 3667-3686, 2013.

[228] J. Sheriff, A. R. Pelton and L. A. Pruitt, "Hydrogen effects on nitinol fatigue," in *Proceedings of the International Conference on Shape Memory and Superelastic Technologies,* Kurhaus Baden-Baden, Germany, 2004, pp. 111-116.

[229] Z. Zeng, b. Panton, J. P. Oliveira, A. Han and Y. N. Zhou, "Dissimilar laser welding of NiTi shape memory alloy and copper," *Smart Materials and Structures,* vol. 24, pp. 1-8, 2015.

[230] R. Hahnlen, G. Fox and M. J. Dapino, "Fusion welding of nickel–titanium and 304 stainless steel tubes: Part I: laser welding," *Journal of Intelligent Material Systems and Structures,* vol. 0, pp. 1-17, 2012.

[231] B. Panton, A. Pequegnat and Y. Zhou, "Dissimilar Laser Joining of NiTi SMA and MP35N Wires," *Metallurgical and Materials Transactions A,* vol. 45, pp. 3533-3544, 2014.

[232] J. P. Oliveira, B. Panton, Z. Zeng, C. M. Andrei, Y. N. Zhou, R. M. Miranda and F. M. Braz Fernandes, "Laser Joining of NiTi to Ti6Al4V Using a Niobium Interlayer," *Acta Materialia,* vol. 105, pp. 9-15, 2015.

[233] B. Tam, M. I. Khan and Y. N. Zhou, "Mechanical and Functional Properties of Laser-Welded Ti-55.8 Wt Pct Ni NitinolWires," *Metallurgical and Materials Transactions A,* vol. 42A, pp. 2166-2175, 2011.

[234] A. Falvo, F. M. Furgiuele and C. Maletta, "Laser welding of a NiTi alloy: Mechanical and shape memory behaviour," *Materials Science & Engineering A,* vol. 412, pp. 235-240, 2005.

[235] L. A. Vieira, F. M. B. Fernandes, R. M. Miranda, R. J. C. Silva, L. Quintino, A. Cuesta and J. L. Ocaña, "Mechanical behaviour of Nd:YAG laser welded superelastic NiTi," *Materials Science & Engineering A,* vol. 528, pp. 5560-5565, 2011.

[236] J. P. Oliveira, F. M. Braz Fernanandes, N. Schell and R. M. Miranda, "Shape memory effect of laser welded NiTi plates," *Functional Materials Letters,* vol. 8, pp. 1-5, 2015.

[237] X. J. Yan, D. Z. Yang and X. P. Liu, "Influence of heat treatment on the fatigue life of a laser-welded NiTi alloy wire," *Materials Characterization,* vol. 58, pp. 262-266, 2007.

[238] C. W. Chan, H. C. Man and F. T. Cheng, "Fatigue behavior of laser-welded NiTi wires in small-strain cyclic bending," *Materials Science & Engineering A,* vol. 559, pp. 407-415, 2013.

[239] J. P. Oliveira, R. M. Miranda, N. Schell and F. M. Braz Fernandes, "High strain and long duration cycling behavior of laser welded NiTi sheets," *International Journal of Fatigue,* vol. 83, Part 2, pp. 195-200, 2016.

[240] A. Falvo, F. M. Furgiuele and C. Maletta, "Functional behaviour of a NiTi-welded joint: Two-way shape memory effect," *Materials Science & Engineering A,* vol. 481-482, pp. 647-650, 2008.

[241] C. Chan, H. Man and T. Yue, "Effect of Postweld Heat Treatment on the Microstructure and Cyclic Deformation Behavior of Laser-Welded NiTi-Shape Memory Wires," *Metallurgical and Materials Transactions A,* vol. 43, pp. 1956-1965, 2012.

[242] X. J. Yan, D. Z. Yang and M. Qi, "Rotating-bending fatigue of a laser-welded superelastic NiTi alloy wire," *Materials Characterization,* vol. 57, pp. 58-63, 2006.

[243] P. Sevilla, F. Martorell, C. Libenson, J. A. Planell and F. J. Gi, "Laser welding of NiTi orthodontic archwires for selective force application," *Journal of Materials Science: Materials in Medicine,* vol. 19, pp. 525-529, 2008.

[244] E. G. Welp and S. Langbein, "Survey of the in situ configuration of cold-rolled, nickel-rich NiTi sheets to create variable component functions," *Materials Science & Engineering A,* vol. 481-482, pp. 602-605, 2008.

[245] Q. Meng, Y. Liu, H. Yang, B. S. Shariat and T. Nam, "Functionally graded NiTi strips prepared by laser surface anneal," *Acta Materialia,* vol. 60, pp. 1658-1668, 2012.

[246] Y. Bellouard, T. Lehnert, J. E. Bidaux, T. Sidler, R. Clavel and R. Gotthardt, "Local annealing of complex mechanical devices: a new approach for developing monolithic micro-devices," *Materials Science and Engineering: A,* vol. 273-275, pp. 795-798, 1999.

[247] D. Cluff, S. Corbin and R. Gorbet, "Powder metallurgy fabrication of hybrid monolithic SMA actuators," in *Cansmart 2009, International Workshop, Smart Materials and Structures,* Montreal, Quebec, Canada, 2009, pp. 1-10.

[248] M. Whitney, S. F. Corbin and R. B. Gorbet, "Investigation of the mechanisms of reactive sintering and combustion synthesis of NiTi using differential scanning calorimetry and microstructural analysis," *Acta Materialia,* vol. 56, pp. 559-570, 2008.

[249] A. Pequegnat, M. Vlascov, M. Daly, Y. Zhou and M. I. Khan, "Dynamic actuation of a multiple memory material processed nitinol linear actuator," *ASME 2011 Conference on Smart Materials, Adaptive Structures and Intelligent Systems,* pp. 1–5, 2011.

[250] M. M. Collur, A. Paul and T. DebRoy, "Mechanism of alloying element vaporization during laser welding," *Metallurgical Transactions B,* vol. 18, pp. 733-740, 1987.

[251] A. Block-Bolten and T. Eagar, "Metal vaporization from weld pools," *Metallurgical Transactions B-Process Metallurgy,* vol. 15, pp. 461-469, 1984.

[252] M. Jandaghi, P. Parvin, M. J. Torkamany and J. Sabbaghzadeh, "Alloying element losses in pulsed Nd : YAG laser welding of stainless steel 316," *Journal of Physics D: Applied Physics,* vol. 41, pp. 1-9, 2008.

[253] P. A. A. Khan and T. Debroy, "Alloying element vaporization and weld pool temperature during laser welding of AISI 202 stainless steel," *Metallurgical Transactions B,* vol. 15B, pp. 641-644, 1984.

[254] X. He, T. DebRoy and P. W. Fuerschbach, "Alloying element vaporization during laser spot welding of stainless steel," *Journal of Physics D: Applied Physics,* vol. 36, pp. 3079-3088, 2003.

[255] X. He, T. DebRoy and P. W. Fuerschbach, "Composition change of stainless steel during microjoining with short laser pulse," *Journal of Applied Physics,* vol. 96, pp. 4547-4555, 2004.

[256] S. Koelemijer Chollet, L. Benmayor, J. M. Uehlinger and J. Jacot, "Cost effective micro-system assembly automation," in *Proceedings of the 7th IEEE International Conference on Emerging Technologies and Factory Automation,* 1999, pp. 359-366.

[257] B. Tam, A. Pequegnat, M. Khan and Y. Zhou, "Resistance Microwelding of Ti-55.8 wt pct Ni Nitinol Wires and the Effects of Pseudoelasticity," *Metallurgical and Materials Transactions A,* vol. 43, pp. 2969-2978, 2012.

[258] A. Schuessler, T. Haas, P. Schlossmacher and H. Borgmann, "Micro Welding of NiTi Shape Memory Alloys," *Proc. Actuator 94 : 4th Internat. Conf. on New Actuators, Bremen, June 15-17, 1994,* pp. S.372-376, .

[259] J. Zhang, D. C. Weckman and Y. Zhou, "Effects of Temporal Pulse Shaping on Cracking Susceptibility of 6061-T6 Aluminum Nd:YAG Laser Welds," *Welding Research,* vol. 87, pp. 18-s-30-s, 2008.

[260] C. B. Churchill, J. A. Shaw and M. A. Iadicola, "Tips and tricks for characterizing shape memory alloy wire: Part 2— fundamental isothermal responses," *Experimental Techniques,* pp. 51-62, 2009.

[261] J. A. Shaw and S. Kyriakides, "Thermomechanical aspects of NiTi," *Journal of the Mechanics and Physics of Solids,* vol. 43, pp. 1243-1281, 8, 1995.

[262] M. A. Iadicola and J. A. Shaw, "An experimental method to measure initiation events during unstable stress-induced martensitic transformation in a shape memory alloy wire," *Smart Materials and Structures,* vol. 16, pp. S155-S169, 2007.

[263] J. A. Shaw, C. B. Churchill and M. A. Iadicola, "Tips and tricks for characterizing shape memory alloy wire: Part 1—Differential scanning calorimetry and basic phenomena," *Experimental Techniques,* pp. 55-62, 2008.

[264] C. B. Churchill, J. A. Shaw and M. A. Iadicola, "Tips and tricks for characterizing shape memory alloy wire: Part 3 - localization and propagation phenomena," *Experimental Techniques,* vol. 33, pp. 70-78, 2009.

[265] C. B. Churchill, J. A. Shaw and M. A. Iadicola, "Tips and tricks for characterizing shape memory alloy wire: Part 4 - thermo-mechanical coupling," *Experimental Techniques,* vol. 34, pp. 63-80, 2010.

[266] B. Reedlunn, S. Daly, L. Hector Jr., P. Zavattieri and J. Shaw, "Tips and trick for characterizing shape memory wire part 5: full-field strain measurements by digital image correlation," *Experimental Techniques,* vol. 37, pp. 78, 2013.

[267] X. He, J. T. Norris, P. W. Fuerschbach and T. DebRoy, "Liquid metal expulsion during laser spot welding of 304 stainless steel," *Journal of Physics D: Applied Physics,* vol. 39, pp. 525-534, 2006.

[268] L. Corbin, "Dies & ceramics," in *Nonferrous Wire Handbook,* 3rd ed.Anonymous Guilford, CT: The Wire Association,Inc., 1995, pp. 477.

[269] K. Kazemi-Choobi, J. Khalil-Allafi and V. Abbasi-Chianeh, "Investigation of the recovery and recrystallization processes of Ni50.9Ti49.1 shape memory wires using in situ electrical resistance measurement," *Materials Science & Engineering A,* vol. 551, pp. 122-127, 2012.

[270] M. H. Elahinia, M. Hashemi, M. Tabesh and S. B. Bhaduri, "Manufacturing and processing of NiTi implants: A review," *Progress in Materials Science,* vol. 57, pp. 911-946, 2012.

[271] X. Ren, N. Miura, J. Zhang, K. Otsuka, K. Tanaka, M. Koiwa, T. Suzuki, Y. I. Chumlyakov and M. Asai, "A comparative study of elastic constants of Ti–Ni-based alloys prior to martensitic transformation," *Materials Science and Engineering: A,* vol. 312, pp. 196-206, 2001.

[272] T. Waitz, V. Kazykhanov and H. P. Karnthaler, "Martensitic phase transformations in nanocrystalline NiTi studied by TEM," *Acta Materialia,* vol. 52, pp. 137-147, 2004.

[273] H. C. Lin, S. K. Wu, T. S. Chou and H. P. Kao, "The effects of cold rolling on the martensitic transformation of an equiatomic TiNi alloy," *Acta Metallurgica Et Materialia,* vol. 39, pp. 2069-2080, 1991.

[274] J. P. Oliveira, F. M. Braz Fernandes, R. M. Miranda and N. Schell, "On the Mechanisms for Martensite Formation in YAG Laser Welded Austenitic NiTi," *Shape Memory and Superelasticity,* pp. 1-7, 2015.

[275] S. Miyazaki, Y. Kohiyama and K. Otsuka, "Effects of several factors on the ductility of the Ti-Ni alloy," *Materials Science Forum,* vol. 56-58, pp. 765-770, 1990.

[276] M. I. Khan, S. K. Panda and Y. Zhou, "Effects of Welding Parameters on the Mechanical Performance of Laser Welded Nitinol," *Materials Transactions,* vol. 49, pp. 2702-2708, 2008.

[277] Q. P. Sun and Y. J. He, "A multiscale continuum model of the grain-size dependence of the stress hysteresis in shape memory alloy polycrystals," *International Journal of Solids and Structures,* vol. 45, pp. 3868-3896, 2008.

[278] J. P. Oliveira, F. M. Braz Fernanandes, N. Schell and R. M. Miranda, "Martensite Stabilization During Superelastic Cycling of Laser Welded NiTi Plates," *Materials Letters,* vol. 171, pp. 273-276, 2016.

[279] K. Otsuka and K. Shimizu, "Pseudoelasticity and shape memory effects in alloys," *International Metals Reviews,* vol. 31, pp. 93-114, 1986.

[280] G. Scirè Mammano and E. Dragoni, "Effects of Loading and Constraining Conditions on the Thermomechanical Fatigue Life of NiTi Shape Memory Wires," *Journal of Materials Engineering and Performance,* vol. 23, pp. 2403-2411, 2014.

[281] H. C. Lin, S. K. Wu and J. C. Lin, "The martensitic transformation in Ti-rich TiNi shape memory alloys," *Materials Chemistry & Physics,* vol. 37, pp. 184-190, 1994.

[282] S. Kou, *Welding Metallurgy.* Hoboken, NJ: John Wiley Sons, Inc., 2003.

[283] A. Schuessler, T. Haas, P. Schlossmacher and H. Borgmann, "Micro Welding of NiTi Shape Memory Alloys," *Proc. Actuator 94 : 4th Internat. Conf. on New Actuators, Bremen, June 15-17, 1994,* pp. S.372-376, .

[284] T. Waitz, T. Antretter, F. D. Fischer and H. P. Karnthaler, "Size effects on martensitic phase transformations in nanocrystalline NiTi shape memory alloys," *Materials Science and Technology,* vol. 24, pp. 934-940, 2008.

[285] Q. P. Sun, A. Aslan, M. P. Li and M. X. Chen, "Effects of grain size on phase transition behavior of nanocrystalline shape memory alloys," *Science China Technological Sciences,* vol. 57, pp. 671-679, 2014.

[286] J. Schaffer, "Structure-Property Relationships in Conventional and Nanocrystalline NiTi Intermetallic Alloy Wire," *Journal of Materials Engineering and Performance,* vol. 18, pp. 582-587, 2009.

[287] D. Stoeckel, "The Shape Memory Effect – Phenomenon, Alloys and Applications," *Proceedings: Shape Memory Alloys for Power Systems EPRI,* pp. 1-13, 1995.

[288] S. K. Bhaumik, K. V. Ramaiah and C. N. Saikrishna, "Nickel–Titanium shape memory alloy wires for thermal actuators," in *Micro and Smart Devices and Systems*, K. J. Vinoy, Ed. Springer India, 2014, pp. 181-198.

[289] X. Shi, L. Cui, D. Jiang, C. Yu, F. Guo, M. Yu, Y. Ren and Y. Liu, "Grain size effect on the R-phase transformation of nanocrystalline NiTi shape memory alloys," *Journal of Materials Science,* vol. 49, pp. 4643-4647, 2014.

[290] J. R. Trelewicz and C. A. Schuh, "The Hall–Petch breakdown in nanocrystalline metals: A crossover to glass-like deformation," *Acta Materialia,* vol. 55, pp. 5948-5958, 2007.

[291] M. Dao, L. Lu, R. J. Asaro, J. T. M. De Hosson and E. Ma, "Toward a quantitative understanding of mechanical behavior of nanocrystalline metals," *Acta Materialia,* vol. 55, pp. 4041-4065, 2007.

[292] A. Ahadi and Q. Sun, "Stress hysteresis and temperature dependence of phase transition stress in nanostructured NiTi—Effects of grain size," *Applied Physics Letters,* vol. 103, 2013.

[293] B. Erbstoeszer, B. Armstrong, M. Taya and K. Inoue, "Stabilization of the shape memory effect in NiTi: an experimental investigation," *Scripta Materialia,* vol. 42, pp. 1145-1150, 2000.

[294] X. Zhao, W. Wang, L. Chen, F. Liu, J. Huang and H. Zhang, "Microstructures of cerium added laser weld of a TiNi alloy," *Materials Letters,* vol. 62, pp. 1551-1553, 2008.

[295] X. Zhao, L. Lan, H. Sun, J. Huang and H. Zhang, "Mechanical properties of additive laser-welded NiTi alloy," *Mater Lett,* vol. 64, pp. 628-631, 3/15, 2010.

[296] F. Yang, D. R. Coughlin, P. J. Phillips, L. Yang, A. Devaraj, L. Kovarik, R. D. Noebe and M. J. Mills, "Structure analysis of a precipitate phase in an Ni-rich high-temperature NiTiHf shape memory alloy," *Acta Materialia,* vol. 61, pp. 3335-3346, 2013.

[297] X. He, T. DebRoy and P. W. Fuerschbach, "Probing temperature during laser spot welding from vapor composition and modeling," *Journal of Applied Physics,* vol. 94, pp. 6949-6958, 2003.

[298] A. Nespoli and S. Besseghini, "A complete thermo-mechanical study of a NiTiCu shape memory alloy wire," *Journal of Thermal Analysis and Calorimetry,* vol. 103, pp. 821-826, 2011.

[299] G. Bigelow, S. Padula, A. Garg, D. Gaydosh and R. Noebe, "Characterization of Ternary NiTiPd High-Temperature Shape-Memory Alloys under Load-Biased Thermal Cycling," *Metallurgical and Materials Transactions A,* vol. 41, pp. 3065-3079, 2010.

[300] D. N. Fang, W. Lu, W. Y. Yan, T. Inoue and K. C. Hwang, "Stress–strain relation of CuAlNi SMA single crystal under biaxial loading—constitutive model and experiments," *Acta Materialia,* vol. 47, pp. 269-280, 1998.

[301] J. P. Oliveira, B. Panton, Z. Zeng, T. Omori, Y. Zhou, R. M. Miranda and F. M. Braz Fernandes, "Laser welded superelastic Cu–Al–Mn shape memory alloy wires," *Materials and Design,* vol. 90, pp. 122-128, 2016.

[302] A. Michael, Y. N. Zhou and M. I. Khan, "Experimental validation of a one-dimensional model for monolithic shape memory alloys with multiple pseudoelastic plateaus," *Journal of Intelligent Material Systems and Structures,* 2015.